Ministry of Water Resources

Bangladesh Water Development Board

Coastal Embankment Improvement Project, Phase-I (CEIP-I)

Long Term Monitoring, Research and Analysis of Bangladesh Coastal Zone (Sustainable Polders Adapted to Coastal Dynamics)

Climate Change Scenarios
Deliverable 4C: Meteorology

August 2021

Ministry of Water Resources

Bangladesh Water Development Board

Coastal Embankment Improvement Project, Phase-I (CEIP-I)

Long Term Monitoring, Research and Analysis of Bangladesh Coastal Zone (Sustainable Polders Adapted to Coastal Dynamics)

Climate Change Scenarios
Deliverable 4C: Meteorology

August 2021

Contents

FIGURES

ACRONYMS AND ABBREVIATIONS

ASLR	Absolute Sea Level Rise
BMD	Bangladesh Meteorological Department
BoB	Bay of Bengal
BWDB	Bangladesh Water Development Board
CEIP	Coastal Embankment Improvement Project
CMIP	Climate Model Intercomparison Project
COV	Coefficient of Variation
GBM	Ganges, Brahmaputra and Meghna
GCM	Global Circulation Model
GMSL	Global Mean Sea Level
IWM	Institute of Water Modelling
JTWC	Joint Typhoon Warning Center
RCP	Representative Concentration Pathway
RSLR	Relative Sea Level Rise
SLR	Sea Level Rise
SROCC	Special Report on the Ocean and Cryosphere in a Changing Climate
TC	Tropical Cyclones
TRM	Tidal River Management

1   INTRODUCTION

1.1 Background

Bangladesh is widely recognized to be one of the most climate vulnerable countries in the world. According to the "Global Climate Risk Index 2020" (Germanwatch, 2019), Bangladesh ranks at number seven in the world among most affected countries by natural disasters with an estimated loss of 0.41% per unit GDP for the period 1999 – 2018. By 2050, Bangladesh could face incremental costs of flood protection (against sea and river floods) of US$2.6 billion initial costs and US$54 million annual recurring costs (2009 prices; Dasgupta et al. 2010). Ahmed and Suphachalasai (2014), estimated that Bangladesh is projected to face 2.0% loss of annual GDP by 2050 and more than 9% by 2100 under a business-as-usual (BAU) scenario as a result of climate change. The same figures are also reported as part of the Delta Plan (GED, 2018). To avoid the damage and economic losses from climate change under the BAU scenario, the region would need to provide an average adaptation expenditure of 0.48% of GDP per annum by 2050 and 0.86% of GDP per annum by 2100. These adaptation costs could be reduced if global target mitigation efforts would be met.

The effects that climate change could have on the Ganges, Brahmaputra and Meghna (GBM) delta system are multiple: for example, changes in rainfall patterns will affect river discharges (averaged and peaks) and sediment loads, with possible effects on flooding as well as on the river and delta morphology. Similarly, sea level rise will affect the development of the GBM morphology. The effect of climate change and sea level rise on tropical cyclones (frequency and intensity) will lead to more frequent and extreme flooding. Sea level rise will also enhance salinity levels and intrusion within the GBM delta.

The effects on the physical system will in turn affect the economic activities, livelihood and ecosystems of the GBM delta. The effect of climate change on several sectors has been described, among others, in the Delta Plan 2100 (General Economics Division (GED) – 2018), including impacts on agriculture, health, land loss, infrastructures, energy, forest and other ecosystems.

The end goal of the "Long-Term Monitoring, Research and Analysis of Bangladesh Coastal Zone" project, as stated in the projects Terms of Reference, is to develop relevant and state-of-the-art knowledge for the Bangladesh coastal zone, which can be used as a basis towards the development of long-term sustainable polders. The knowledge development is based on monitoring, modelling (at different spatial and temporal scale) and sharing of knowledge. It is therefore of primary importance that the conceptual design of resilient polders (i.e. the end-goal of this project) will properly account for the effects that climate change may have on the physical system and which can in turn affect the different coastal polders across the region.

The present deliverable (Deliverable 4C: Meteorology) will specifically focus on defining plausible scenarios for future precipitation, temperature, sea level rise and cyclone frequency and intensity. These scenarios will then be used as a basis for further numerical modelling analysis, in separate modelling deliverables, and towards the development of a polder management and investment plan as described in Section 1.2.

1.2 Specific objectives of this report

Following the ToR of this project, the present report is part of project Component-4D ("Meteorology") which has, as main goal, the definition of current and future trends in **rainfall**, **temperature**, **cyclone frequency** and **intensity** as a result of climate change. In addition, and for completeness, we have opted to include as part of this report the assessment of **sea level rise** scenarios based on available data and recent literature. This deliverable provides the input to a number of project components as described in Figure 1.1, including both model- and non-model deliverables. Possible climate scenarios will be put forward for the different variables analysed and (whenever possible) until the end of the century. These scenarios will be used to assess the response of the physical system, based on numerical modelling, and towards the definition of new conceptual polder designs and the investment plan.
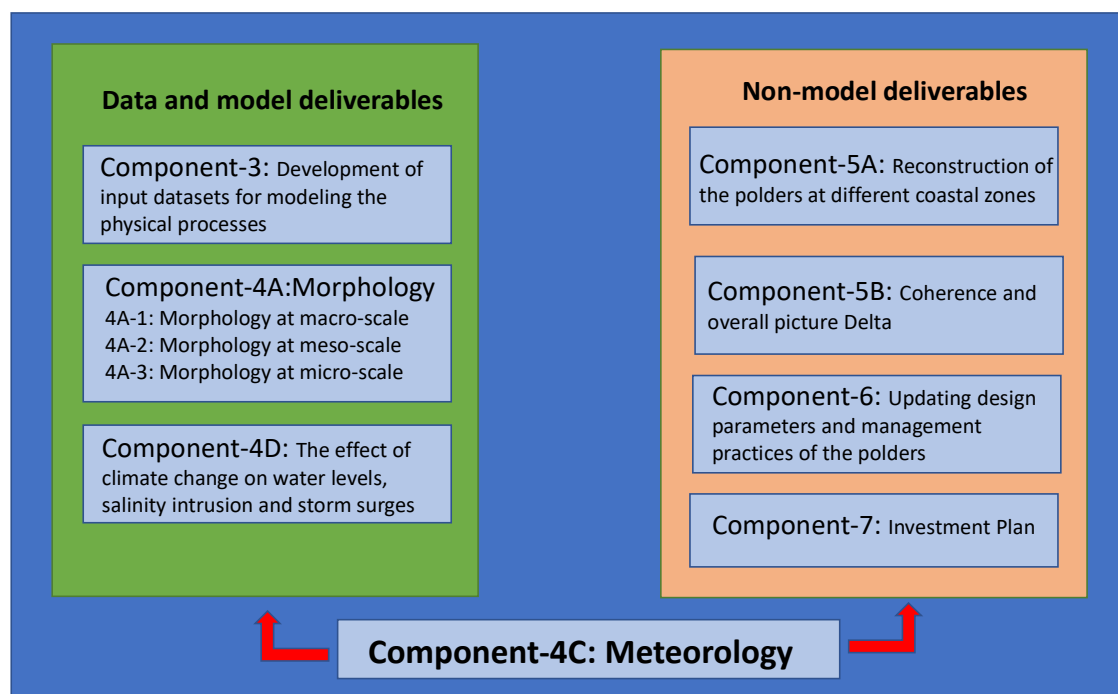
Figure 1.1   Overview of project components to which this report is providing input.

The spatial scale will be focusing both on the entire coastal region (and even GBM catchment for temperature and precipitation) and with particular emphasis on the five polders which will be analysed more in details as part of Component 5-A (i.e. 15, 29, 40/1 & 40/2, 59/2, 64/1a & 64/1b).

As it will be demonstrated in this report, variations in climate change projections are large. Different climate models provide substantially different projections. This means uncertainties in climate change are substantial and cannot be ignored. We therefore strongly advise against selecting a single climate scenario as input for model simulations, as such a scenario might be confused with a *prediction* instead of one of many possible *projections*. It is relevant to show stakeholders that there is large uncertainty involved and that it is important to be prepared for a range of scenarios.

> Because climate change is highly uncertain and because different applications require focus on different climate characteristics, it is important to consider multiple climate change scenarios.

For this reason, we propose to apply a 'tipping point approach' (Kwadijk et al., 2010) in the follow-up phases of the project. This means we will evaluate a number of plausible 'fixed" scenarios without directly putting a label on it like a year, an emission scenario or a high/low bound'. For example, this

can be a scenario like +10% precipitation, +30% precipitation or +2 degrees Celsius. We then analyse how the various systems (macro-, meso- and microscale) respond to those changes and report on major "tipping points" i.e. where the system starts to behave significantly different from todays' situation. Subsequently, we can *qualitatively* describe the likelihood of those scenarios in a particular year and emission scenario, based on the available climate projections.

1.3 This report

This report is organized as follows: **Chapter 1** provides a general introduction to the report, while **Chapter 2** describes the approach and methodology used for the analysis. The data used for the analysis of the different variables are described as part of **Chapter 3**. **Chapter 4** presents an overview of major results and, finally, a summary of major conclusions and proposed scenarios for further use in upcoming model and non-model deliverables.

2 Approach & Methodology

2.1 Rainfall and temperature

The general concept is as follows: first we analyse the current climate conditions and quantify its most relevant statistical characteristics. Then we analyse projections from various Global Climate Models (GCMs) and quantify how these relevant characteristics may change over time in the coming decades. Projected changes in climate conditions will be quantified in terms of percentages (precipitation) or absolute differences (temperature). These projected changes will be superimposed on data from historic records, if available. For rainfall and temperature in Bangladesh, we will superimpose projected changes on available records of the approximately 30 climate stations spread over the country (see section 3.2).

Climate change projections for the GBM basin as a whole are relevant for the delta as they will result in changes in river discharges and sediment loads. However, for the GBM basin we cannot do the same analysis as for Bangladesh, since we do not have historical climatological records available for the whole basin. The following approach will be followed to assess changes in river discharges and sediment loads:

1. Assess current climate

    a. Derive a reference climate scenario (precipitation, temperature) from the historical bias-corrected GCM data (current report)

    b. Apply resulting time series as input in the Hydrotrend model (Deliverable 4A-1: macro-scale morphology)

    c. Store resulting time series of discharge and sediment loads (Deliverable 4A-1: macro-scale morphology)

2. Assess future climate projections

    a. Derive representative scenarios (precipitation, temperature) from the GCMs (current report)

    b. Apply resulting time series as input in the Hydrotrend model (Deliverable 4A-1: macro-scale morphology)

    c. Store resulting time series of discharge and sediment loads (Deliverable 4A-1: macro-scale morphology)

3. Derive future projections of discharge and sediment loads

    a. Derive the percentage change in discharge and sediment by comparing 1c) with 2c)

    b. Superimpose results on historic discharge records and estimated historic sediment loads

Note that regarding river discharges and sediment loads, the current report will only focus on steps 1a and 2a. The results of the other steps of the procedure will be discussed as part of Component-4A (Macro-scale morphology).

In the current report we will quantify various statistical characteristics of precipitation and temperature and which may be relevant for different purposes. For example:

- Extreme rainfall events in Bangladesh are relevant for polder design as flood impacts of these events should be minimized as much as possible. For the polders selected for further analysis

under Component 5.A (i.e. 15, 29, 40/1 & 40/2, 59/2, 64/1a & 64/1b), we therefore need to quantify projected changes in daily rainfall extremes.

- Annual sediment loads in the delta are related to precipitation totals in the GBM basin. Especially the precipitation volumes in the monsoon season are relevant in this respect. We therefore need to assess potential changes in annual and monsoon total precipitation in the GBM basin.

- Prolonged drought periods pose a serious threat for agricultural productivity. We therefore need to assess potential changes in precipitation in the dry season of the GBM basin.

Further details on the statistical tests and indicators used to analyse the rainfall and temperature data is provided in Appendix A, B and C.

2.2   Sea level rise

Changes in sea level, determined from changes to the volume of the global ocean over time, are generally referred as **eustatic (or absolute) sea level rise** (see for example Syvitski et al., 2009). However, for most applications within this project (e.g. morphological changes at the different scale, polder drainage, etc.), the most relevant parameter is the **relative sea level rise,** defined as the local changes of the sea level compared to a land reference system (i.e. therefore including processes such as, for example, land subsidence).

To assess relative changes in sea level the following approach was used:

- We first analyse past trends of absolute (ASLR) and relative sea level rise (RSLR) and subsidence based on most recent literature. Note that subsidence will be further analysed based on new data collected under this project as part of Component 4B.

- Then we retrieve regional projection of ASLR based on different future projections and until the end of the century. For our analysis, we will use four coastal regions as basis as done, for example, in the Bangladesh Delta Plan (GED, 2018)[1].

- Additionally, we provide future subsidence values available at the same regions, and which can be used to obtain RSLR values.

As different projections are expected to provide very different values, finally we will provide a suggestion of plausible values for further use in the project.

2.3   Cyclone frequency and intensity

Possible changes in cyclone frequency and intensity will be analysed as follow:

- We will first look into possible trends based on past data;

- We will then analysis and compare different future projections;

- Finally, we will give suggestion of plausible values for further use in the project based on the analysis of past and future trends.

---

[1] The four coastal regions are: South West (Sundarbans), South Central (Ganges tidal flats), South East (Ganges Meghna Flats), Easter Hill (Chittagong Coastal Plain)

3　Data

3.1　Introduction

Climate data consist of time series. There are three types of time series relevant here:

[1]　Observed data from gauging stations (section 3.2);

[2]　Re-analysis data: estimates of historic time series by a combination of combination of models and observations (section 3.3);

[3]　Projected future scenarios from climate models (section 3.3);

We will use [1] and [2] to characterise the current ('reference') climate conditions, whereas [3] will be used to characterise projections of future conditions. We will compare results from [2] and [3] to assess relative changes in climate conditions.

3.2　Measured data

3.2.1　Rainfall

Time series of 32 rainfall stations collected by the Bangladesh Meteorological Department (BMD) were available to the project, see Figure 3.1 and Table 3-1. Figure 3.2 shows the data availability for these stations; gaps in the lines represent missing data. It shows there is substantial variation in data availability for the various stations. Years with more than 5% missing data were excluded from the analysis.

Figure 3.3 shows the annual average rainfall as derived from this data set. For verification purposes, a comparison is made with an annual average rainfall map from Shahid et al (2011). It shows these results are in very good accordance. This seems logical as the same data is likely to be the basis of both figures, but nevertheless a useful verification/validation for both studies.
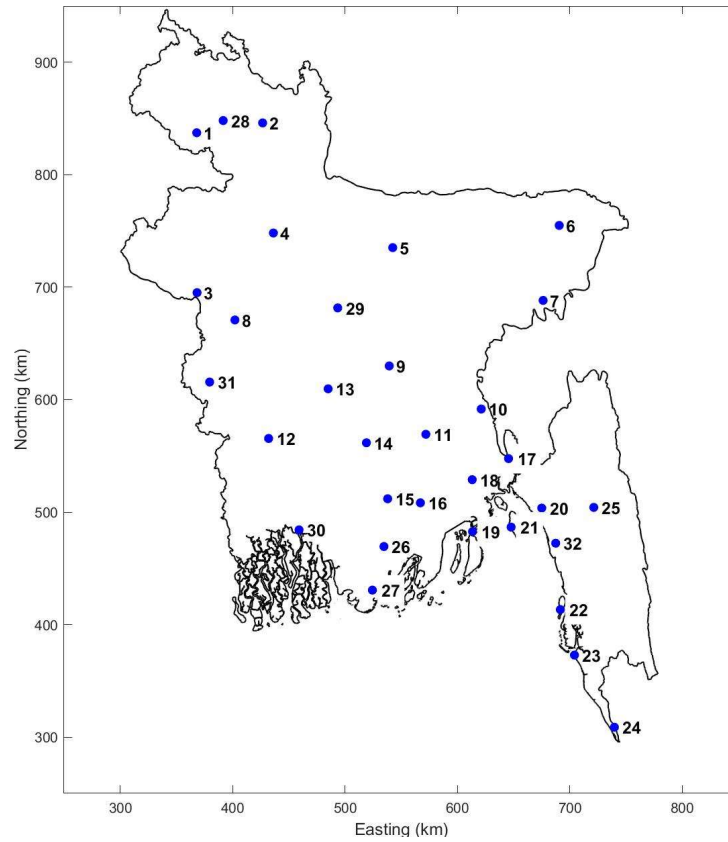
Figure 3.1   Rainfall stations (32 in total) for which data was available to this project.

Table 3-1   Names and coordinates of the 32 rainfall stations of Figure 3.1.

no	station	Lat	lon		no	station	lat	lon
1	Dinajpur	25.65	88.68		17	Feni	23.03	91.42
2	Rangpur	25.73	89.27		18	Maijdee Court	22.87	91.10
3	Rajshahi	24.37	88.70		19	Hatiya	22.45	91.10
4	Bogra	24.85	89.37		20	Sitakunda	22.63	91.70
5	Mymensingh	24.73	90.42		21	Sandwip	22.48	91.43
6	Sylhet	24.90	91.88		22	Kutubdia	21.82	91.85
7	Srimangal	24.30	91.73		23	Coxs Bazar	21.45	91.97
8	Ishwardi	24.15	89.03		24	Teknaf	20.87	92.30
9	Dhaka	23.78	90.38		25	Rangamati	22.63	92.15
10	Comilla	23.43	91.18		26	Patuakhali	22.33	90.33
11	Chandpur	23.23	90.70		27	Khepupara	21.98	90.23
12	Jessore	23.20	89.33		28	Syedpur	25.75	88.92
13	Faridpur	23.60	89.85		29	Tangail	24.25	89.93
14	Madaripur	23.17	90.18		30	Mongla	22.47	89.60
15	Barisal	22.72	90.37		31	Chuadanga	23.65	88.82
16	Bhola	22.68	90.65		32	Chittagong (City)	22.35	91.82
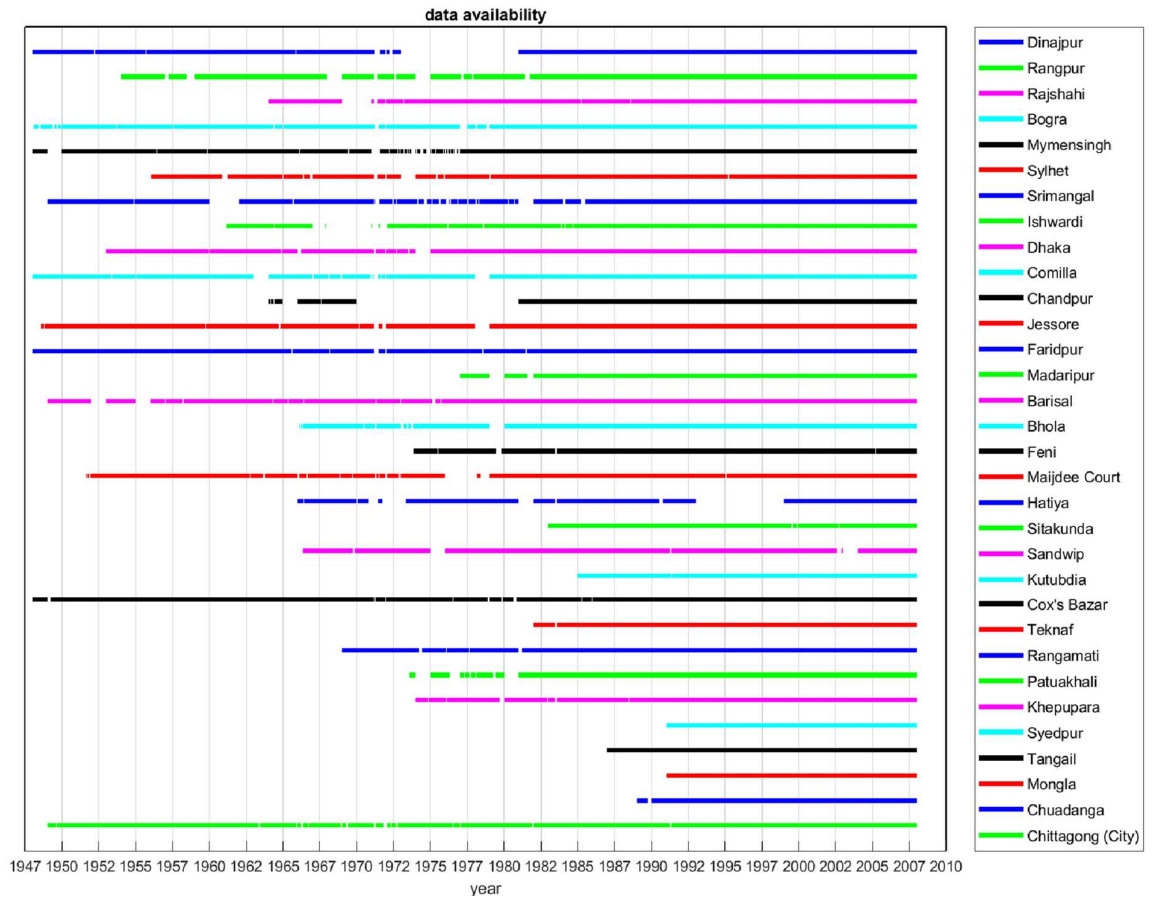
Figure 3.2   Data availability for the 32 rainfall stations. Gaps in the line indicate missing data.
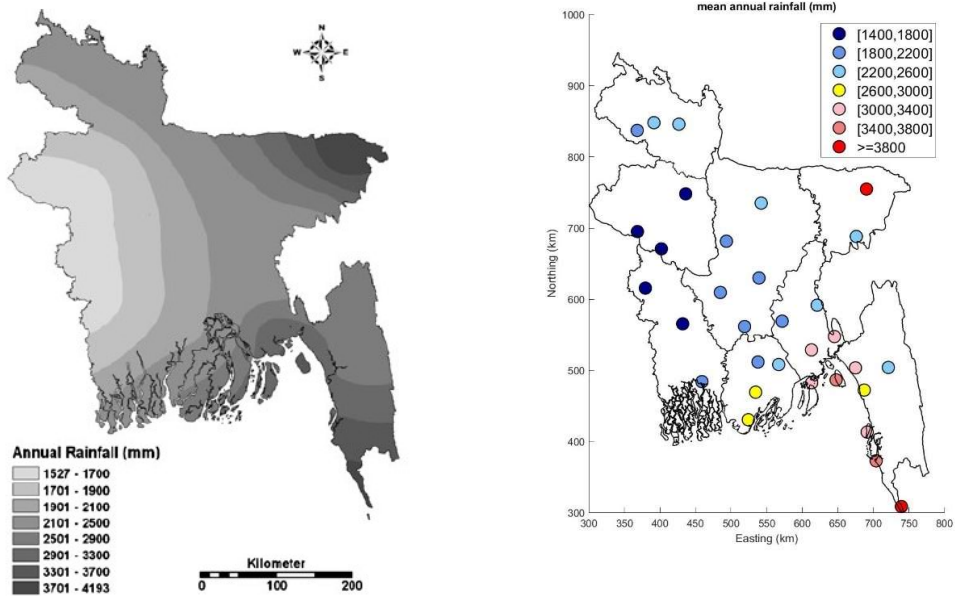
Figure 3.3   Annual average rainfall: comparison between results from Shahid et al [2011] (left) and this report (right).

3.2.2 Temperature

Time series of 34 temperature stations and collected by the Bangladesh Meteorological Department (BMD) were available to the project, see Figure 3.4. Figure 3.5 shows the data availability for these stations; gaps in the lines represent missing data. It shows there is substantial variation in data availability for the various stations. Years with more than 5% missing data were excluded from the analysis. Figure 3.6 shows derived annual average temperatures (right) and compares them with corresponding results from MOEF (2005) (left). Both figures show a clear temperature gradient from east to west. The values from MOEF (2005) are higher, though, this is most likely the difference between mean daily rainfall (our data) and daily maximum temperature (MOEF, 2005).
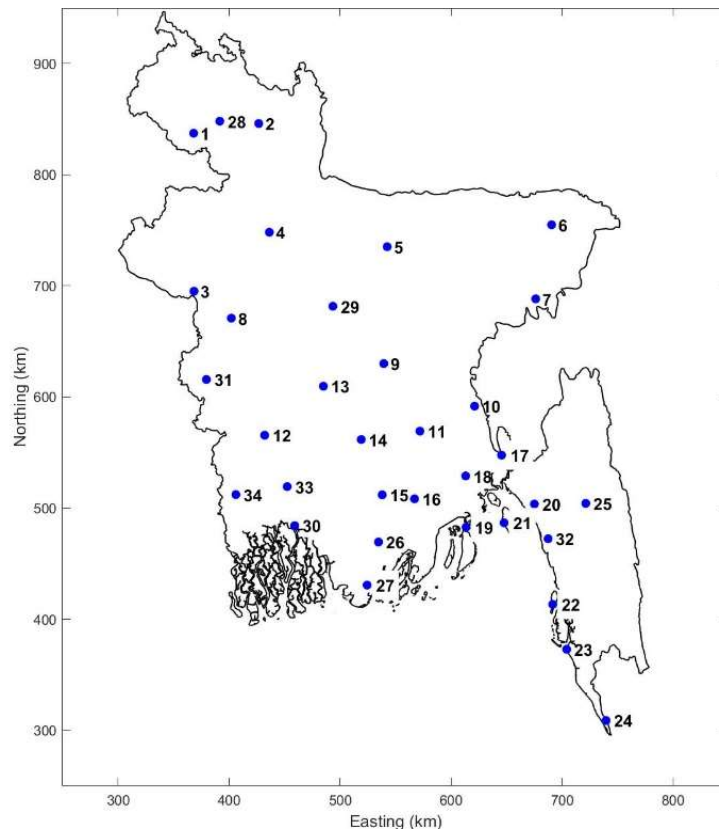
Figure 3.4   Temperature stations (34 in total) for which data was available to this project.

Table 3-2   Names and coordinates of the 34 rainfall stations of Figure 3.4.

no	station	Lat	lon		no	station	lat	lon
1	Dinajpur	25.65	88.68		18	Bhola	22.68	90.65
2	Rangpur	25.73	89.27		19	Feni	23.03	91.42
3	Rajshahi	24.37	88.70		20	Maijdee Court	22.87	91.10
4	Bogra	24.85	89.37		21	Hatiya	22.45	91.10
5	Mymensingh	24.73	90.42		22	Sitakunda	22.63	91.70
6	Sylhet	24.90	91.88		23	Sandwip	22.48	91.43
7	Srimangal	24.30	91.73		24	Kutubdia	21.82	91.85
8	Ishwardi	24.15	89.03		25	Coxs Bazar	21.45	91.97
9	Dhaka	23.78	90.38		26	Teknaf	20.87	92.30
10	Comilla	23.43	91.18		27	Rangamati	22.63	92.15
11	Chandpur	23.23	90.70		28	Patuakhali	22.33	90.33

no	station	Lat	lon		no	station	lat	lon
12	Jessore	23.20	89.33		29	Khepupara	21.98	90.23
13	Faridpur	23.60	89.85		30	Syedpur	25.75	88.92
14	Madaripur	23.17	90.18		31	Tangail	24.25	89.93
15	Khulna	22.78	89.53		32	Mongla	22.47	89.60
16	Satkhira	22.72	89.08		33	Chuadanga	23.65	88.82
17	Barisal	22.72	90.37		34	Chittagong (City)	22.35	91.82
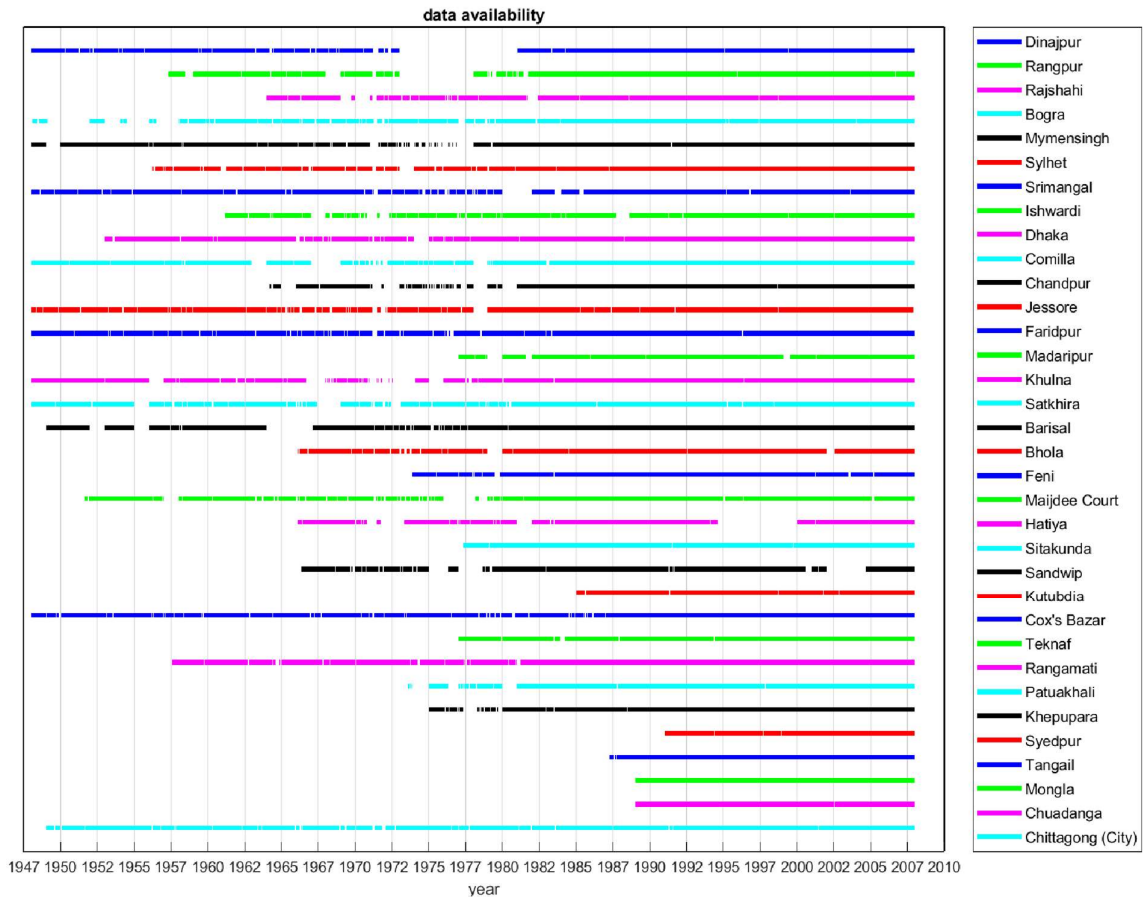
Figure 3.5   Data availability for the 34 temperature stations. Gaps in the lines indicate missing data.
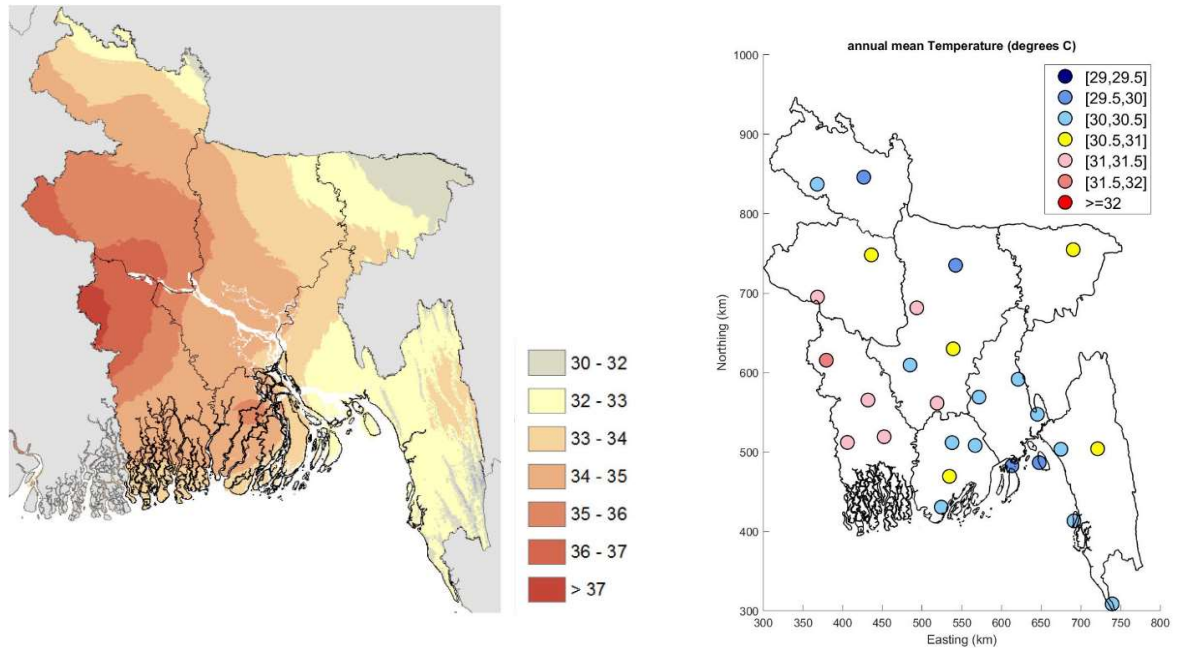
Figure 3.6   Annual average temperature: comparison between MOEF [2005] (left) and the results from our analyses (right).

3.2.3   Sea level rise

The GBM delta is considered one of the most vulnerable deltas in the world to the effects of sea level rise and subsidence. RSLR data from literature were analysed. This included analysis of the following data sources:

- Syvitski et al (2009), including analysis of high-resolution satellite images at 33 representative deltas;

- SMRC (2003), which used 22 years historical tidal data at three coastal stations (Hiron Point, CharChanga, and Cox's Bazar);

- Becker et al. (2020), who based the analysis on 101 water level gauges across the delta, and which were also available to the project. The same authors made also use of satellite altimetric data from the ESA Sea Level Climate Change Initiative (v1.1) over the period 1993 to 2012 to estimate past ASLR and maximum subsidence rates over the region.

The results are further discussed in Section 4.2.3.

3.2.4   Cyclone frequency and intensity

Bangladesh is a global hotspot for tropical cyclones (TC) and its adverse impacts on society (Dasgupta et al., 2016). Between 1960-2004 more than half a million inhabitants of Bangladesh died as a consequence of TCs, primarily due to storm surge (Schultz et al., 2005). For example, the 1991 Bangladesh cyclone (BOB 01) caused about US$1.7 billion (1991 USD) in damage.

TCs generate in the Bay of Bengal, propagate northwards and make landfall in Bangladesh following a southwest / northeast direction. Once on land, the intensity of the TC decreases due to lack of warm water supplying energy to the TC and increase in land roughness. Generation occurs both during the

early summer time period (April, May, June, July) as in the late rainy season period (September, October, November, December; see for more information Dasgupta et al., 2016).

In this study, information on TC events derived from the IBTrACS database (Knapp et al., 2010; Knapp et al. 2018) and specifically from the subset by the Joint Typhoon Warning Center (JTWC) were used as a basis to assess possible historical changes in TC frequency and intensity. In particular, the most recent data starting from 1972 based on satellite detection, provides more accurate information on both historical tracks and cyclone intensity for the North Indian Ocean (see e.g. Singh (2010)). This information is used in combination with future projections (Section 3.3.3) to derive reliable projections (Chapter 4).

3.3 Modelled data (future scenarios)

3.3.1 Rainfall and temperature

To assess changes in rainfall and temperature in Bangladesh and the GBM basin, the downscaled climate datasets from the 5th Assessment report of the Intergovernmental Panel on Climate Change (IPCC-AR5) have been used. More specifically, we used the precipitation and temperature datasets from General Circulation Models (GCMs) that were part of the international inter-sectoral impact model inter-comparison project (ISI-MIP; Warszawski et al., 2013). The ISI-MIP project (https://www.isimip.org/) developed future climate projections that were later used as input for the IPCC 5th assessment report.

The database contains bias-corrected GCM data existing of global daily grids with a resolution of 0.5 degrees for 5 GCMs:

- GFDL-ESM2M
- HadGEM2
- IPSL-CM5A
- MIROC_ESM_CHEM
- NORESM-M

For the bias-correction of the ISI-MIP dataset, an advanced method was used (Hempel et al., 2013) that preserves the absolute changes in monthly temperature, and relative changes in monthly values of precipitation while correcting the daily variability around the monthly mean.

GCM data was obtained for the following three scenarios and periods:

- Reference scenario: period 1951-2005
- RCP4.5 emission scenario: period 2006-2099
- RCP8.5 emission scenario: period 2006-2099

The temporal resolution is one day (daily data). For each day in the period, we extracted precipitation and temperature data for a rectangular grid in which the GBM basin is embedded, see Figure 3.7. The spatial resolution of the grid is 0.5 degrees lat-lon, which is approximately equal to 50 km.

Precipitation (mm) on 01-09-2000; model: GFDL-ESM2M
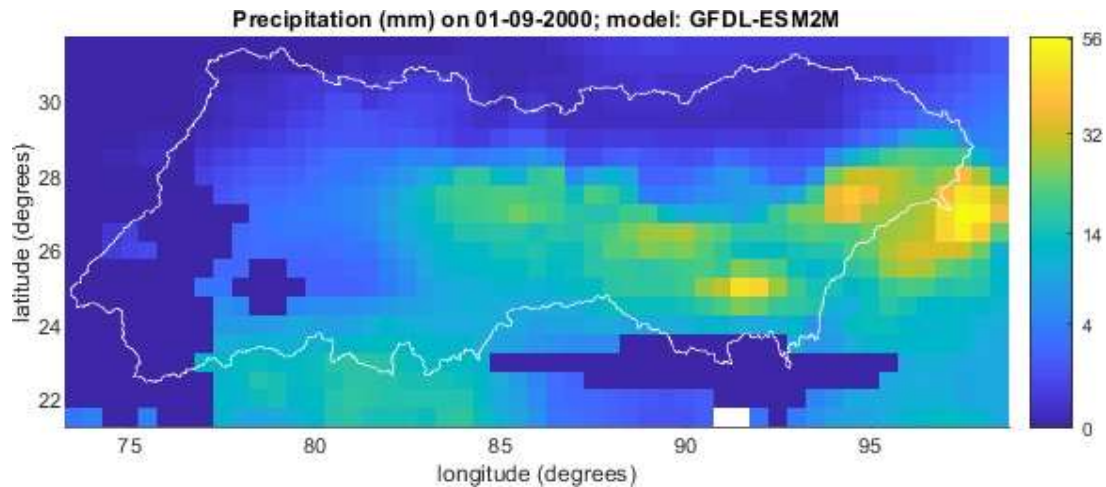
Figure 3.7   Example precipitation grid map, the white line shows the contours of the GBM basin.

The GCM data of the reference period (1951-2005) is the result of a run with the GCM models and historic radiation as forcing. Furthermore, a bias correction is applied afterwards to correct for differences with observations from gauging stations. Comparing GCM data from the reference period with GCM data of future periods will provide information on projected climate change characteristics. The projected changes will be superimposed on data from historic records, if available, as described in section 2.1.

3.3.2   Sea level rise

For future sea level rise projections, the IPCC SROCC regional projections for Bangladesh based on IPCC (2019) were used (Oppenheimer et al. 2019). This is the most recent and scientifically accepted published update of the IPCC AR5 report. In the report, the upper bound of the likely range for a high emission scenario has been adjusted upwards. This is because more recent modelling suggests a larger contribution from the Antarctic Ice Sheet (medium confidence). In addition, we have added considerations based on recent literature concerning sea level rise scenarios for planning purposes and accounting for ice sheet contribution to future sea-level rise (see e.g. DeConto et al., 2016, Kopp et al., 2017, Bamber et al., 2019 and Haasnoot et al., 2020).

3.3.3   Cyclone frequency and intensity

As further described in Section 4.2.4, it is hard to define statistically significant trends on TC frequency/intensity only based on data. However, both available data and literature seem to suggest an increase in TC intensity and frequency for the most extreme cyclone events in the Bay of Bengal.

To further quantify possible future changes in cyclone frequency and intensity, regional projections available from literature were analysed and compared in Section 4.4.4.

4 Results

4.1 Introduction

In this chapter, results from the analysis are presented at different spatial scale, depending on the variable analysed:

- For the entire country;

- For the four morphological zones as defined for example in the Bangladesh Delta Plan (Figure 4.1);

- For the five selected polders (i.e. 15, 29, 40/1 & 40/2, 59/2, 64/1a & 64/1b) (Figure 4.2).
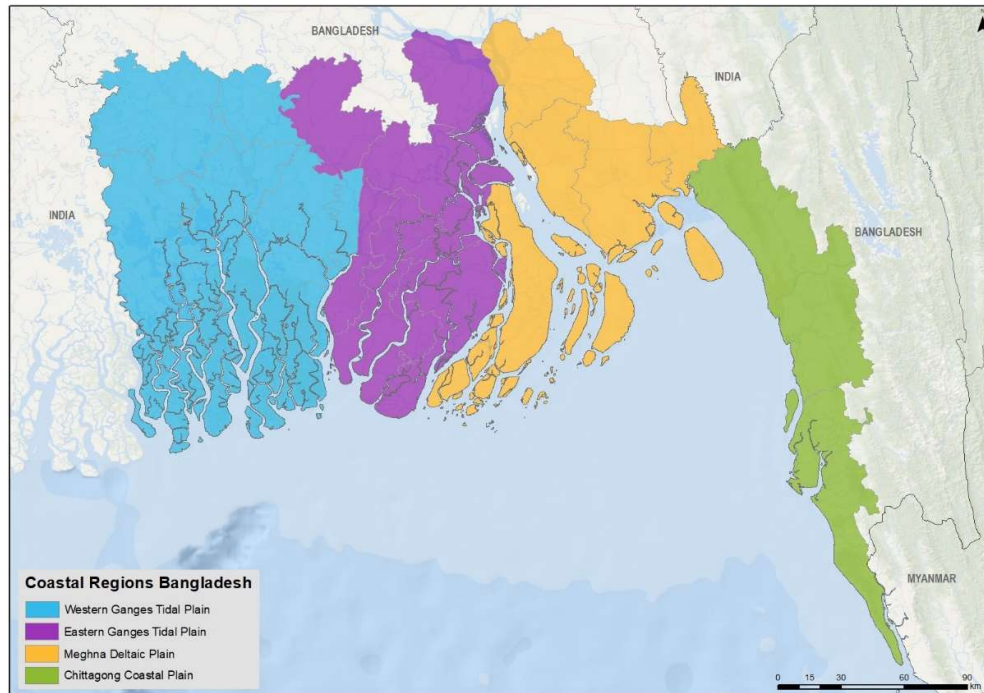
Figure 4.1   Morphological zones of the coastal area of Bangladesh as used in the Delta Plan (GED, 2018).
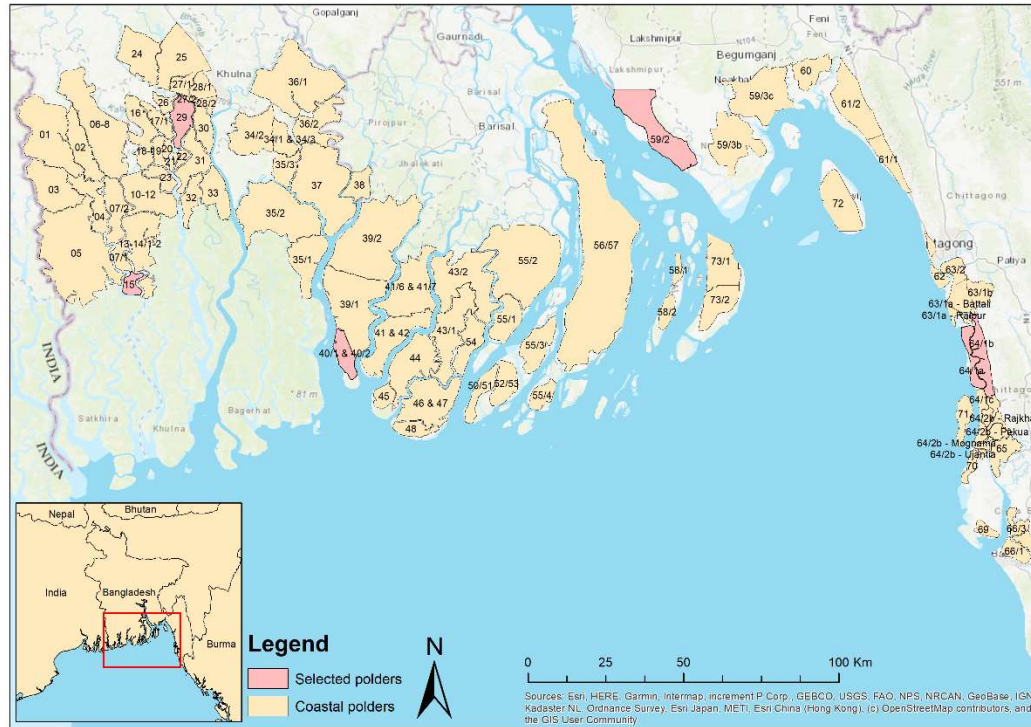
Figure 4.2   Map of the five selected polders.

4.2 Measured data (past trends)

4.2.1 Precipitation

For the purpose of spatial visualization of trends in precipitation and temperature, seven trend classes were defined. For each trend class, a colour code is used, ranging from dark blue (very likely decreasing trend) to dark red (very likely increasing trend; see Table 4-1),

Table 4-1   Definition of trend classes.

Colour code	Description
	Very likely decreasing trend
	Likely decreasing trend
	Possible decreasing trend
	No trend
	Possible increasing trend
	Likely increasing trend
	Very likely increasing trend

Figure 4.3 shows derived trend classes based on the measured data presented in Section 3.2.1 for the annual total (sum) rainfall, using the Mann-Kendall statistical test (right subplot). The results are compared to the results of Shahid (2009) (left plot). It shows no major trends over Bangladesh as both darkest red (indicating an increase) to darkest blue colours (indicating a decrease) are observed. Overall, there are more locations with an increasing trend than locations with a decreasing trend. In

particular, in the northwest and along the coastline there are several locations with an increasing trend.
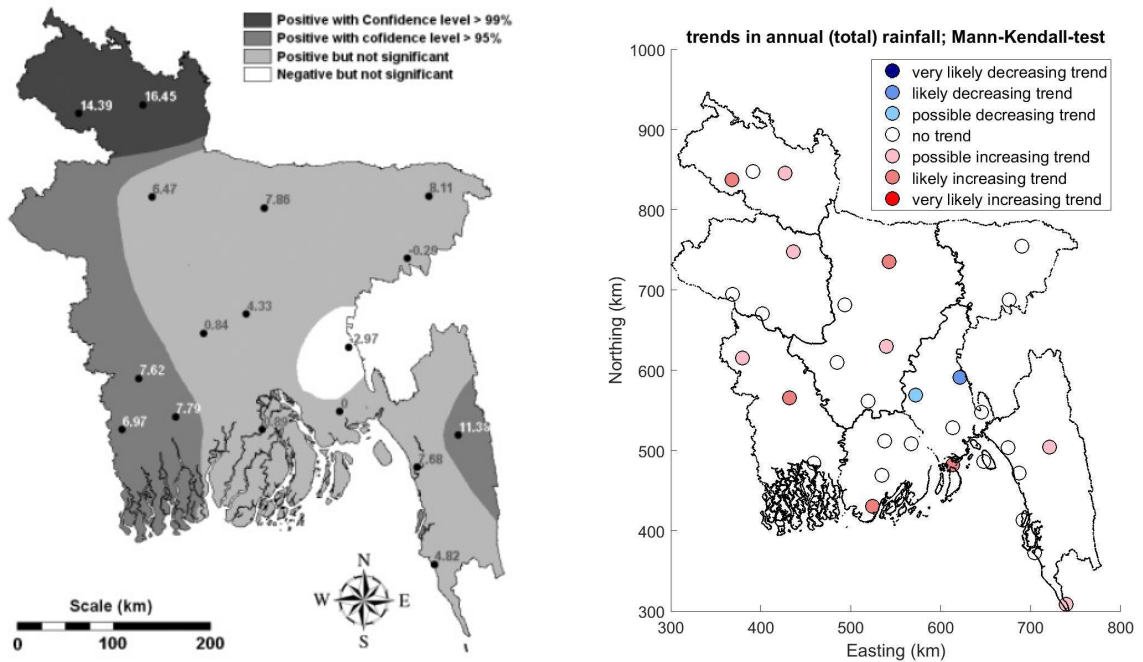
Figure 4.3   Trends in annual total rainfall: comparison between the results from Shahid (2010) (left) and this report (right). The numbers in the left plot show the magnitude of rainfall change in millimeter per year during the time period 1958–2007.

Appendix B shows similar plots for other statistical tests, the various seasons and the annual daily maximum rainfall. No analyses were done for the annual minimum daily rainfall because that value is always equal to 0. The trend classes for the annual total rainfall as derived with the other three statistical tests are very similar to the one shown for the Mann-Kendall test in Figure 4.3; as such confirming the seemingly apparent increasing trend in the Northwest and along the coastline.

The figures for the *monsoon* season in Appendix B are different to the ones for the annual total rainfall. There are less locations with an increasing trend in the monsoon season compared to the number of locations with an increasing trend in the whole year. For the monsoon season, the number of locations with an increasing trend is similar to the number of locations with a decreasing trend. The stations that do have an increasing trend are (again) mainly in the northwest and along the coast. The *pre-monsoon* season shows increasing trends mainly for the locations along the north-west to south-east diagonal. The *post-monsoon* season shows similar spatial patterns as the monsoon season, albeit with somewhat "weaker" trends. In the *winter* season there are more stations with a *decreasing* trend than stations with an increasing trend suggesting a trend towards dryer winters. As such, the winter trend pattern deviates from the trend pattern in the other seasons.

The figures for the annual (or seasonal) maximum daily rainfall are fairly similar to those of the annual (seasonal) totals. The main difference is that the number of locations with an increasing trend is slightly smaller for most seasons compared to the total rainfall sum.

Table 4-2 shows the resulting trend classes when all 32 stations are combined with the method as described in Appendix A. Several tests indicate that the winter season has an overall negative trend, whereas the post-monsoon season and the whole year have an increasing trend.

Table 4-2   Derived trend classes for rainfall for the combination of all stations. Results are shown for two indicators, four statistical tests, and five different seasons (including the whole year). Refer to Table 4-1 for a description of the colour codes. The four statistical tests are: Pearson (PS), Mann-Kendal (MK), Spearman rank test (SM) and Wilcoxon-Mann-Whitney (WMW), see appendix A-2.

Indicator:	Total rainfall (sum)				Maximum daily rainfall			
test:	PS	MK	SM	WMW	PS	MK	SM	WMW
Year	[red]		[red]					
Pre-monsoon								
Monsoon					[red]			
Post-monsoon	[red]		[red]			[red]		
Winter		[blue]	[blue]		[blue]	[blue]	[dark blue]	

Besides the likelihood of a (potential) trend, it is also relevant to quantify the magnitude of the trend. There is a relation between the likelihood and magnitude, but this relation is not 100% deterministic. The left plot of Figure 4.4 shows the decadal change in rainfall based on a linear trend analysis. So, for example, a value of 100 mm means on average the annual rainfall increases 100 mm in a period of 10 years (so 10 mm/year). And, similarly, a value of -50 means on average the annual rainfall decreases 50 mm in a period of 10 years (so 5 mm/year).

The pattern of the left plot of Figure 4.4 is similar to the pattern of the right plot of Figure 4.3; with generally larger increases in the western part of the country. However, there are also some striking differences. For example, the dark blue dot in the left plot of Figure 4.4 indicates a substantial negative trend at location Sitakunda, whereas the right plot of Figure 4.3 indicates there is no significant trend at that location. This has to do with the fact that the annual average rainfall at Sitakunda is relatively high. This means a substantial decrease in absolute sense may be moderate in relative sense.

Therefore, an additional plot (right plot of Figure 4.4) was produced that shows relative changes (decadal change as a percentage of the annual mean rainfall). The pattern of this plot is (even) more similar to the right plot of Figure 4.3. The main difference is noted at location Syedpur in the northwest, which has a dark red colour in Figure 4.4 (indicating a major increasing trend) whereas it has a white colour in Figure 4.3, indicating that no likely trend was detected. This has to do with the fact that the time series of this location is relatively short, only about 17 years. The observed trend is more than 15 mm/year, but the time is too short to qualify this as statistically significant.
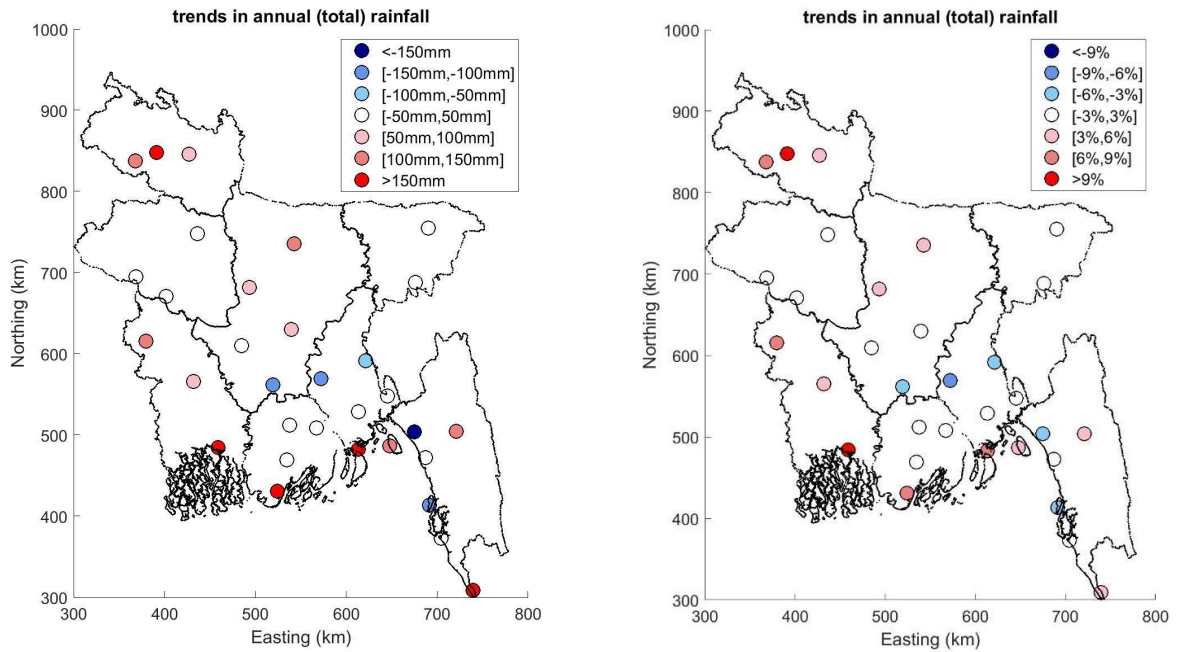
Figure 4.4   Decadal change in rainfall based on a linear trend analysis. The left plot shows absolute values (mm/decade), the right plot shows the same numbers as a percentage of the annual average rainfall.

4.2.2 Temperature

Figure 4.5 shows the trend classes for the annual mean temperature, as derived with the Mann-Kendall test. Nearly all locations have an increasing trend, about half even have a very likely increasing trend. In the Northwest there are a few locations with a decreasing trend. But generally, the trend is increasing, therefore suggesting a clear variation towards warmer conditions.

Appendix C shows similar plots for other statistical tests and the various seasons. The trend classes for the annual mean temperature for the other three statistical tests are very similar to the one shown for the Mann-Kendall test in Figure 4.5, as such confirming the seemingly apparent increasing trend in the Northwest and along the coastline. The increase in mean temperature is mainly happening in the monsoon and post-monsoon season. In these seasons, almost all stations have an increasing trend and no stations have a decreasing trend. In the winter and pre-monsoon season the results are more mixed. In these two seasons, the stations in the south have an increasing trend, while the stations in the north have a decreasing trend.

Table 4-3 shows the resulting trend classes when all 34 stations are combined with the method as described in Appendix A. This shows significant overall increasing trends in mean temperature are observed in the monsoon and post-monsoon season and, consequently, also increasing trends in the annual mean temperature. The winter season has negative trends for maximum and minimum temperatures, but not for mean temperatures.

trends in annual (mean) temperature; Mann-Kendall-test

Legend:
- very likely decreasing trend
- likely decreasing trend
- possible decreasing trend
- no trend
- possible increasing trend
- likely increasing trend
- very likely increasing trend
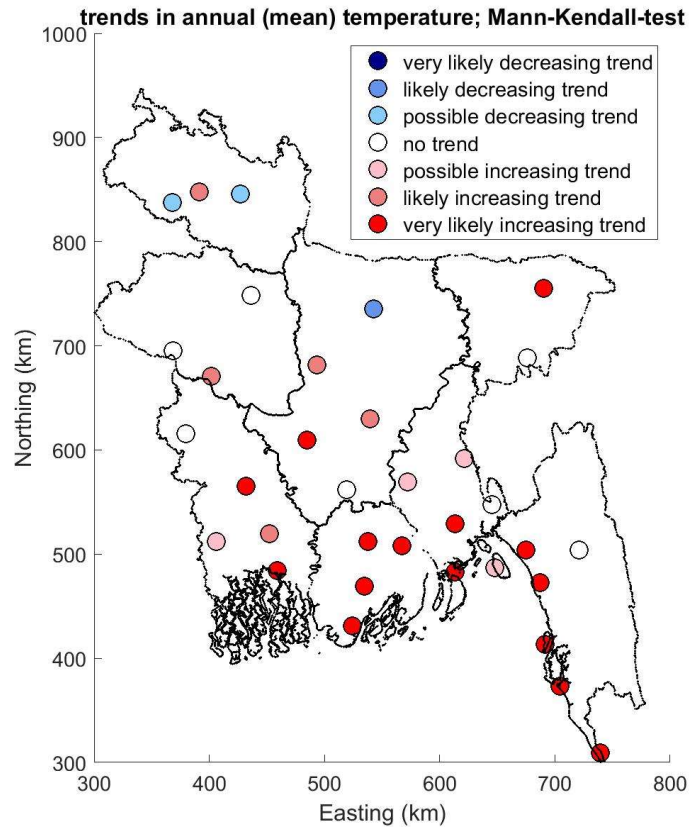
Figure 4.5   Trends in annual mean temperature; Mann-Kendal test.

Table 4-3   Derived trend classes for temperature for a combination of all stations. Results are shown for three indicators, four statistical tests and five different seasons (including the whole year). Refer to Table 4-1 for a description of the classes and colour codes.

Indicator:	Mean temperature				Maximum daily temperature				Minimum daily temperature			
test:	PS	MK	SM	WMW	PS	MK	SM	WMW	PS	MK	SM	WMW
Year												
Pre-monsoon												
Monsoon												
Post-monsoon												
Winter												

Figure 4.6 shows the magnitude of the temperature trend (in degrees Celsius per decade). The spatial pattern is similar to the pattern of Figure 4.5. It shows that most stations have a positive trend.

19

trends in annual (mean) temperature

Legend:
- $< -0.3\,^{\circ}C$
- $[-0.3\,^{\circ}C, -0.2\,^{\circ}C]$
- $[-0.2\,^{\circ}C, -0.1\,^{\circ}C]$
- $[-0.1\,^{\circ}C, 0.1\,^{\circ}C]$
- $[0.1\,^{\circ}C, 0.2\,^{\circ}C]$
- $[0.2\,^{\circ}C, 0.3\,^{\circ}C]$
- $> 0.3\,^{\circ}C$
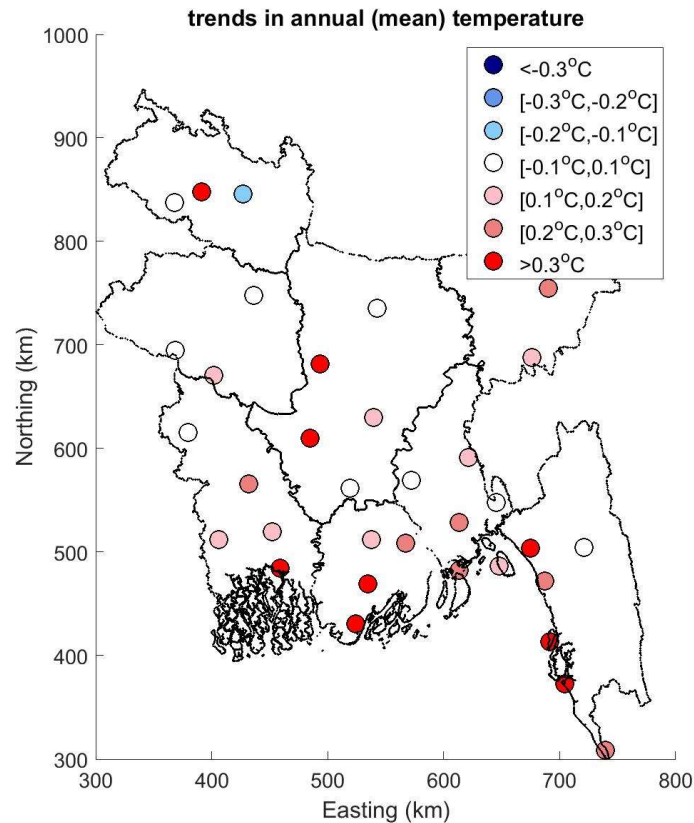
Figure 4.6   Decadal change in temperature based on a linear trend analysis (degrees Celsius/decade).

4.2.3 Sea level rise

Syvitski et al (2009) estimated the RSLR rate by means of high-resolution satellite images at 33 representatives deltas. For the Bangladesh coastal zone, the RSLR (i.e. including subsidence) was estimated between 8-18 mm/year. Similar conclusions can be retrieved from the study by the SAARC Meteorological Research Council (SMRC, 2003), which carried out a study on RSLR at the Bangladesh coast. The study used 22 years historical tidal data at three coastal stations. The study showed that the RSLR rate along the Bangladesh coast is several times higher than the mean global rate; in particular, 4 mm/year at Hiron Point, 6 mm/year at CharChanga and 7 mm/year at Cox's Bazar.

Becker et al. (2020) reconstructed the RSLR changes over 1968 to 2012, using 101 water level gauges across the delta, which were also available to the project. Although uncertainties are large, the study showed that during the 1968 to 2012 period, the average RSLR at the different coastal regions (Section 4.1) has increased slightly faster ($\approx$ 3 mm/y) than absolute global mean sea level ($\approx$ 2 mm/y). However, estimates are largely lower than local relative sea-level rise trends reported earlier (between 6 and 21 mm/y over $\approx$ 30y; see e.g. FFWC (2012), CCC (2012), Singh (2002), Sarwar (2013), Higgins et al. (2018), Steckler et al. (2010). Interannual fluctuations are strongly modulated by the El Niño Southern Oscillation (ENSO) and the Indian Ocean Dipole (IOD) variability.

Based on Becker et al. (2020), an overview of estimated RSLR for the different coastal regions (Figure 4.1) is reported in Table 4-4. The values estimated indicate relatively minor differences across the first three regions (i.e. Western Ganges Tidal Plain, Eastern Ganges Tidal Plain, Meghna Deltaic Plain), which are within the uncertainty band. The region with the lowest RSLR is the Chittagong Coastal Plain, however statistical trends are not significant for this region.

ASLR rates were also estimated by Becker et al (2020) based on satellite altimeter datasets over 1993 to 2012 (Table 4-4). Surprisingly, reported estimated values of ASLR are on the same range as reported RSLR. However, the two datasets have been derived based on completely different datasets and periods and therefore should not be compared directly due to interannual and decadal sea level variability (see e.g. Figure 3 from Becker et al., 2021). Maximum subsidence rates within the region, estimated as local differences between RSLR and ASLR over 1993 to 2012, can be considerable and up to 7 mm/y (Table 4-4). These values were estimated based on a Monte Carlo resampling on this difference and taking the 10% lower bound obtained from the resampling. No value was reported for Chittagong Coastal Plain area in view of the large differences with the rest of the delta and enhanced tectonic activity in this region, as discussed in Becker et al. (2020).

Subsidence rates in the coastal region are also being analysed based on new data collected under this project as part of Component 4B. Preliminary results suggest maximum subsidence rates up to ≈ 15 mm/year in areas of active sedimentation (Steckler et al., 2021). Values expected for buildings and embankments are lower, up to ≈ 8 mm/y. Different values are observed depending on the methodology used to measure subsidence and whether the device measures very shallow subsidence in the upper few meters (e.g., RSET-MH instruments) or only from deeper layers (e.g., river gauges and GNSS mounted on buildings). This may also explain why reported values by Becker et al. (2020) and based on water level gauges (i.e., therefore not recoding shallow subsidence) are lower than the preliminary values obtained as part of this project. In addition, local differences in subsidence rates are also expected depending on local conditions.

As also discussed in Becker et al (2020), local subsidence is expected to largely enhance the effect of ASLR locally (Section 4.4.3).

Table 4-4   Relative sea level rise estimated based on water level gauges for the period 1968-2012, absolute sea level rise estimated based on satellite altimetry data for the period 1993-2012 and expected max subsidence for the period 1993-2012. The P-values in brackets provide an indication of how statistically significant trends are (see Appendix A) (adapted from Becker et al., 2020).

Region	Relative sea level rise 1968-2012 (mm/y)	Absolute sea level rise 1993-2012 (mm/y)	Expected max subsidence 1993-2012 (mm/y)
Western Ganges Tidal Plain	2.7 ± 1.3 (P≤0.001)	2.1 ± 1.4 (P≤0.1)	2.4
Eastern Ganges Tidal Plain	3.6 ± 1.8 (P≤0.001)	3.2 ± 1.6 (P≤0.001)	7.0
Meghna Deltaic Plain	3.0 ± 2.6 (P≤0.1)	3.4 ± 1.6 (P≤0.001)	5.2
Chittagong Coastal Plain	1.3 ± 1.4	3.4 ± 1.7 (P≤0.001)	-

4.2.4   Cyclone frequency and intensity

Information on TC events derived from the IBTrACS database (Knapp et al., 2010; Knapp et al. 2018) and specifically from the subset by the Joint Typhoon Warning Center (JTWC) were used as a basis to assess possible historical changes in TC frequency and intensity (Section 3.2.4). The historic TC tracks are plotted in Figure 4.7. At first, we have analysed the probability of TC genesis (Figure 4.8a) and termination (Figure 4.8b). The probability is, in this case, estimated as number of events within a 200 km radius and divided by the total number of events. Figure 4.8a shows that most TC are generated in the middle of the Bay of Bengal (BoB), west of the Andaman and Nicobar Islands. Once generated, the TCs propagate through the BoB and they make landfall in eastern India, with a hotspot in Andhra Pradesh and in Bangladesh, with a hotspot in the South East region and Eastern Hill (Figure 4.8b). This is consistent with the finding of the literature study presented in Alam and Dominey-Howes (2015).
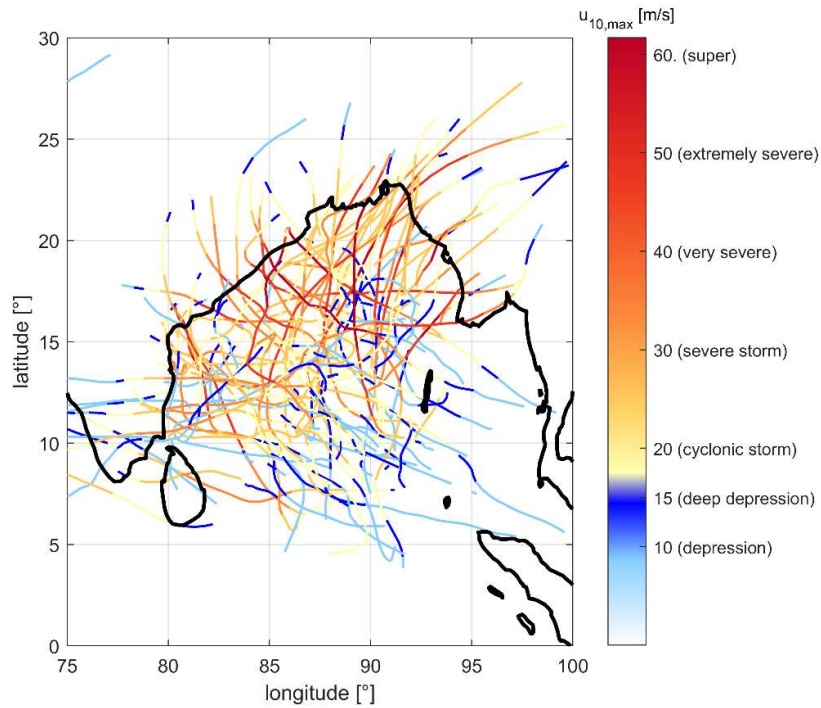
Figure 4.7   Historical TC tracks since 1972 as reported in the JTWC database. Indication of the wind speed and severity is provided according to the classification by the India Meteorological Department (IMD) for the North Indian Ocean.

(a)

(b)
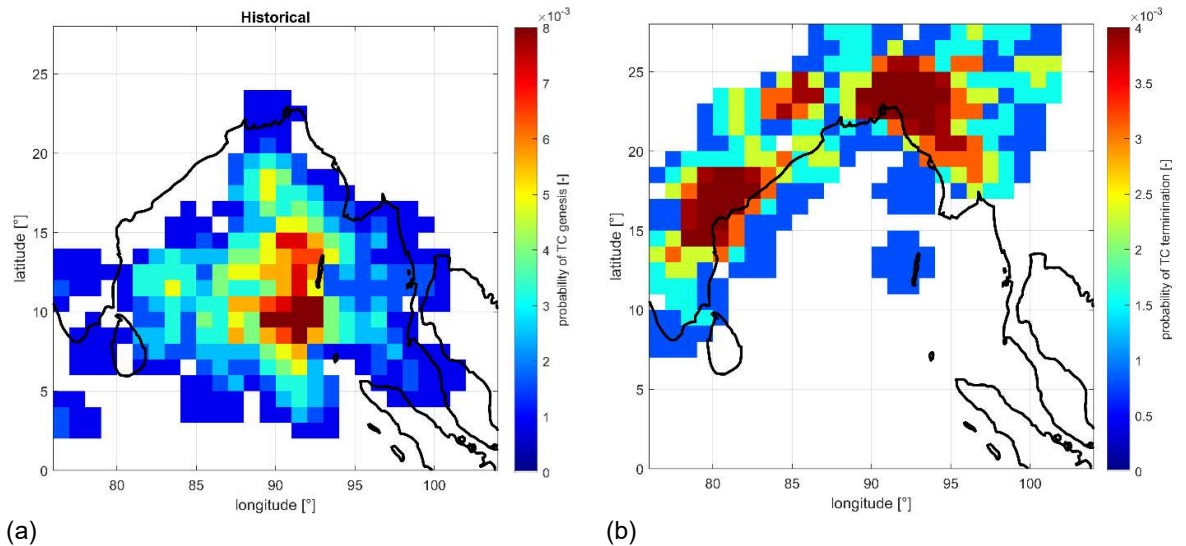
Figure 4.8   Probabilities of genesis (a) and termination (b) for historical TC since 1972. Data retrieved from the JTWC database.

Based on the historical tracks, the yearly probability of TC activity was also determined per grid cell (Figure 4.9). In this case, the probability was estimated by adding the number of TCs within a 200 km radius and dividing by the number of years of observation. The figure shows how, in general, the yearly probability is below one, meaning that it is unlikely that a cell is hit by a cyclone more than once

per year. In fact, the value is approximately once in three years in the region of Bangladesh (value of ≈ 0.3).
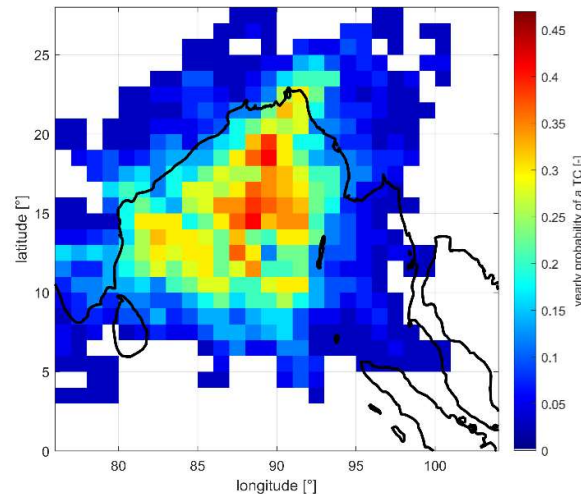
Figure 4.9   Yearly probability of historical TC since 1972. Data retrieved from the JTWC database.

Following the same methodology, the probability of TC generation per month was also plotted in Figure 4.10. The Figure shows how TCs are mostly generated in the pre-monsoon period (May) and post-monsoon period (November), which is consistent with literature (see e.g. Alam et al. (2003), Islam et al. (2009), Dasgupta et al. (2016) and Bhatla et al. (2019)).
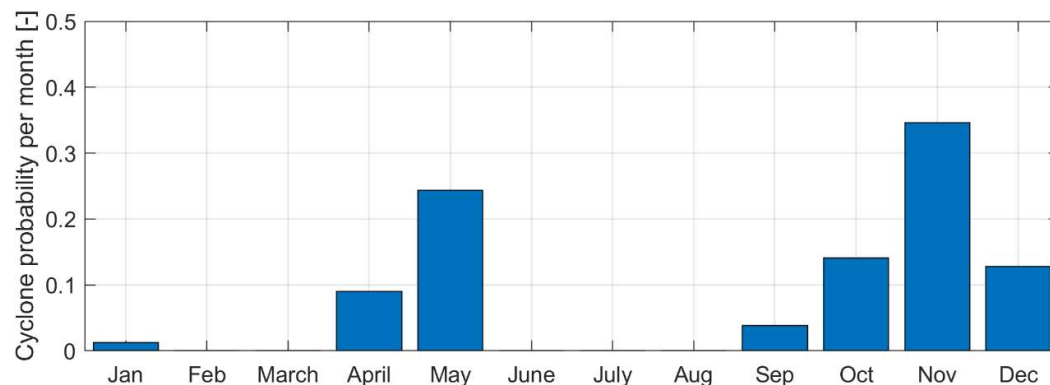
Figure 4.10   Monthly probability of TC generation in the Bay of Bengal based on historical cyclones since 1972. Data retrieved from the JTWC database.

Based on the information from the historical TC from 1972, possible changes in frequency were analysed for the entire Indian Ocean (Figure 4.11a), the Bay of Bengal (Figure 4.11.b) and the Bangladesh coastal zone only (Figure 4.11c). The three regions are visualized in Figure 4.12. Different colours in Figure 4.11 indicate the TC occurrence when taking into account all cyclone events (blue bars) and most extreme TC only (orange bars), characterized by a maximum wind speed larger than 40 m/s. Trend lines have also been added to depict possible trends for both cases. It is important to stress that it is hard to define actual trend lines due to the very limited number of years of observations. For example, these trend lines are very sensitive to one additional year characterized by a larger or lower number of TC. The significance of these trends has been quantified by computing a *p*-value, following three different statistical tests (Pearson t-test, Mann-Kendall test, Wilcoxon-Mann-Whitney test) as described in Appendix A (Table 4-5).

Figure 4.11a suggests that the number of cyclone events and most extreme cyclone events has been slowly increasing through time during the last 5 decades in the North Indian Ocean. Very remarkable has been the year 2019, which was characterized by 6 TCs, all of them in the "severe" category. The increase has been roughly equal to +0.6% and +4.5% per year, respectively for all the TC events and the most extreme ones only. This finding is consistent for example with Singh et al. (2000) and Deo et al. (2011) that have shown an intensification of the most extreme TCs. All different statistical tests qualify the increasing trends in several cyclones as "possible trends".

When we focus on the Bay of Bengal only (Figure 4.11b), one can see that the number of TCs has been decreasing, however the number of most extreme TCs has been increasing through time. The estimated changes have been equal to -0.4% per year and +1.7% respectively for all the TC events and the most extreme ones only. Similar conclusions were reported for example by Webster et al. (2005) and in the Delta Plan (GED, 2018), indicating that the number of TC is decreasing but the intensity is increasing. A very recent review by Knutson et al. (2021) also reaches very similar conclusions: the number of very intense TCs has increased and it is projected to increase globally as a result of climate change. In contrary, the total number of TCs each year is projected to decrease or remain approximately the same.

Finally, Figure 4.11c focuses on the Bangladesh coastal zone only. The figure suggests that, if we focus on the Bangladesh coastal area only, it is difficult to draw firm conclusions on whether the number of events and intensity has decreased/increased over time. Therefore, we have decided not to add a trend line in this last figure.

The yearly number of TC is also dependent on additional multi-year processes such as El Niño-Southern Oscillation (ENSO) (Singh et al., 2000; Hoarau et al. 2012).
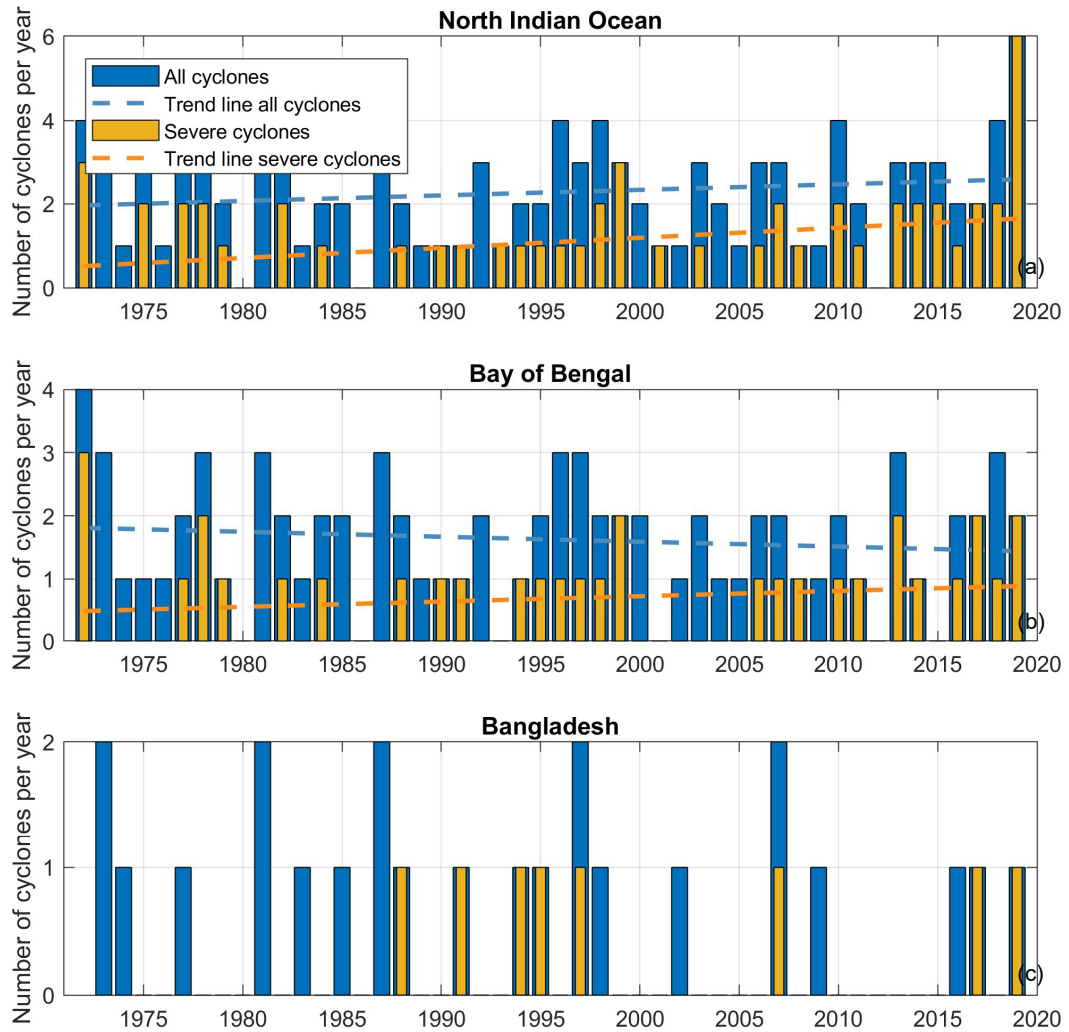
Figure 4.11   Number of cyclones per year since 1972 as retrieved from the JTWC database for: (a) the North Indian Ocean, (b) the Bay of Bengal and (c) the Bangladesh coastal zone. Plots are made for all cyclones (in blue) and only the severe cyclones (maximum wind speed larger than 40 m/s) (in orange). Linear trend lines have been added to show estimated changes in cyclone frequency over the time period.

Table 4-5   *p*-value derived according to different statistical tests, as defined in Section A.2, and for different regions, both including all cyclone events and only the most extreme ones. Cells with a pink colour indicate values characterized by a "possible slightly increasing trend" (*p*-value<0.2), while cells with a white colour "do not exhibit a significant trend".

Region	Test		
	PS	MK	WMW
North Indian Ocean (all cyclones)	0.32	0.51	0.17
North Indian Ocean (severe cyclones)	0.04	0.05	0.08
Bay of Bengal (all cyclones)	0.45	0.59	0.87
Bay of Bengal (severe cyclones)	0.29	0.11	0.23
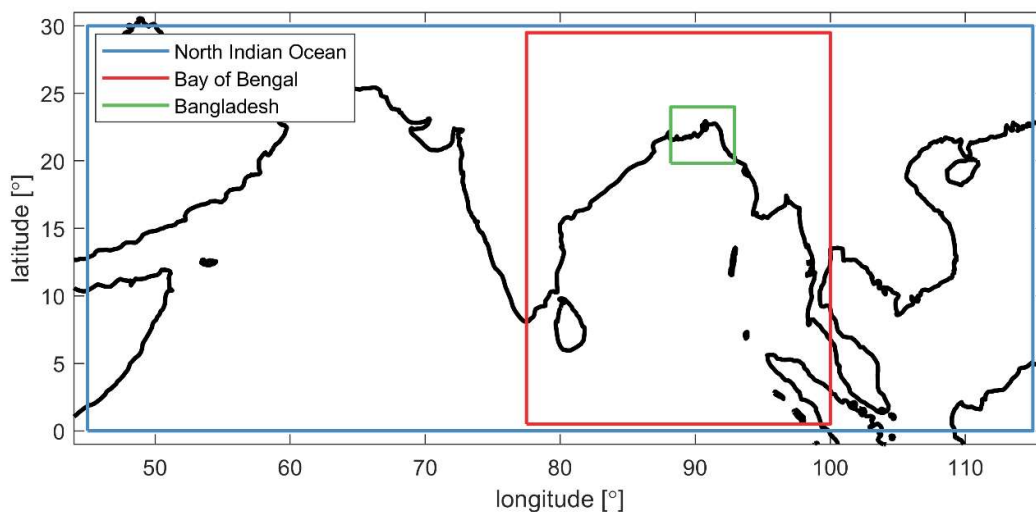
Figure 4.12   Boundaries of the three regions: North Indian Ocean, Bay of Bengal and Bangladesh.

4.3 GCM data of historical periods

The bias-corrected historical simulations from the GCMs will be used to establish a reference downscaled climate scenario. Future climate scenarios (section 4.4) will be compared with this reference scenario to establish relative changes in climate conditions. To ensure we are able to establish a reliable reference scenario, the historical GCM data is analysed and validated in this section, respectively for precipitation (Section 4.3.1) and temperature (Section 4.3.2).

4.3.1 Precipitation

4.3.1.1   GBM basin

First, we assessed precipitation data from the GCMs for the reference period (1976-2005). Figure 4.13 shows spatial plots of the mean annual precipitation. Each subplot represents one of the five

climate models. As can be seen, spatial patterns are very similar; in that respect the models are very consistent.

Figure 4.14 shows bar charts of mean precipitation over the entire GBM basin for four different seasons and for the entire year. Again, the climate models are very much in agreement with each other. This is most likely "enhanced" by the fact that the model results have been "bias-corrected" to be as much as possible in accordance with historical records. We also produced similar plots for smaller areas within the GBM basin (not shown here). In each case, no significant differences were found between the models.

With regard to the year-to-year variation of annual and seasonal precipitation, differences between the models are more substantial. Figure 4.15 shows the coefficient-of-variation (COV, the standard deviation divided by the mean) of the annual precipitation and seasonal precipitation in the GBM basin over the period 1976-2005. A higher value of this coefficient indicates a higher inter-annual variability.

It turns out the COV of the IPSL-CM5A model is about twice as large as for the other GCMs, which means it generates substantially more inter-annual variability than the other models. Also, between the other four models the relative differences in COV are larger than the observed differences in annual mean precipitation. Figure 4.16 provides additional insights in the inter-annual variability, as it shows empirical distribution functions of annual precipitation for the five models and the various seasons. It shows that the IPSL-CM5A model is the clear "outlier" with respect to annual rainfall and monsoon rainfall. It has outliers on the high end as well as on the low end. Note that these findings do not necessarily imply that the IPSL-CM5A model is wrong, it may also be that the other models underestimate the inter-annual variability.

The differences between inter-annual variability between the models are not consistent all over the basin. This is demonstrated in the spatial plot of Figure 4.17, which shows the COV for all grid cells in the GBM basin. It shows that the COV for IPSL-CM5A is particularly large in the western half of the Ganges basin compared to the other models. All models display a decrease in COV going from west to east. This is in part explained by the fact that the mean annual precipitation is lower in the western part of the basin and therefore less consistent from year to year. As a result, the COV in the Ganges basin (summarized in Figure 4.18) is substantially larger than the COV in the Brahmaputra basin (Figure 4.19). Both these Figures show that IPSL-CM5A model consistently has the largest variation in the monsoon period and from the whole year. For the Brahmaputra basin, however, the differences with the other four models are less substantial. Also worth noting is that the ranking-order of the other four models vary strongly between Figure 4.18 and Figure 4.19. This shows there seems to be no consistent pattern regarding the year-to-year variation.

The inter-annual variability of the precipitation and, hence, river discharge, is relevant for the delta. For that reason, the fact that the climate models disagree on the inter-annual variability of historical rainfall, is of some concern. We therefore delve deeper into this subject in Section 4.3.1.2 , where model data are compared with historical station records.

mean of historical annual rainfall; results of 5 climate models

Figure 4.13   Mean annual precipitation (mm) over the period 1976-2005; data from five GCMs.

mean of historical seasonal rainfall; results of 5 climate models

Figure 4.14   Mean precipitation in the GBM basin for five different seasons over the period 1976-2005; data from five GCMs. The cyan colour on the bottom right shows the region (grid cells) that was included in the computation.

Figure 4.15   Coefficient-of-variation (year-to-year variation) of precipitation in the GBM basin for five different seasons over the period 1976-2005; data from five GCMs. The cyan colour on the bottom right shows the region (grid cells) that was included in the computation.
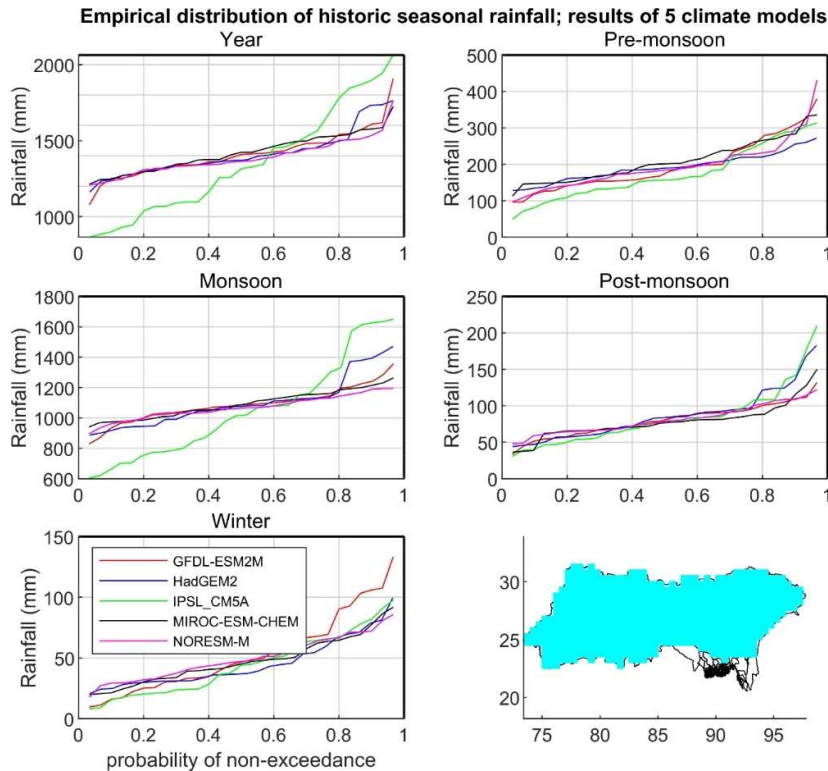
Figure 4.16   Empirical distributions (year-to-year variation) of precipitation in the GBM basin for five different seasons over the period 1976-2005; data from five GCMs. The cyan colour on the bottom right shows the region (grid cells) that was included in the computation.

Coefficient of variaton of historic annual rainfall; results of 5 climate models
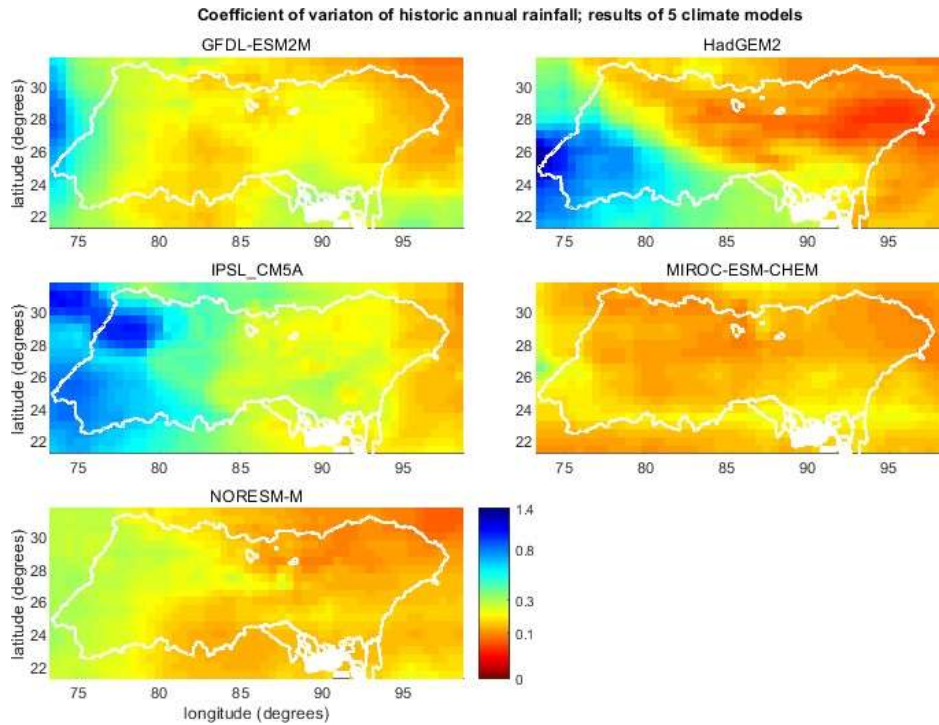
Figure 4.17   Coefficient-of-variation of annual precipitation over the period 1976-2005; data from five GCMs.

Coefficient of variaton of historical seasonal rainfall; results of 5 climate models
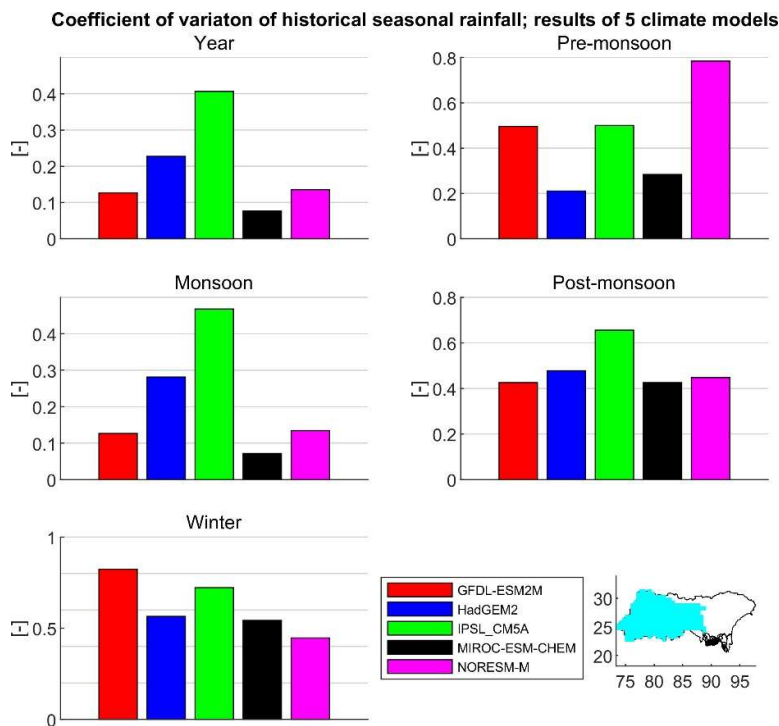
Figure 4.18   Coefficient-of-variation (year-to-year variation) of precipitation in the Ganges basin for five different seasons over the period 1976-2005; data from five GCMs. The cyan colour on the bottom right shows the region (grid cells) that was included in the computation.
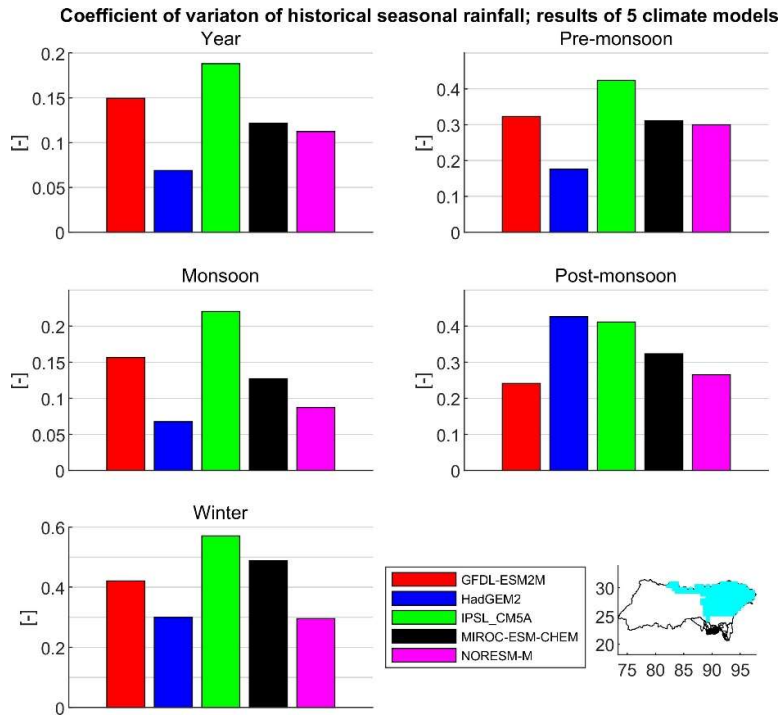
Figure 4.19   Coefficient-of-variation (year-to-year variation) of precipitation in the Brahmaputra basin for five different seasons over the period 1976-2005; data from five GCMs. The cyan colour on the bottom right shows the region (grid cells) that were included in the computation.

4.3.1.2   Bangladesh

Similar figures as produced in the previous section for the GBM basin were made for Bangladesh to verify to what extent the five climate models agree on the rainfall characteristics in the reference period. Figure 4.20 and Figure 4.21 show maps of mean annual precipitation and the COV of the annual precipitation in Bangladesh according to the five GCMs. The models show mutually consistent patterns for the mean, while at the same time the patterns for the COV differ substantially between the models. This is similar to what was concluded in the previous section on the GBM basin. However, even though the patterns for the COV are different, the absolute differences between models are not as large as seen in other areas of the GBM basin. The COV is relatively low all over Bangladesh according to the GCMs. This means the choice of a preferred GCM (if any) will have less consequences for projected changes in precipitation patterns in Bangladesh than it has for the GBM basin as a whole.

Additionally, we compared these characteristics with corresponding values of the available historical rainfall record as a form of validation. Note that comparing rainfall data at recording stations ("point data") with rainfall data form models at a spatial resolution of 0.5 degrees lat-lon (~50km) has to be done with care. This is especially the case for high intensity rainfall events, because return values for such events are expected to be substantially higher at point locations than for larger areas like the 0.5 degree grid cells for which extremes "average out". For annual and seasonal totals, on the other hand, differences should not be as large unless there are substantial spatial variations within the 0.5 degree grid cells.

Figure 4.22 and Figure 4.23 show bar charts of mean annual precipitation and the COV of the annual precipitation at location Dhaka. Results of the five GCMs are compared with historical records (light blue). Figure 4.22 shows that mean rainfall of the five GCMs is very similar to mean historical rainfall, and this is the case for all 32 available rainfall stations (not shown here). The COV (Figure 4.23) shows larger differences between models and station, but still they are in the same order of magnitude (as is the case for all 32 stations). Figure 4.24 compares the empirical distributions of the five GCMs

31

and the rainfall record and they are clearly in accordance. This is the case for almost all (32) available records from rainfall stations in Bangladesh, with a few exceptions where we suspect the spatial variation within single grid cells are relatively large due to orographic effects or land/sea boundaries.

So far, we showed statistics of annual/seasonal precipitation. For polder design, extreme rainfall events can be relevant as well. The GCMs only provide information on a daily scale on a 0.5-degree lat/lon spatial scale, so detailed information on local extreme rainfall bursts cannot be obtained from these data sets. The best possible indicator on (changes in) extremes from these datasets are annual maximum values of the daily rainfall per grid cell. Figure 4.25 shows maps of the mean value of annual maximum daily rainfall over the period 1976-2005 for the five GCMs. It shows that spatial patterns are largely the same for each model, while relative differences in absolute values are substantially larger than observed for annual mean rainfall (compare with Figure 4.20). This is confirmed by Figure 4.26, which shows bar charts of mean annual daily maximum precipitation at location Dhaka. Results of the five GCMs are compared with historical records. It shows, again, that mutual differences between models are larger than was the case for annual means (compare with Figure 4.22). This is to be expected because the annual maximum daily rainfall is "by nature" more erratic than the annual mean. Nevertheless, a difference of 50 mm between two GCMs in the mean annual maximum daily rainfall of a historical record is of some concern.
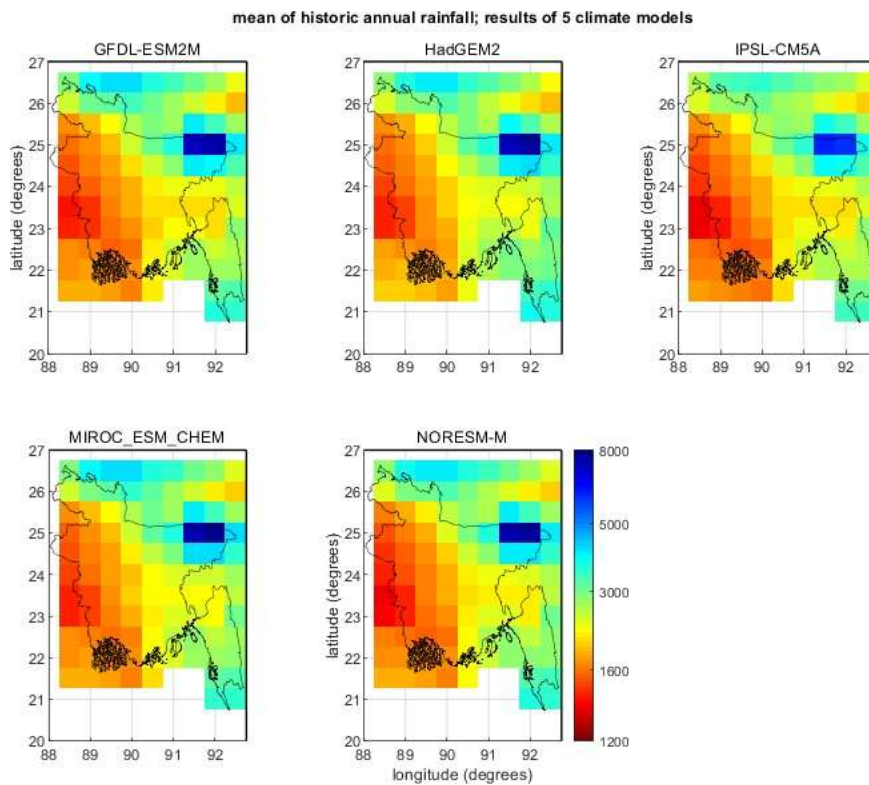
Figure 4.20   Mean annual precipitation (mm) over the period 1976-2005; data from five GCMs.
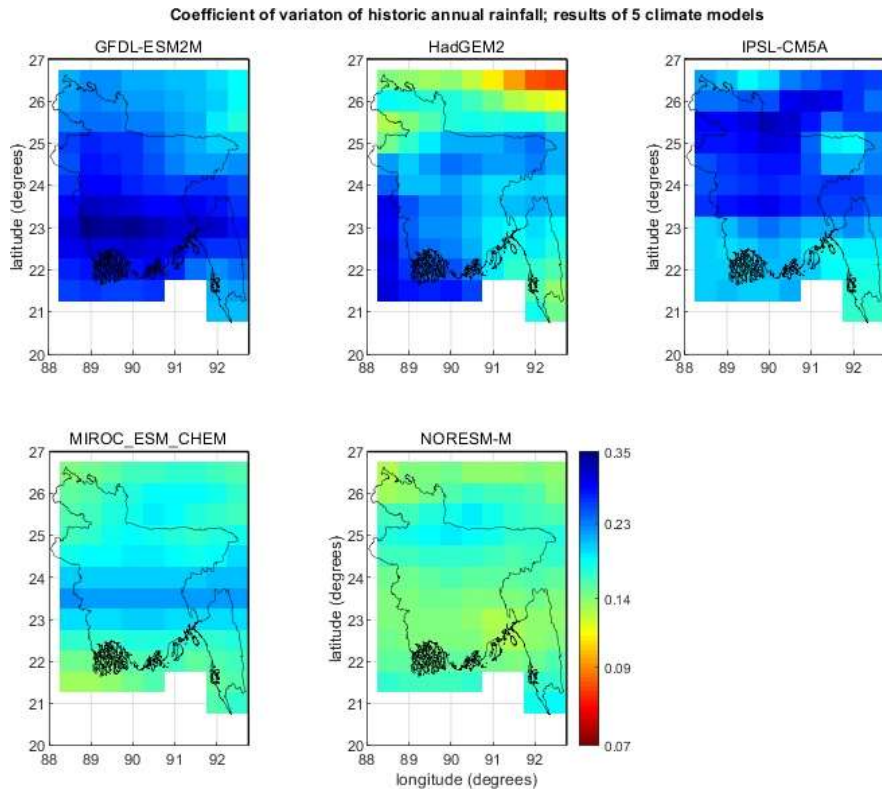
Figure 4.21   Coefficient-of-variation of annual precipitation over the period 1976-2005; data from five GCMs.
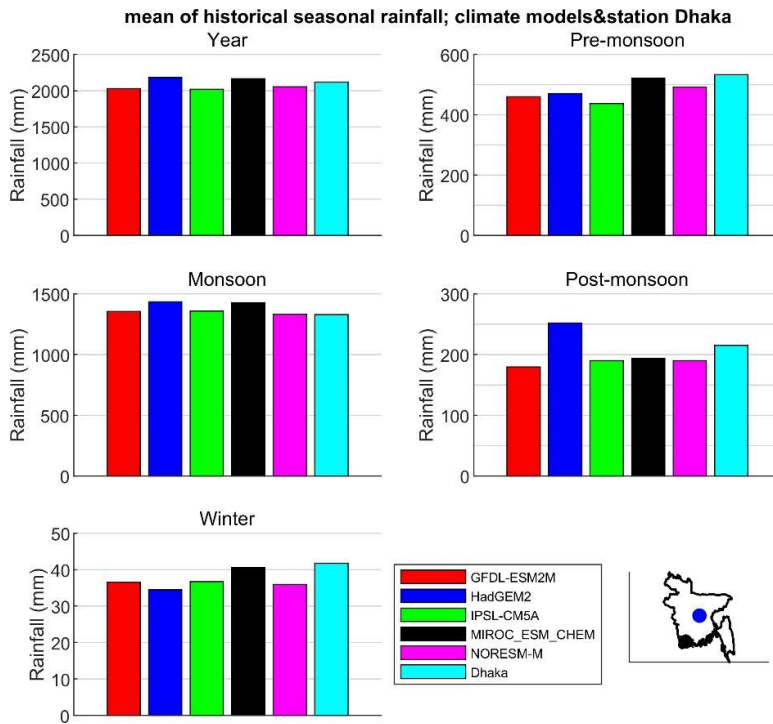
Figure 4.22   Mean annual precipitation (mm) over the period 1976-2005; comparison between recorded rainfall data at Dhaka (light blue bar) and data from five GCMs.

COV of historical seasonal rainfall; climate models&station Dhaka
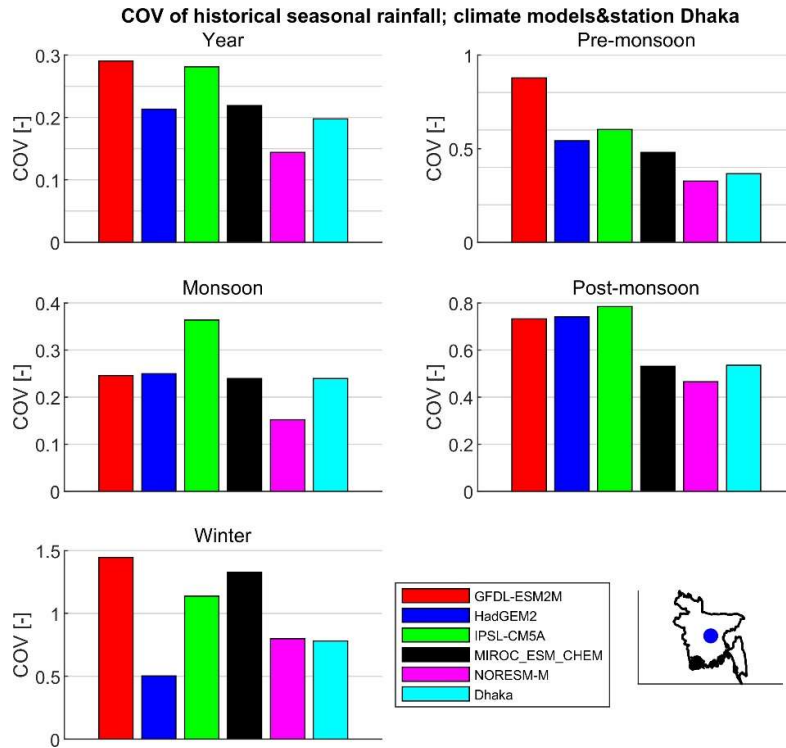
Figure 4.23 Coefficient of variation (COV) of annual precipitation over the period 1976-2005; comparison between recorded rainfall data (light blue bar) at Dhaka and data from five GCMs. The location of the Dhaka station is also provided.

Empirical distribution of seasonal rainfall; 5 climate models & station Dhaka
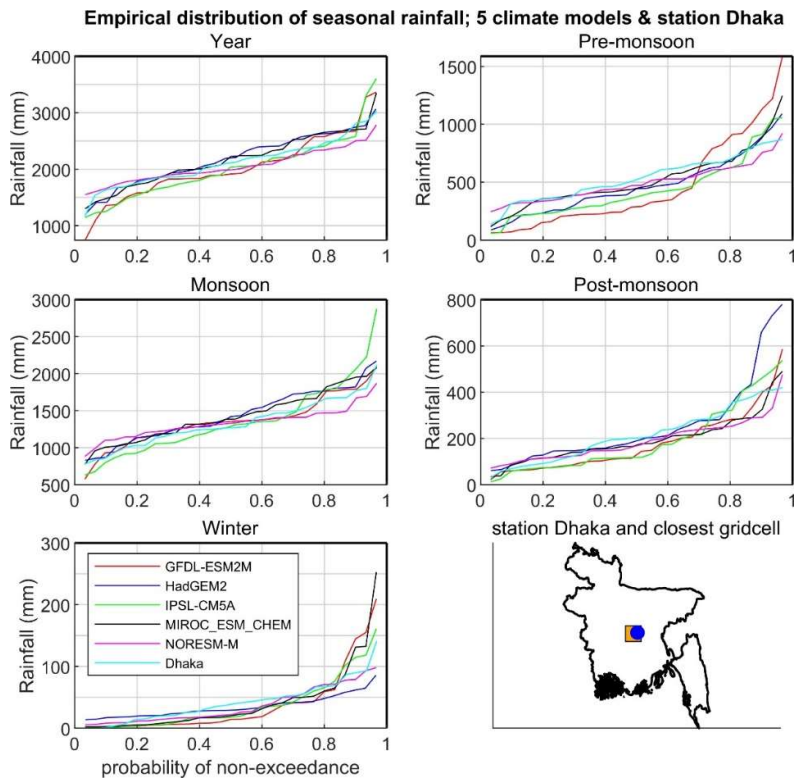
Figure 4.24   Empirical distributions of annual precipitation (mm) over the period 1976-2005; comparison between recorded rainfall data at Dhaka (light blue line) and data from five GCMs. The location of the Dhaka station is also provided.
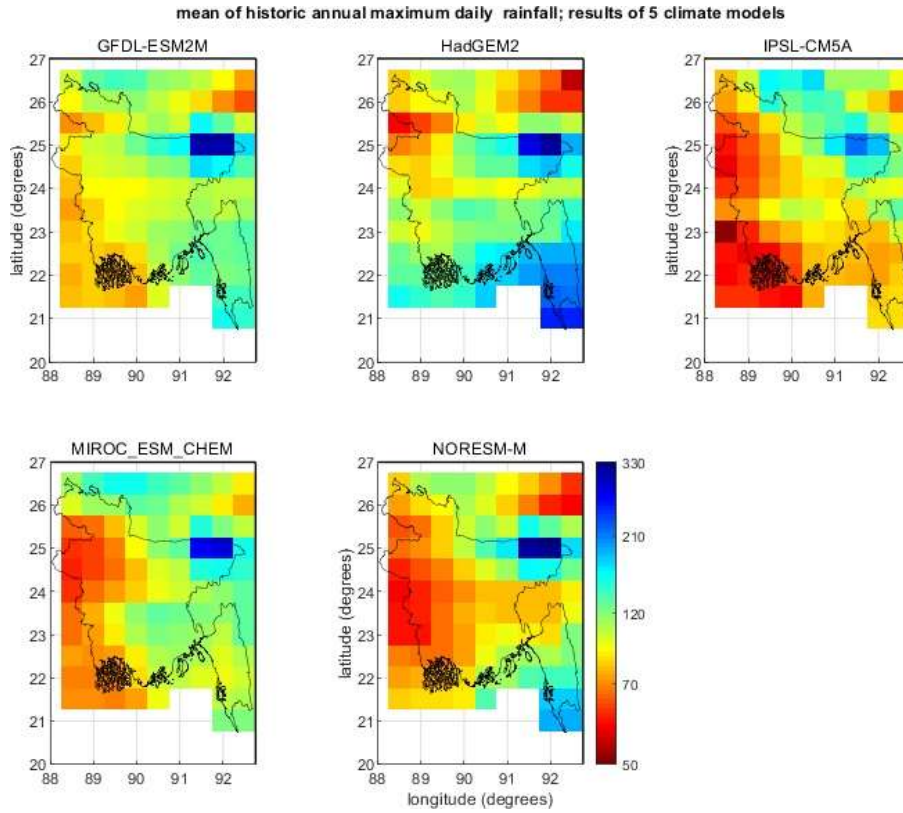
Figure 4.25   Mean annual maximum daily precipitation (mm/day) over the period 1976-2005; data from five GCMs.
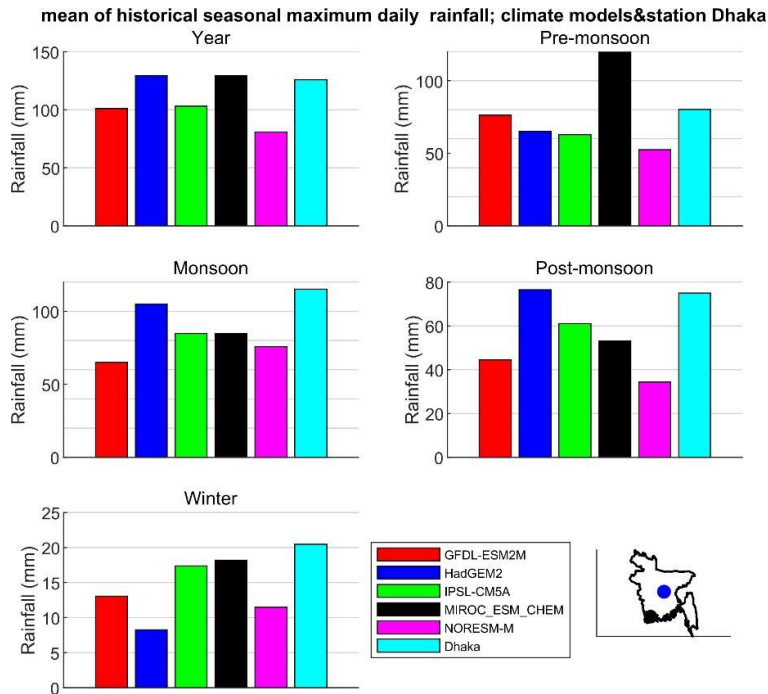
Figure 4.26   Mean annual daily maximum precipitation (mm/day) over the period 1976-2005; comparison between recorded rainfall data at Dhaka (light blue bar) and data from five GCMs. The location of the Dhaka station is also provided.

4.3.2   Temperature

4.3.2.1   GBM basin

Figure 4.27 and Figure 4.28 show spatial patterns of the mean and standard deviation of temperature over the GBM basin. Note that the standard deviation is used here as opposed to the COV which was used for precipitation. The COV is only meaningful for quantities with 0 as the absolute minimum, such as precipitation and wind speed, but not for water level and temperature (unless kelvin is used as unit for temperature).

As with precipitation, patterns for the mean temperature are the same for the five GCMs, whereas patterns for the standard deviation are quite different. However, relative differences in standard deviations are smaller for temperature than for rainfall. This can be seen for example in Figure 4.29 where the mean of the standard deviation over the entire GBM basin is displayed for the five models. Compared to Figure 4.15 (precipitation) relative differences are smaller. The same is observed for the Ganges and Brahmaputra basins separately (Figure 4.30 and Figure 4.31). So, there appears to be no concerns about the reproduction of inter-annual variability of temperature, at least not in the extent as for rainfall (Section 4.3.1).

mean of historical annual temperature; results of 5 climate models
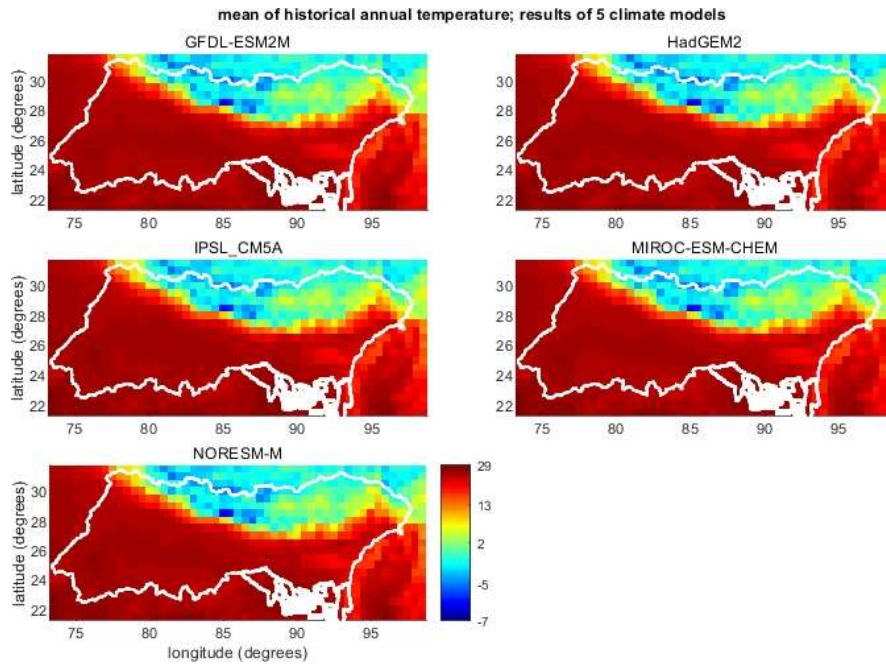
Figure 4.27   Mean annual temperature over the period 1976-2005; data from five GCMs.

standard deviation of historical annual temperature; results of 5 climate models
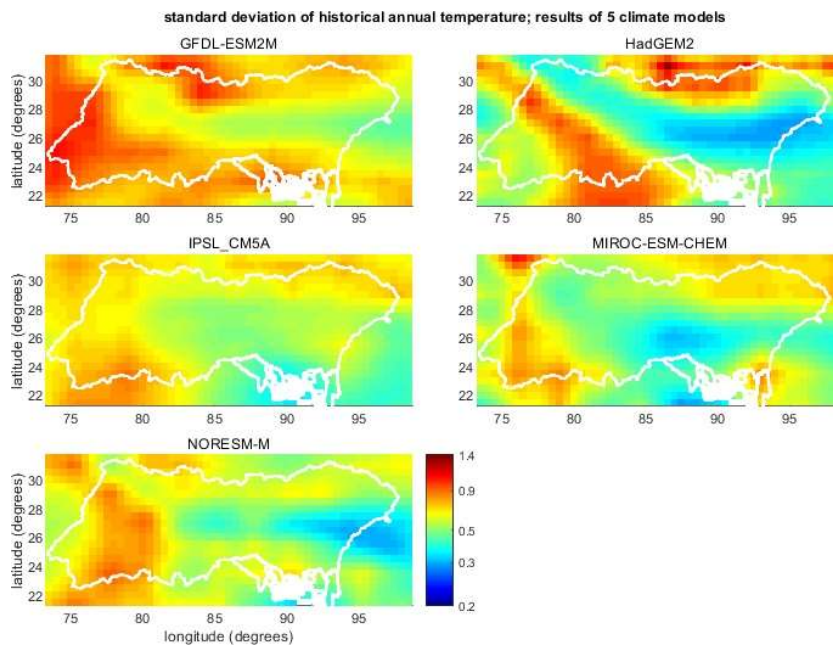
Figure 4.28   Standard deviation of annual temperature over the period 1976-2005; data from five GCMs.

standard deviation of historical seasonal temperature; results of 5 climate models
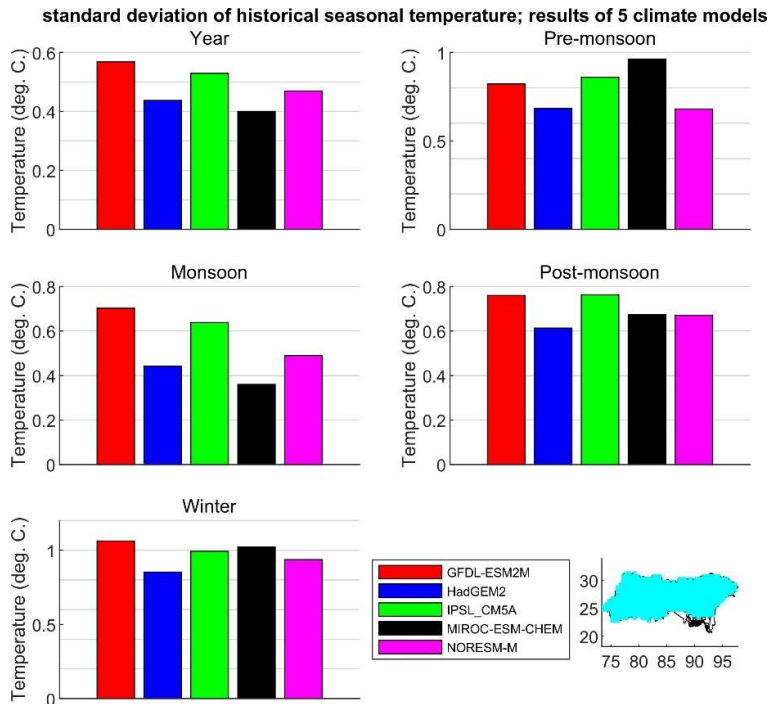
Figure 4.29   Standard deviation (year-to-year variation) of temperature in the GBM basin for five different seasons over the period 1976-2005; data from five GCMs. The cyan colour on the bottom right shows the region (grid cells) that was included in the computation.

standard deviation of historical seasonal temperature; results of 5 climate models
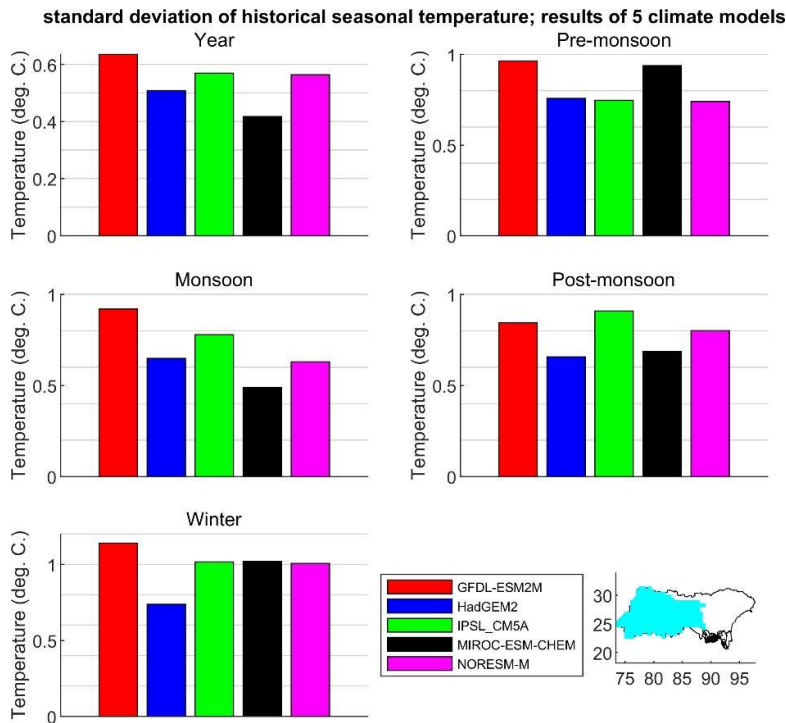
Figure 4.30   Standard deviation (year-to-year variation) of temperature in the Ganges basin for five different seasons over the period 1976-2005; data from five GCMs. The cyan colour on the bottom right shows the region (grid cells) that was included in the computation.

standard deviation of historical seasonal temperature; results of 5 climate models
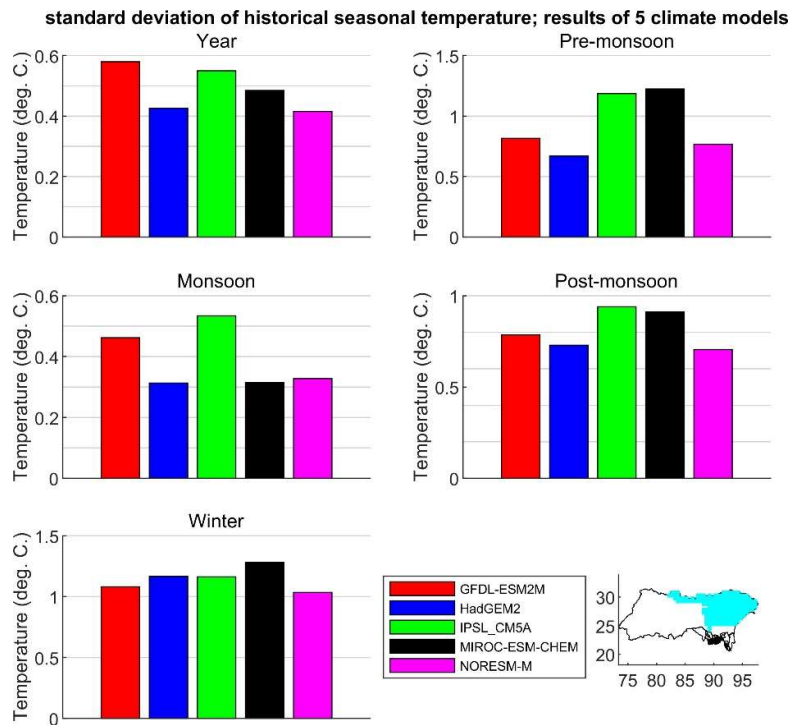
Figure 4.31   Standard deviation (year-to-year variation) of temperature in the Brahmaputra basin for five different seasons over the period 1976-2005; data from five GCMs. The cyan colour on the bottom right shows the region (grid cells) that was included in the computation.

4.3.2.2   Bangladesh

Figure 4.32 shows maps of the mean annual temperature over the period 1976-2005 for grid cells in Bangladesh. Figure 4.33 shows a similar plot for the standard deviation, as a measure of inter-annual variability in temperature. Similar to the GBM basin, it shows that the mean values of the five GCMs are well in accordance, whereas patterns of inter-annual variability differ.

Figure 4.34 compares the recorded annual mean temperature over the period 1976-2005 at Dhaka with corresponding historical data from the five GCMs. It shows that recorded temperatures are on average about four degrees higher than the corresponding temperatures of the GCMs. The same is observed for other stations. The figure suggests that recorded temperatures and GCM temperatures have a different meaning, for example daily maximum temperatures versus daily mean temperatures. This is considered not to be a problem in the current application, because the GCM results are only used to establish temperature *increases* due to climate change; not to establish absolute values. Figure 4.35 shows a similar plot as Figure 4.34 for the standard deviation, as a measure of inter-annual variability in temperature. It shows that the standard deviation is in the same order of magnitude between models. Nevertheless, differences among GCMs and differences between station data and GCMs are not negligible.

mean of historic annual temperature; results of 5 climate models
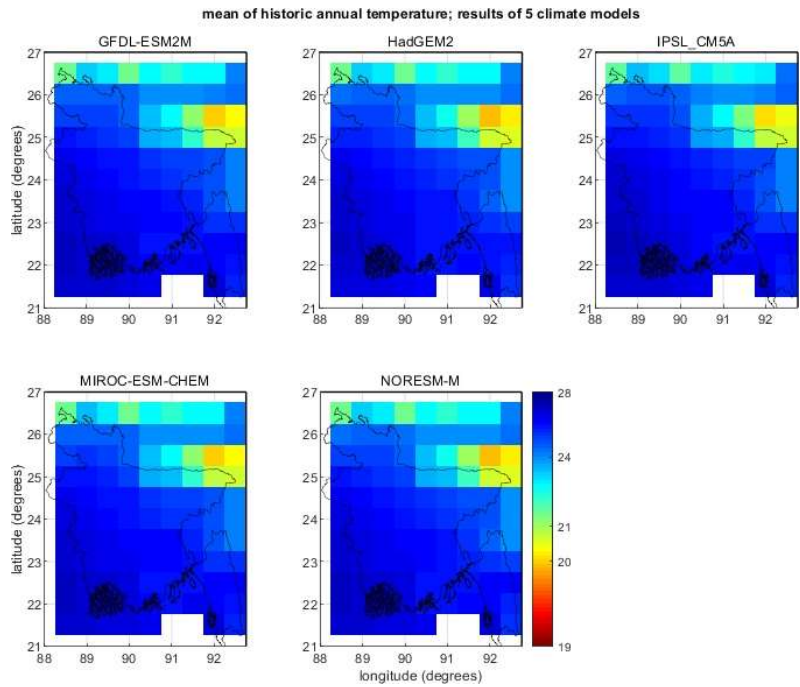
Figure 4.32   Mean annual temperature over the period 1976-2005; data from five GCMs.

standard deviation of historic annual temperature; results of 5 climate models
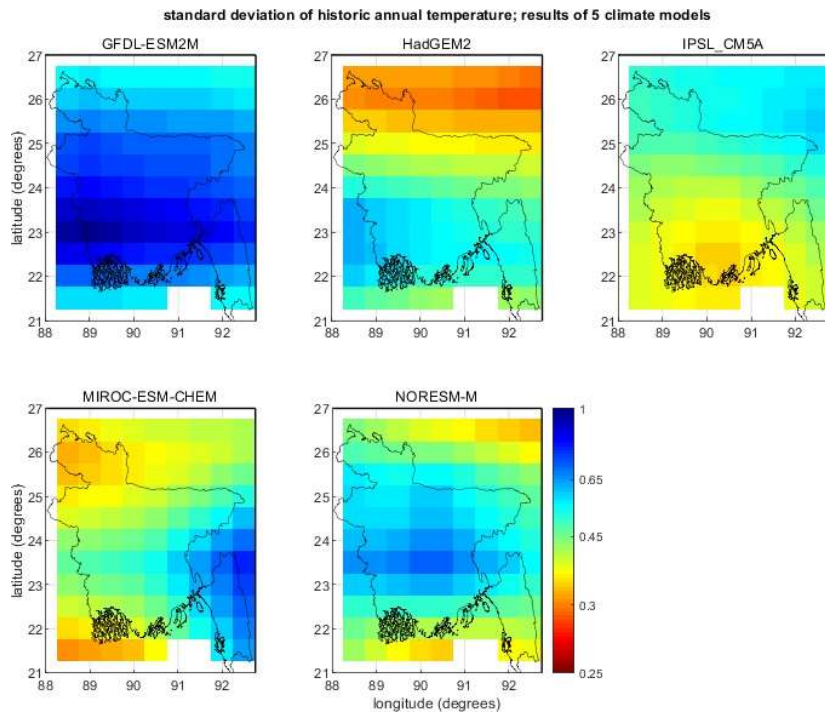
Figure 4.33 Standard deviation of annual mean temperature over the period 1976-2005; data from five GCMs.

mean of historic seasonal temperature; 5 GCMs & station Dhaka
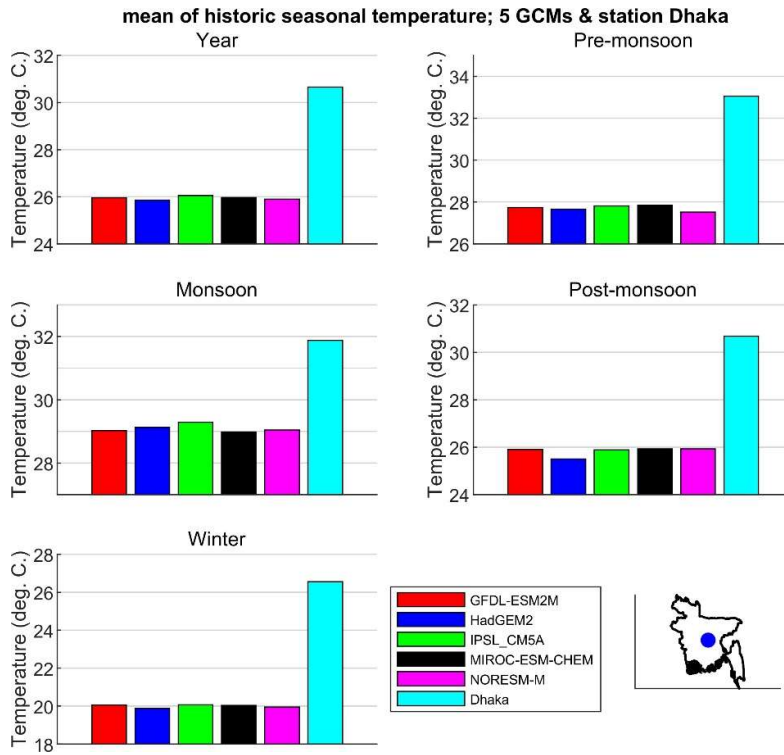
Figure 4.34   Mean annual temperature over the period 1976-2005. Comparison between recorded temperature at Dhaka (light blue bar) and data from five GCMs. The location of the Dhaka station is also provided.

standard deviation of historic seasonal temperature; 5 GCMs & station Dhaka
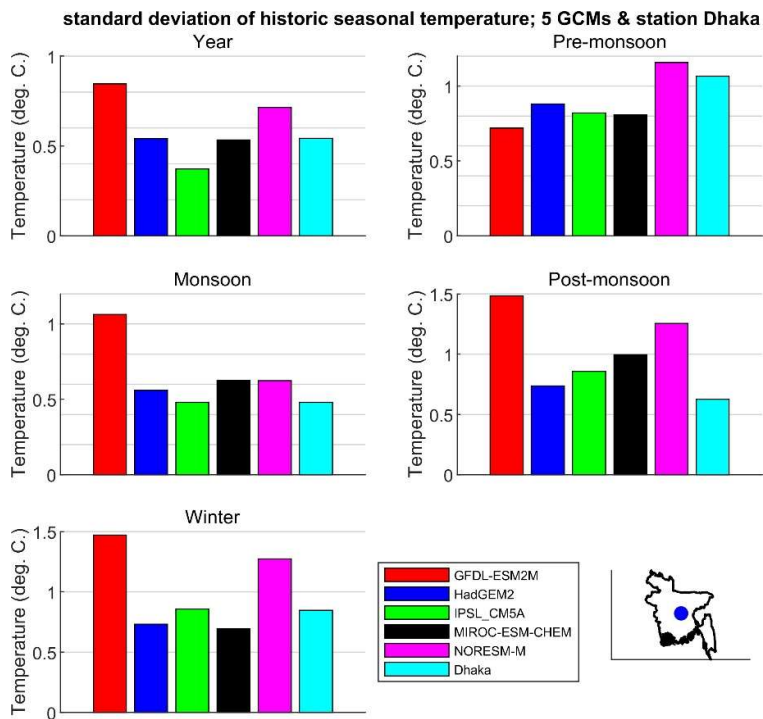
Figure 4.35   Standard deviation of variation of annual temperature over the period 1976-2005. Comparison between recorded rainfall data at Dhaka (light blue bar) and data from five GCMs. The location of the Dhaka station is also provided.

4.4 Modelled data of future periods

4.4.1 Precipitation

4.4.1.1 Introduction

For the future downscaled scenarios of precipitation, we first consider four different periods in our analyses:

- 2006-2035 (representative for the climate of the year 2020)
- 2026-2055 (representative for the climate of the year 2040)
- 2046-2075 (representative for the climate of the year 2060)
- 2066-2095 (representative for the climate of the year 2080)

Climate characteristics as derived from GCM outputs, are compared with characteristics of the reference period (1976-2005; representative for the climate of the year 1990) to establish projections of relative changes in climate conditions.

4.4.1.2 GBM basin

Figure 4.36 shows the projected increase in annual precipitation according to the five GCMs in the year 2020 (period 2006-2035), for the RCP4.5 emission scenario, relative to 1990. It shows that differences in projections between the five GCMs are substantial. This is especially the case for the western part of the Ganges basin. According to the HADGEM2 GCM there may be more than a 20% increase in precipitation over this part of the basin, whereas the GFDL-ESM2M model projects a decrease of more than 10% over the same area. These are large differences, especially given the relative short time horizon (reference period 1976-2005 versus future scenario 2006-2035). These differences are caused by either a structural difference between models or by 'coincidence' related to the inter-annual variability, or a combination of both.

Figure 4.37 shows the projected increase in annual precipitation according to the five GCMs in the year 2080 (period 2066-2095) projected by the RCP8.5 emission scenario. In this more extreme emission scenario, with a longer time horizon, there is more agreement among the models on the *direction* of the trend; the GCMs mostly indicate that an increase in annual precipitation can be expected. Nevertheless, there are still substantial differences in the projected *magnitude* of the increase. Furthermore, for some areas within the GBM basin still a decrease is projected by some GCMs, while an increase is projected by others. Figure 4.38 shows the projected percentage increase in precipitation in 5 sub-areas of the GBM basin for 5 different seasons (including the whole year). Each vertical column of dots (RCP4.5) and triangles (RCP8.5) represents the variation in percentage increase for combinations of RCP-scenarios (2) and climate-models (5). The range that is covered by each combination of five dots and five triangles is an indication of the uncertainty in these projections. The most noteworthy conclusions that can be drawn from this figure and the underlying numbers are:

- The variability in projected changes in precipitation decreases from west to east. Figure 4.39 shows that this is not only the case in relative sense (percentage change) but to a lesser extend also in absolute sense (change in mm).
- In the eastern part of the basin, all projections indicate an increase in precipitation in the monsoon after 2050. Not surprisingly, the same can be stated about the total annual precipitation.
- In the western part of the GBM basin, one GCM (GFDL-ESM2M) projects a decrease in monsoon and annual precipitation after 2050 for both RCP-scenarios, whereas the other four GCMs project an increase.
- For the winter, pre-monsoon, and post-monsoon seasons, the projections are 'mixed' in the sense that some models project an increase after 2050, whereas others project a decrease.
- For the winter season, most models project a decrease in precipitation.

- There does not appear to be a 'rule' for RCP8.5 to result in higher precipitation projections than RCP4.5 or vice versa. Nevertheless, the RCP8.5 scenario results in 65 out of 100 cases in a higher annual rainfall projection than RCP4.5, where each case is a combination of area (5), GCM (5) and time horizon (4).

Percentage increase in mean annual rainfall; rcp4.5-scenario, year: 2020
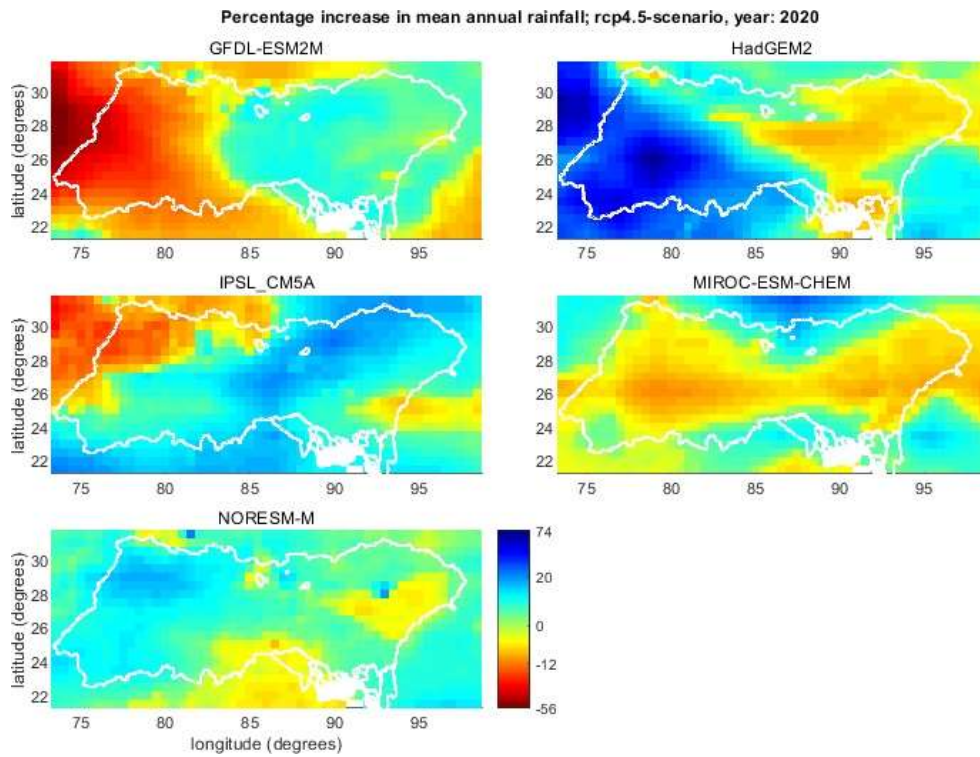
Figure 4.36 Projected percentage change in annual precipitation according to five different GCMs, relative to climate year 1990; RCP-scenario 4.5, year 2020

Percentage increase in mean annual rainfall; rcp8.5-scenario, year: 2080
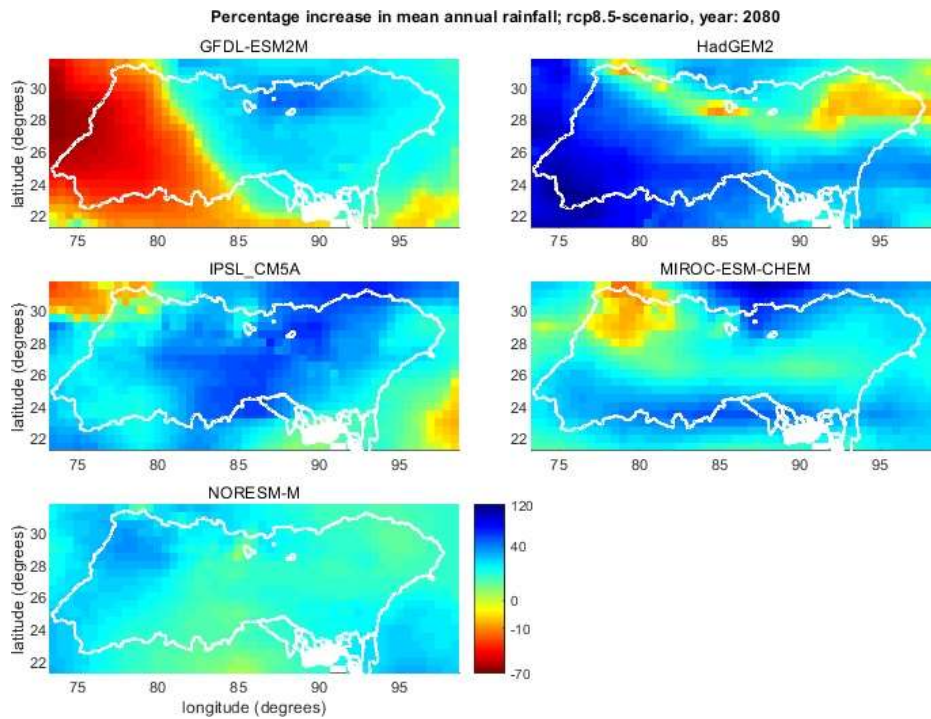
Figure 4.37 Projected percentage change in annual precipitation according to five different GCMs, relative to climate year 1990; RCP-scenario 8.5, year 2080
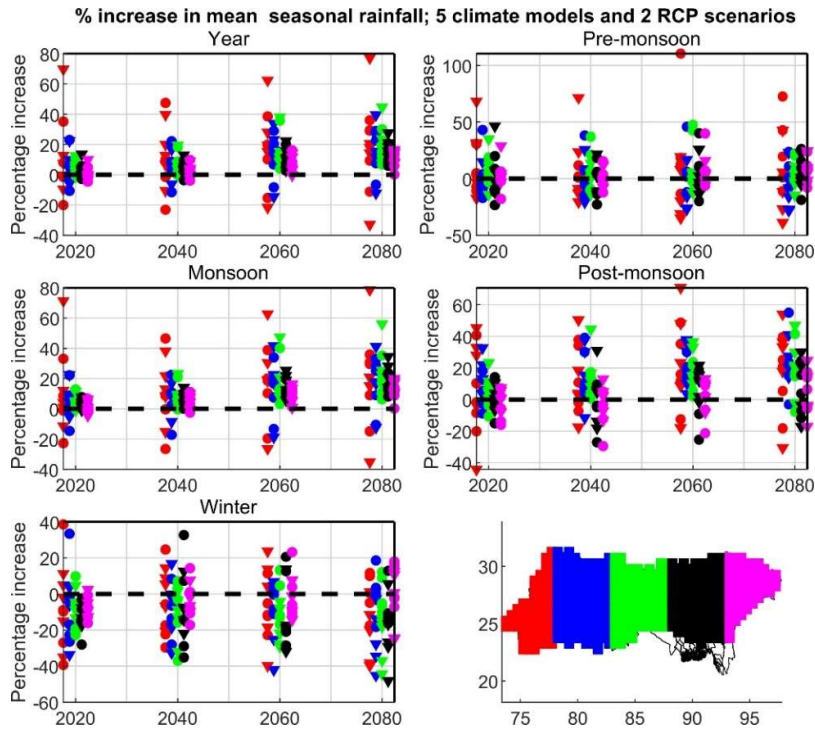
Figure 4.38   Projected percentage change in precipitation in 5 subareas of the GBM basin for 5 different seasons, relative to climate year 1990. Each vertical column of dots (RCP4.5) and triangles (RCP8.5) represents the variation in percentage increase for combinations of RCP-scenarios (2) and climate-models (5).
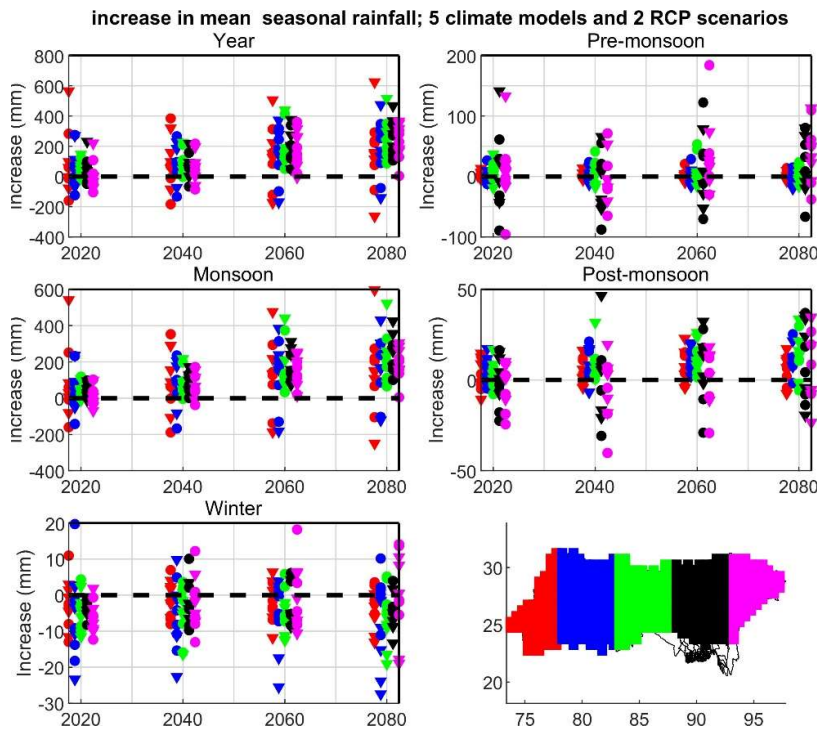
Figure 4.39   Projected absolute change in precipitation in 5 subareas of the GBM basin for 5 different seasons, relative to climate year 1990. Each vertical column of dots (RCP4.5) and triangles (RCP8.5) represents the variation in percentage increase for combinations of RCP-scenarios (2) and climate-models (5).

In this project, projected climate scenarios for rainfall and temperature will serve, among others, as input to the macro-scale Hydrotrend model (Deliverable D4A-1) to assess the potential impact of climate change on upstream river discharges in Bangladesh. Two Hydrotrend models are being developed: one for the Ganges basin and one for the Brahmaputra basin. The climatological input for the Hydrotrend models consists of daily time series of the basin-averaged temperature and precipitation. In that respect, the projected changes in precipitation and temperature on the scale of the Ganges and Brahmaputra basins are particularly relevant for the project. Figure 4.41 shows projected percentage increase in precipitation in the Ganges (red) and Brahmaputra (blue) basins separately for 5 different seasons. Table 4-6 presents summarizing statistics. The results are in line with those from Figure 4.38:

- The variability in projected changes in precipitation is larger for the Ganges basin than for the Brahmaputra basin.
- In the Brahmaputra basin, all models project an increase in precipitation in the monsoon and the whole year after 2050.
- In the Ganges basin, one GCM (GFDL-ESM2M) projects a decrease in monsoon and annual precipitation after 2050 for both RCP-scenarios, whereas the other four GCMs project an increase. The projected increase by those four models are in general substantially higher than projected (percentage) increase for the Brahmaputra basin.
- For the winter, pre-monsoon, and post-monsoon seasons the projections are 'mixed' in the sense that some models project an increase after 2050, whereas others project a decrease. For the winter season, most models project a decrease in precipitation.

Figure 4.41 shows the projected percentage increase in precipitation in the whole GBM basin for 5 different seasons. This figure shows that for the GBM basin as a whole, all models project an increase in precipitation from 2050 onwards. For the other seasons the projections are 'mixed' (both increase and decrease after 2050). For the winter season, most models project a decrease in precipitation.

% increase in mean seasonal rainfall; 5 climate models and 2 RCP scenarios
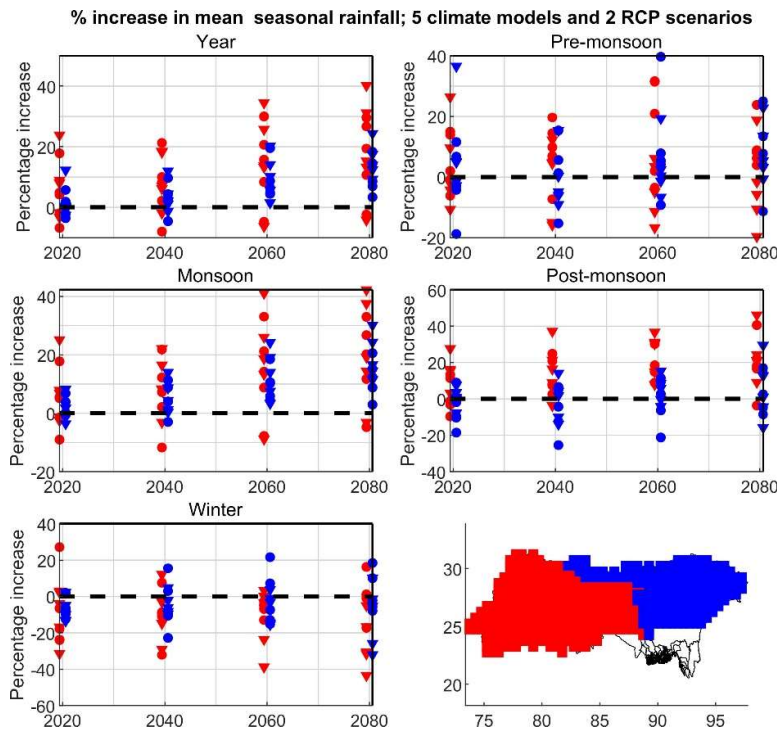
Figure 4.40   Projected percentage change in precipitation in the Ganges (red) and Brahmaputra (blue) basins for 5 different seasons, relative to climate year 1990. Each vertical column of dots (RCP4.5) and triangles (RCP8.5) represents the variation in percentage increase for combinations of RCP-scenarios (2) and climate-models (5).

% increase in mean seasonal rainfall; 5 climate models and 2 RCP scenarios
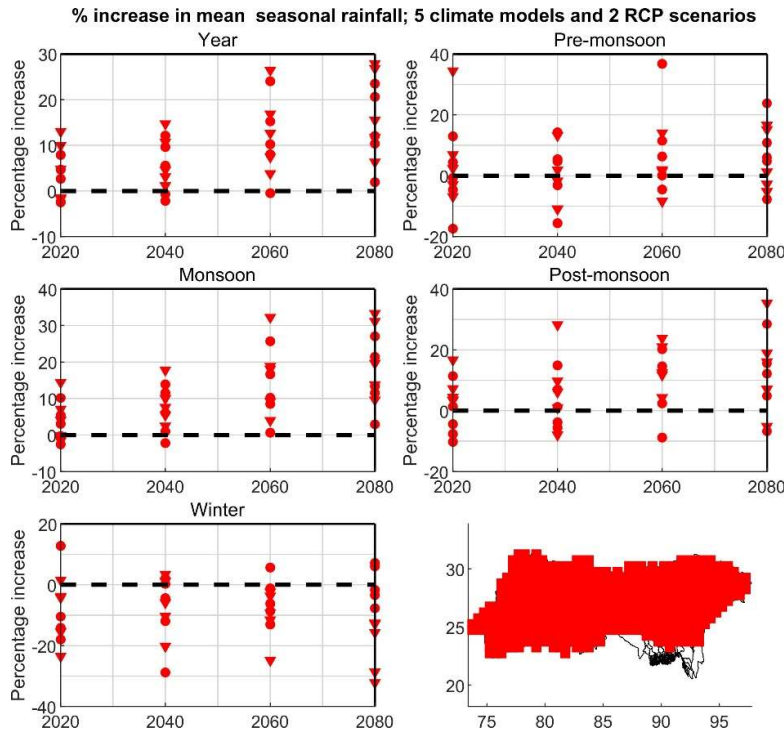
Figure 4.41 Projected percentage change in precipitation in the GBM basin for 5 different seasons, relative to climate year 1990. Each vertical column of dots (RCP4.5) and triangles (RCP8.5) represents the variation in percentage increase for combinations of RCP-scenarios (2) and climate-models (5).

Table 4-6 Summary of projected percentage increase in precipitation in the Ganges and Brahmaputra basin, relative to climate year 1990. The table shows the minimum, mean and maximum over the 10 combinations of RCP-scenarios (2) and climate-models (5).

	in %	2020			2040			2060			2080		
Season	Basin	min	mean	max	min	mean	max	min	mean	max	min	mean	max
Year	Ganges	-7	5	24	-8	8	21	-6	15	34	-4	18	40
	Brahmaputra	-4	1	12	-5	3	12	2	10	20	3	13	24
Pre-monsoon	Ganges	-11	4	26	-16	3	20	-17	6	32	-20	3	24
	Brahmaputra	-19	3	37	-15	0	15	-9	6	40	-11	8	25
Monsoon	Ganges	-9	5	25	-12	8	22	-9	16	41	-5	20	42
	Brahmaputra	-4	1	8	-3	5	14	3	12	24	3	16	30
Post-monsoon	Ganges	-10	7	28	-4	14	37	8	21	37	-4	22	46
	Brahmaputra	-18	-3	9	-25	-3	14	-21	2	15	-16	4	29
Winter	Ganges	-31	-9	27	-32	-9	12	-39	-9	3	-43	-13	16
	Brahmaputra	-13	-7	2	-23	-5	16	-16	-4	22	-32	-4	18

4.4.1.3 Bangladesh

Figure 4.42 shows the projected percentage increase in mean annual precipitation in Bangladesh according to the five GCMs, relative to climate year 1990, RCP-scenario 4.5, year 2020. Figure 4.43 shows similar plots for RCP scenario 8.5, year 2080. As before, in the figures for the GBM basin, spatial patterns differ strongly between models. In areas where some GCMs project an increase in

rainfall, others project a decrease. Not surprisingly, differences between GCM projections are larger for the year 2080 than for the year 2020. Figure 4.44 shows that variations in projections of the mean annual maximum daily rainfall (a proxy for extreme rainfall events) is even larger than it is for annual mean rainfall.
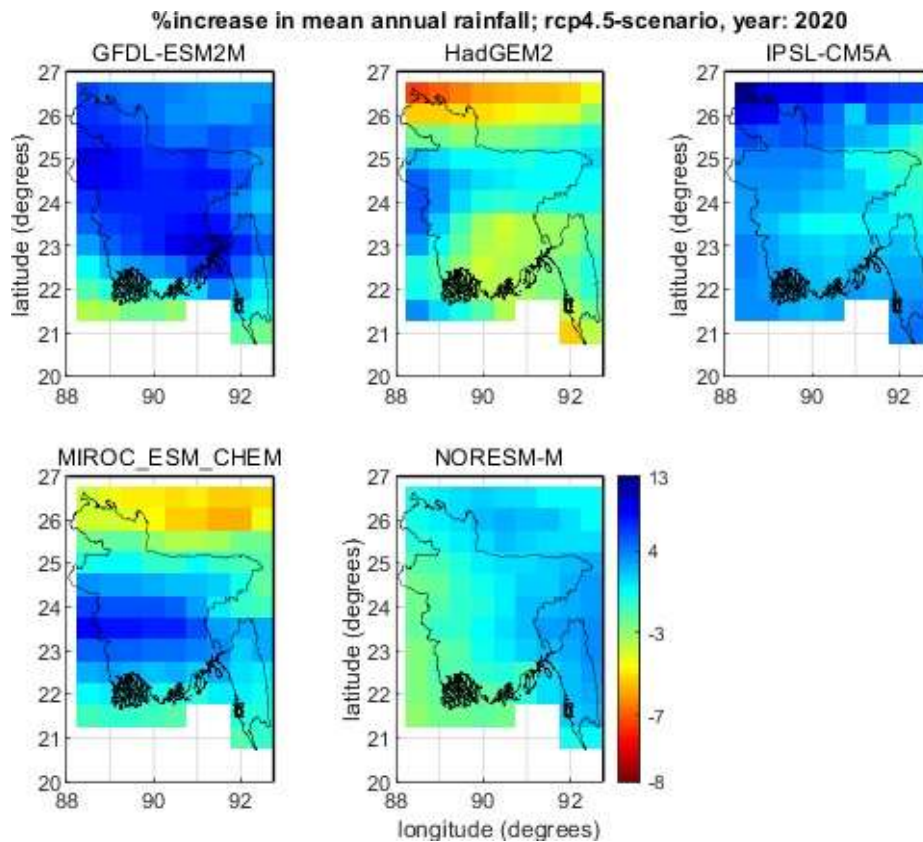
Figure 4.42   Projected percentage change in annual precipitation according to five different GCMs, relative to climate year 1990; RCP-scenario 4.5, year 2020.

%increase in mean annual rainfall; rcp8.5-scenario, year: 2080
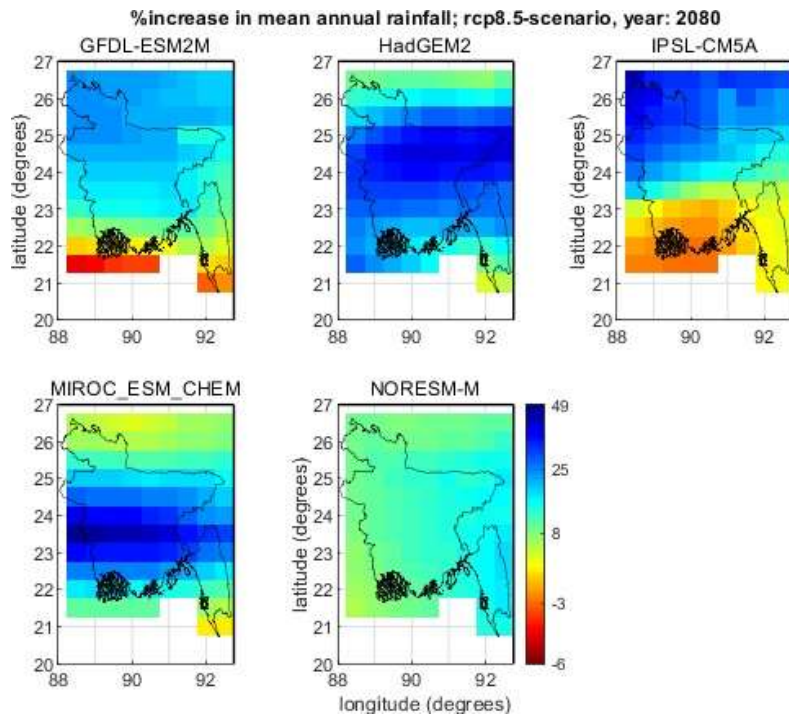
Figure 4.43   Projected percentage change in annual precipitation according to five different GCMs, relative to climate year 1990; RCP-scenario 8.5, year 2080.

%increase in mean annual maximum daily rainfall; rcp8.5-scenario, year: 2080
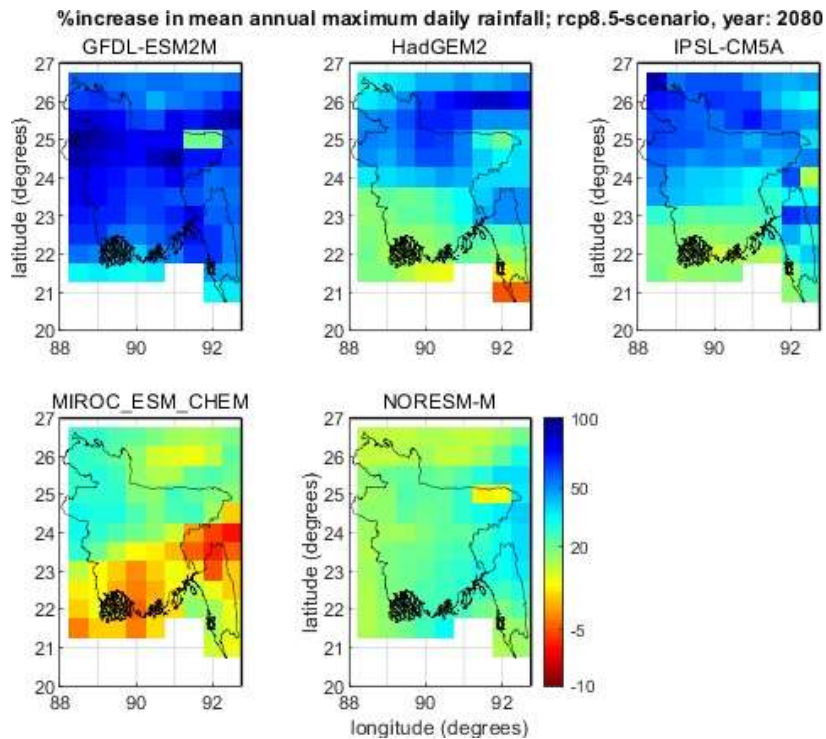
Figure 4.44   Projected percentage change in annual maximum daily precipitation according to five different GCMs, relative to climate year 1990; RCP-scenario 8.5, year 2080.

As part of this project, five polders were selected to define new (resilient) conceptual designs for adaptation (Component 5-A). Figure 4.2 shows a map of the five polders that were selected: polders 15, 29, 40 (1&2), 59/2, 64/1a and 64/1b. Due to the specific interest of the project on these five polders, a detailed analysis and values have been provided for these five polders also. Since the last two polders (64/1 and 64/2) are directly next to each other and therefore in the same GCM grid, we will refer to them as a single polder system 64/1 in the current report.

Figure 4.45 shows the projected percentage increase in precipitation in the 5 selected polders for 4 different seasons and the entire year. Each vertical column of dots (RCP4.5) and triangles (RCP8.5) represents the variation in percentage increase for combinations of RCP-scenarios (2) and climate-models (5). Figure 4.46 show similar plots for the mean annual maximum daily precipitation. From these figures and underlying data, we can conclude that:

- Almost all projections indicate an increase in precipitation in the monsoon season after 2050 for all five polders.
- Almost all projections indicate a decrease in precipitation in the winter season after 2050 at almost all polders.
- For other seasons, the projections show more of a mixture of increases and decreases.
- The GFDL-ESM2M model projects an increase in annual daily maximum rainfall that is substantially larger than those of the other four GCMs.
- The range in projected changes in annual mean precipitation is about 15% in 2020 (-5 to +10%), 20% in 2040 and 30% in 2060 and 2080.
- The range in projected changes in annual maximum daily precipitation is much larger, but that is mainly due to the earlier mentioned 'outlier' projections from the GFDL-ESM2M model (Figure 4.47).
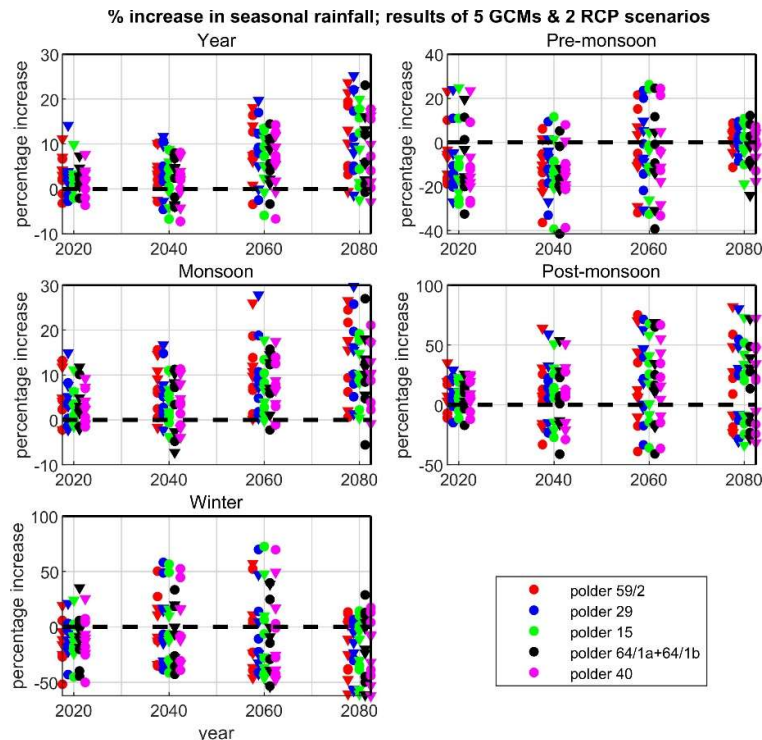
Figure 4.45   Projected percentage change in precipitation in the 5 selected polders for 4 different seasons and for the entire year, relative to climate year 1990. Each vertical column of dots (RCP4.5) and triangles (RCP8.5) represents the variation in percentage increase for combinations of RCP-scenarios (2) and climate-models (5).

Table 4.7 summarises the results of Figure 4.45. It presents the minimum, mean and maximum values for each combination of polders, seasons and time horizons. It is worth noting that these results in some cases appear to be not fully aligned with the trends derived from the historical series (Table 4-2). For example, according to the mean values of Table 4.7, the pre-monsoon rainfall in 2020 shows a decreasing trend, whereas in Table 4-2 no trend was observed. Similarly, the monsoon rainfall in 2020 shows an increasing trend, whereas in Table 4-2 no trend was observed.

In that respect it is better to look at the full range of results from the climate models (difference between the minimum and maximum values in Table 4-2). It shows that using GCMs to determine trends comes with large uncertainties, even when looking at differences between 2020 (period 2006-2035) and 1990 (period 1976-2005). The derived trends from the historic data are well within these uncertainty bounds. The large uncertainty bounds reveal that the predictive power of the GCMs is very limited, which is why it is better to speak of 'projections' than 'predictions'. That is why it was proposed to use various climate scenarios (low, medium and high) to assess potential climate impacts instead of a single scenario (see section 1.2 of this report).

Table 4.7   Summary of projected percentage change in precipitation at five selected polders, relative to climate year 1990. The table shows the minimum, mean and maximum over the 10 combinations of RCP-scenarios (2) and climate-models (5).

		2020			2040			2060			2080		
	in %	min	mean	max	min	mean	max	min	mean	max	min	mean	max
Year	polder 59/2	-7	4	22	-12	4	21	-4	15	52	-8	20	63
	polder 29	-9	2	13	-4	7	35	-9	12	38	-9	15	56
	polder 15	-11	1	13	-3	6	28	-5	10	33	-9	14	43
	polder 64/1	-15	4	22	-11	4	35	-7	14	59	0	18	68
	polder 40	-13	-1	13	-12	1	21	-13	7	32	-8	11	42
Pre-monsoon	polder 59/2	-20	-5	13	-25	-6	19	-24	6	55	-10	9	55
	polder 29	-26	-8	12	-28	-3	20	-30	8	51	-13	4	41
	polder 15	-32	-7	13	-23	-2	24	-25	12	73	-11	7	66
	polder 64/1	-20	-4	37	-28	-3	53	-32	12	91	-13	15	88
	polder 40	-27	-7	14	-25	-5	21	-30	10	75	-12	7	62
Monsoon	polder 59/2	-9	9	42	-13	10	45	-5	17	64	-1	22	94
	polder 29	-15	7	24	-5	10	32	-2	15	56	5	23	105
	polder 15	-15	7	28	-1	9	32	-5	13	48	0	20	88
	polder 64/1	-15	8	44	-14	9	60	-8	15	83	-3	19	85
	polder 40	-17	4	29	-11	5	29	-10	10	41	-13	15	81
Post-monsoon	polder 59/2	-18	9	48	-29	7	88	-36	20	131	-32	21	112
	polder 29	-23	12	52	-21	10	79	-28	18	82	-34	16	57
	polder 15	-20	7	31	-22	5	47	-26	14	57	-31	13	53
	polder 64/1	-25	8	40	-33	7	58	-42	18	60	-26	19	66
	polder 40	-23	10	34	-20	7	59	-26	14	47	-35	13	54
Winter	polder 59/2	-27	-6	15	-34	-1	25	-52	-2	60	-50	-16	21
	polder 29	-21	1	18	-29	4	41	-47	2	75	-54	-14	12
	polder 15	-25	-2	20	-27	5	49	-55	-3	60	-55	-16	17
	polder 64/1	-32	-10	21	-27	-7	22	-52	-11	24	-49	-13	36
	polder 40	-27	-3	19	-30	3	47	-59	-5	55	-54	-17	18
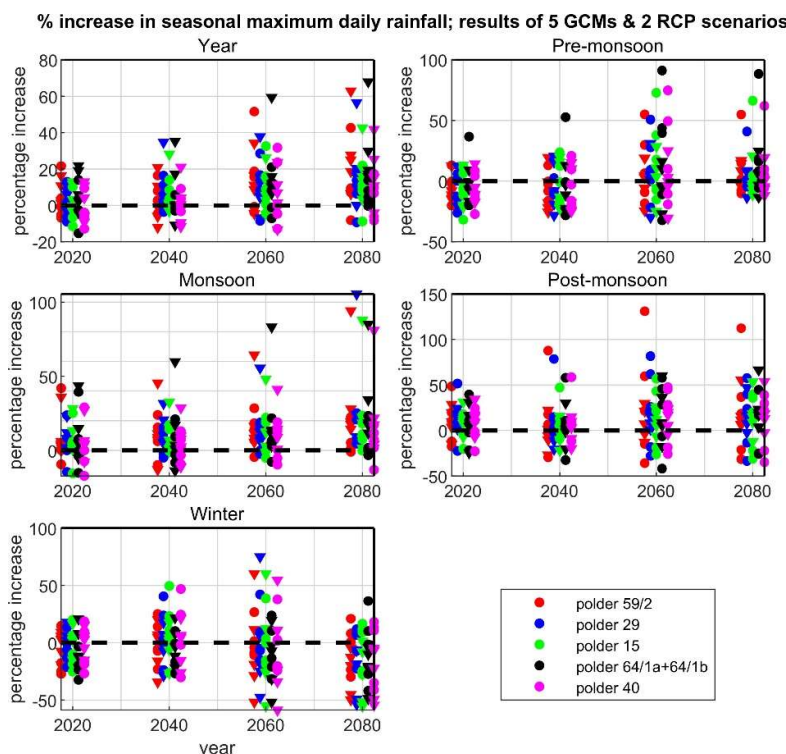
Figure 4.46   Projected percentage change in maximum daily precipitation in the 5 selected polders for 4 different seasons, relative to climate year 1990. Each vertical column of dots (RCP4.5) and triangles (RCP8.5) represents the variation in percentage increase for combinations of RCP-scenarios (2) and climate-models (5).

We made a comparison between the projections above and the projections as reported in the Bangladesh Delta Plan (GED, 2018). GED (2018) reported a projected increase in precipitation in the years 2030 and 2050 for seven regions in Bangladesh (see Table 4.8). To make the comparison, we derived projections for the years 2030 and 2050, as reported in the Delta Plan, for the five polders from the available GCM outputs. For each polder we compared results with Delta Plan projections of the associated region. So, for example, we compared projections of polder 15 with projections of region 'southwest', because polder 15 is in region southwest. The five polders are located in the regions southwest (polders 15 and 29), south central (polder 40), southeast (polder 59/2) and eastern hills (polder 64/1). This means the three northern regions of Table 4.8 were not included in the comparison.

Figure 4.47 shows the results of the comparison. The vertical lines represent projected percentage increase in maximum daily rainfall in the 5 selected polders for 5 different seasons from the analyses of the current report. Each vertical line represents the range in percentage increase for combinations of RCP-scenarios (2) and climate-models (5). The dots show the projections from the Bangladesh Delta Plan (GED, 2018). There are clearly some differences worth noticing:

- The data from the Delta Plan report indicate a decrease in annual rainfall between 2030 and 2050 for most polders/regions, whereas the GCM results of our report suggest a slight increase. The same can be stated for the monsoon season.

- The Delta Plan indicates an increase in pre-monsoon rainfall in the year 2030, whereas the GCM results of our report suggest a decrease in most cases. The projections from the Delta Plan report are in some cases outside the range of the 10 scenarios of our report.

- The Delta Plan indicates a substantial increase (>40%) in winter precipitation for a number of regions whereas the GCM results of our report suggest a decrease in most cases. The

projections from the Delta Plan report are in some cases far outside the range of the 10 scenarios of our report.

- For the post-monsoon season, the projections from the Delta Plan report are also in some cases far outside the range of the 10 scenarios of our report.

This shows that the projections of our report and of the Delta Plan report are far from being mutually consistent, despite the fact that in both cases the projections are based on IPCC approved GCMs. This is, yet again, an indication of the large uncertainty in climate projections.

Table 4.8   Projection of percentage change in precipitation in seven regions in Bangladesh in the "business-as-usual" scenario, as reported in The Bangladesh Delta Plan (GED, 2018).

	2030				
Region	**Year**	**Pre-monsoon**	**Monsoon**	**Post-monsoon**	**Winter**
Northwest	-0.1	19.9	-6.1	116.1	134
North-central	19	34.1	14.8	47.7	107.6
Northeast	13.1	7.1	15	8.1	32
Southwest	6	11.9	1.4	76.4	68.8
South-central	6.3	15.7	3.4	45.4	-6.7
Southeast	12.3	26.6	10.9	6.6	-5.1
Eastern Hills	-2.8	-20.1	1.8	-35.4	-32.9
	2050				
Region	**Year**	**Pre-monsoon**	**Monsoon**	**Post-monsoon**	**Winter**
Northwest	4.5	-18.6	5.6	28.8	119.3
North-central	16.9	-5.1	20.6	12.6	31.2
Northeast	13.2	-0.9	17.9	9.8	12.1
Southwest	-1.5	-20.3	0.7	-7.8	58.2
South-central	-2.5	-1.5	-2.1	-11.4	0.2
Southeast	5.4	9.6	5	0.6	7.2
Eastern Hills	-1.6	2.2	-1.3	-33.7	45

% increase in seasonal rainfall; results of 5 GCMs & 2 RCP scenarios
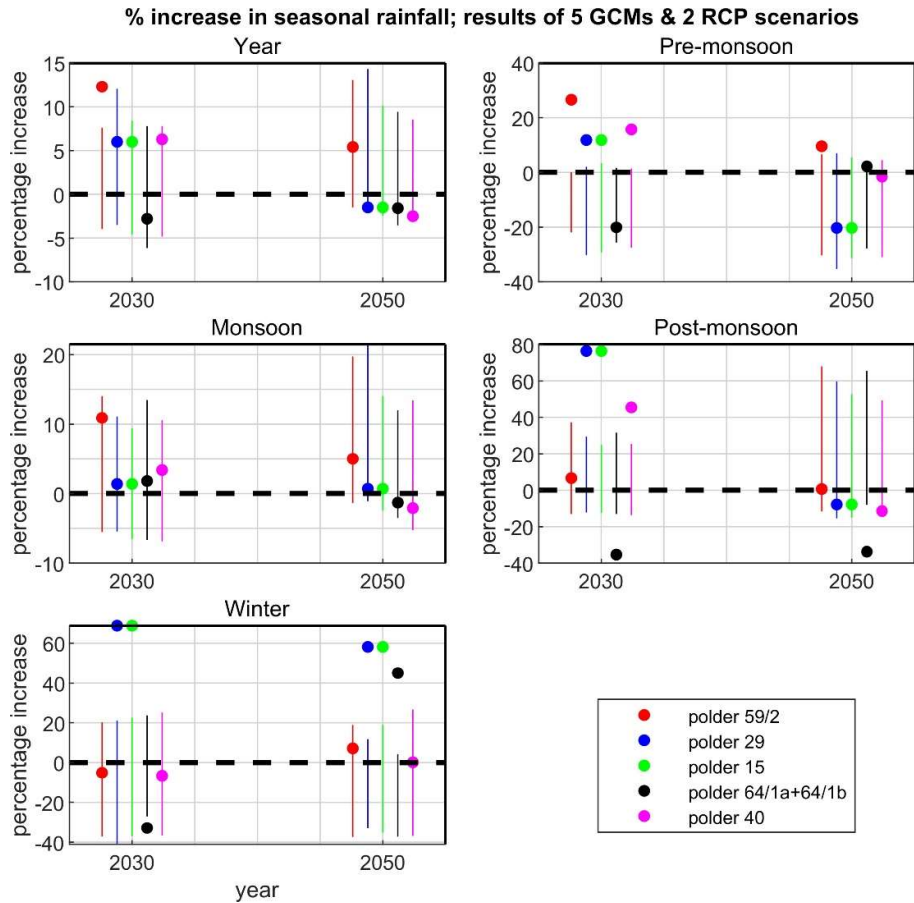
Figure 4.47 Projected percentage change in maximum daily precipitation in the 5 selected polders for 4 different seasons and for the entire year, relative to climate year 1990. Each vertical line represents the range in percentage increase for combinations of RCP-scenarios (2) and climate-models (5). The dots show the projections from the Bangladesh Delta Plan (GED, 2018).

4.4.2 Temperature

4.4.2.1 Introduction

For the downscaled future scenarios of temperature, we consider four different periods in our analyses:

- 2006-2035 (representative for the climate of the year 2020)
- 2026-2055 (representative for the climate of the year 2040)
- 2046-2075 (representative for the climate of the year 2060)
- 2066-2095 (representative for the climate of the year 2080)

Climate characteristics as derived from GCM outputs, are compared with characteristics of the reference period (1976-2005; representative for the climate year 1990) to establish projections of relative changes in climate conditions.

4.4.2.2 GBM basin

Figure 4.48 shows maps with projected increases in annual mean temperature relative to climate year 1990, according to the five GCMs in the year 2020 (period 2006-2035), assuming the RCP4.5 emission scenario. Figure 4.49 shows similar maps for the RCP8.5 scenario in the year 2080 (period

2066-2095). The models agree that temperatures are expected to increase all over the basin, but nevertheless there are clear differences in spatial patterns and spatial means. Most models indicate the largest temperature increases are expected in the Himalayas.

Figure 4.50 shows the projected increase in temperature in 5 sub-areas of the GBM basin for 4 different seasons (including the whole year). Each vertical column of dots (RCP4.5) and triangles (RCP8.5) represents the variation in increase for combinations of RCP-scenarios (2) and climate-models (5). The figure shows that projected temperatures in the RCP8.5 scenario are generally higher than the corresponding projected temperatures in the RCP4.5 scenario. Projected increases are substantial in all scenarios. The projected increases are largest for the winter season. Figure 4.51 shows similar plots for five sub-areas in the Himalayan part of the GBM basin. It shows the projected temperature increases are even larger for this part of the basin.
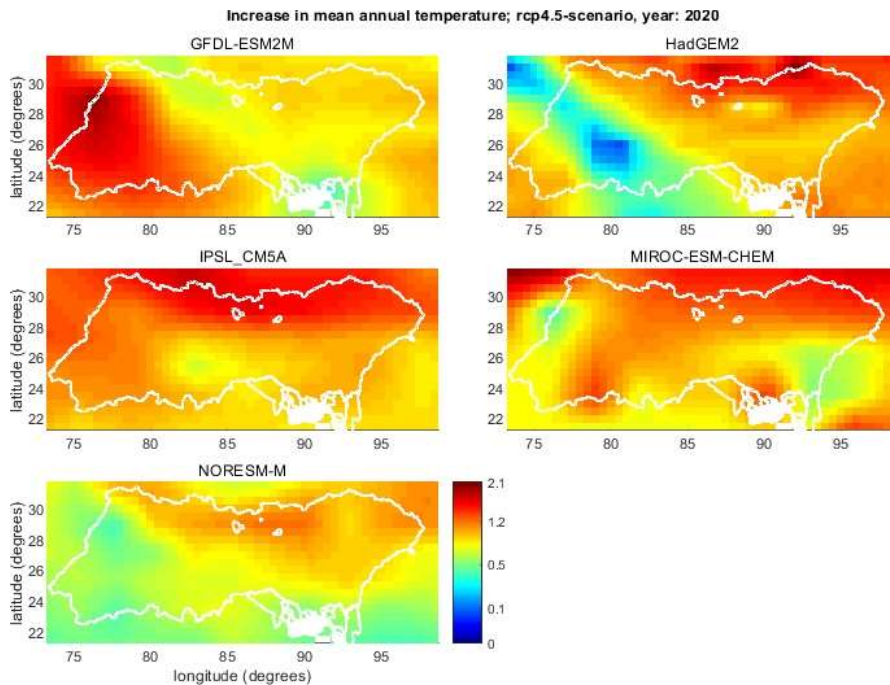
Figure 4.48   Projected absolute change in annual mean temperature relative to climate year 1990, according to five different GCMs; RCP-scenario 4.5, year 2020.

Increase in mean annual temperature; rcp8.5-scenario, year: 2080
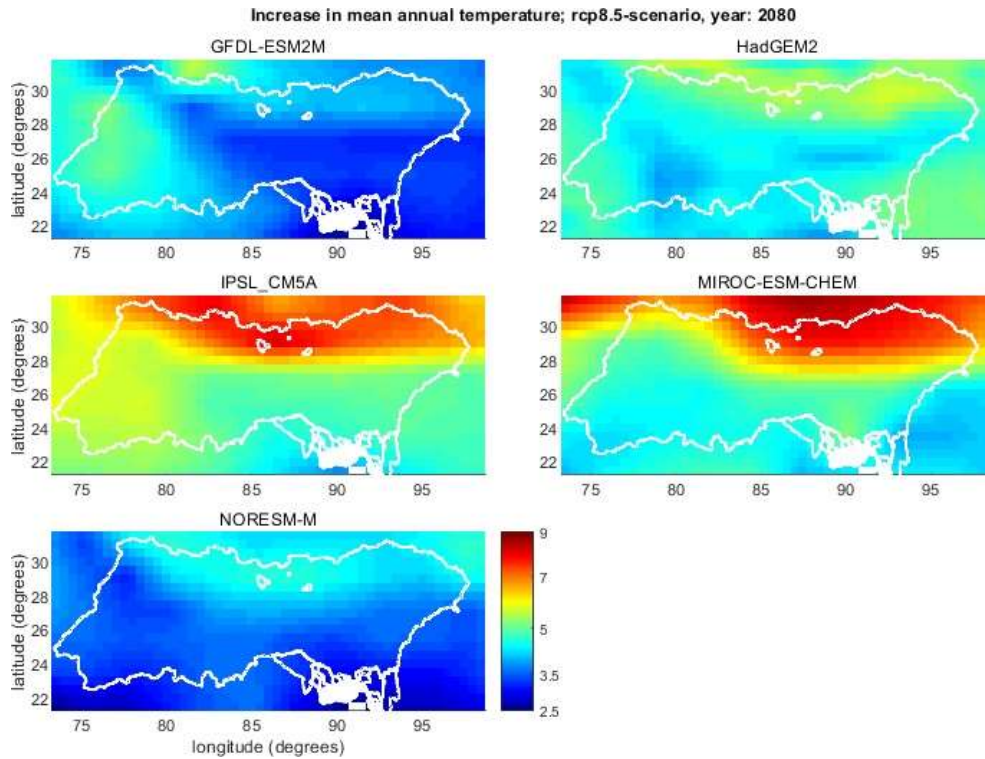
Figure 4.49   Projected absolute change in annual mean temperature relative to climate year 1990, according to five different GCMs; RCP-scenario 8.5, year 2080.
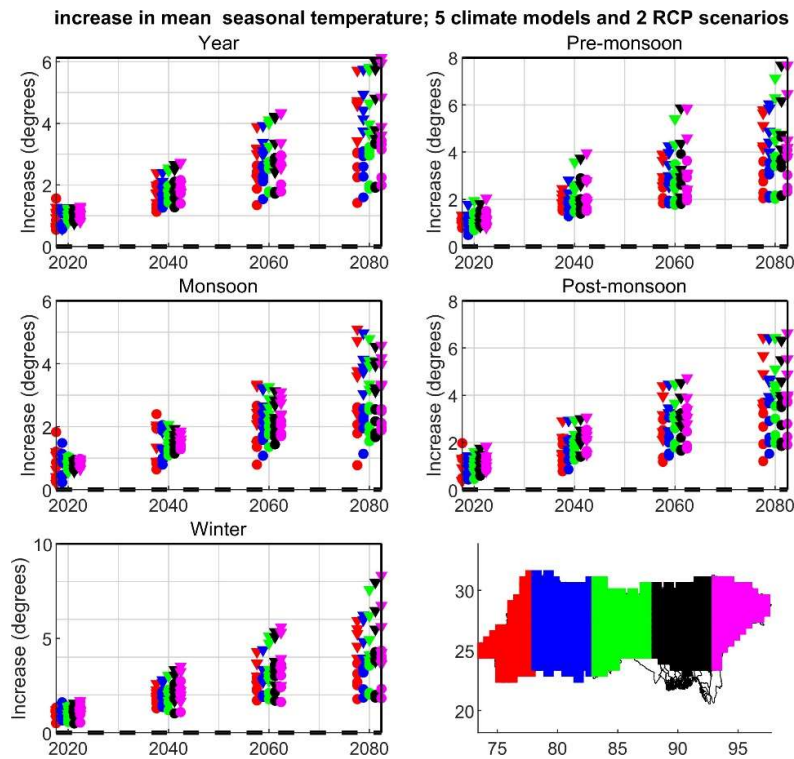
Figure 4.50   Projected change in temperature, relative to climate year 1990, in 5 sub-areas of the GBM basin for 4 different seasons and for the entire year. Each vertical column of dots (RCP4.5) and triangles

(RCP8.5) represents the variation in increase for combinations of RCP-scenarios (2) and climate-models (5).
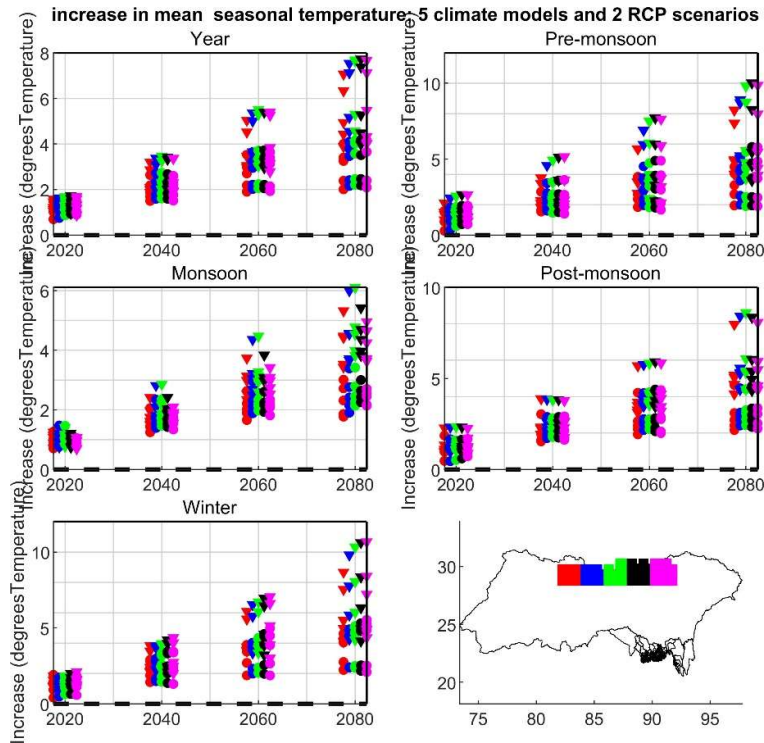
Figure 4.51   Projected change in temperature, relative to climate year 1990, in 5 subareas of the Himalayan part of the GBM basin for 4 different seasons and for the entire year. Each vertical column of dots (RCP4.5) and triangles (RCP8.5) represents the variation in increase for combinations of RCP-scenarios (2) and climate-models (5).

Figure 4.52 shows similar graphs for the Ganges and Brahmaputra basins and Table 4.9 summarizes these results. Figure 4.53 shows the graphs for the GBM basin as a whole. Results of the Ganges and Brahmaputra basin are similar. The main difference is that the Brahmaputra basin has one or two more extreme projections of temperature increase for some seasons, especially the Winter and Pre-Monsoon seasons.

increase in mean seasonal temperature; 5 climate models and 2 RCP scenarios
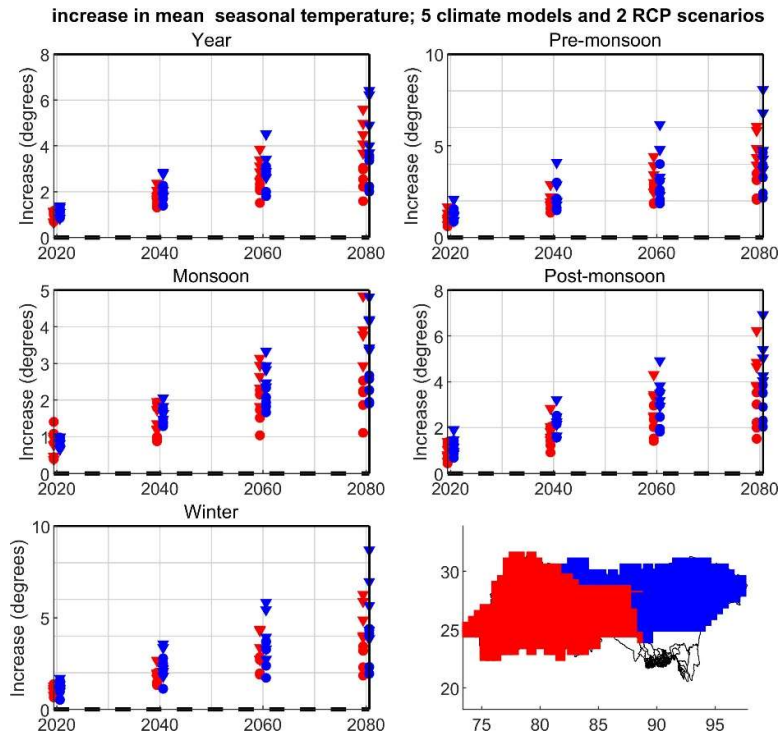
Figure 4.52   Projected change in temperature, relative to climate year 1990, in the Ganges and Brahmaputra basins for 4 different seasons and for the entire year. Each vertical column of dots (RCP4.5) and triangles (RCP8.5) represents the variation in increase for combinations of RCP-scenarios (2) and climate-models (5).

Table 4.9   Summary of projected change in temperature, relative to climate year 1990, in the Ganges and Brahmaputra basin. The table shows the minimum, mean and maximum over the 10 combinations of RCP-scenarios (2) and climate-models (5).

Season	Basin	2020			2040			2060			2080		
		min	mean	max	min	mean	max	min	mean	max	min	mean	max
Year	Ganges	0.7	0.9	1.2	1.3	1.7	2.4	1.5	2.6	3.9	1.6	3.5	5.6
	Brahmaputra	0.8	1.1	1.4	1.4	2.1	2.9	1.8	3.1	4.5	2.0	4.0	6.4
Pre-monsoon	Ganges	0.6	1.1	1.7	1.4	1.9	2.9	1.9	2.9	4.4	2.1	3.9	6.1
	Brahmaputra	0.9	1.2	2.1	1.5	2.3	4.1	1.9	3.3	6.2	2.2	4.4	8.1
Monsoon	Ganges	0.4	0.8	1.4	0.9	1.4	2.0	1.0	2.2	3.1	1.1	2.9	4.8
	Brahmaputra	0.7	0.9	1.0	1.3	1.6	2.1	1.7	2.4	3.3	1.9	3.1	4.8
Post-monsoon	Ganges	0.4	0.9	1.4	0.9	1.7	2.8	1.4	2.6	4.3	1.5	3.6	6.2
	Brahmaputra	0.7	1.2	1.9	1.6	2.1	3.2	1.8	3.1	4.9	2.0	4.0	6.9
Winter	Ganges	0.7	1.0	1.4	1.3	2.0	2.7	1.9	3.0	4.4	1.8	3.9	6.3
	Brahmaputra	0.5	1.2	1.7	1.1	2.4	3.6	1.7	3.6	5.8	2.0	4.7	8.7

modelling_report_metereology_climate_changev_2nd_submission_clean.docx / AG / 2021-06-21

increase in mean seasonal temperature; 5 climate models and 2 RCP scenarios
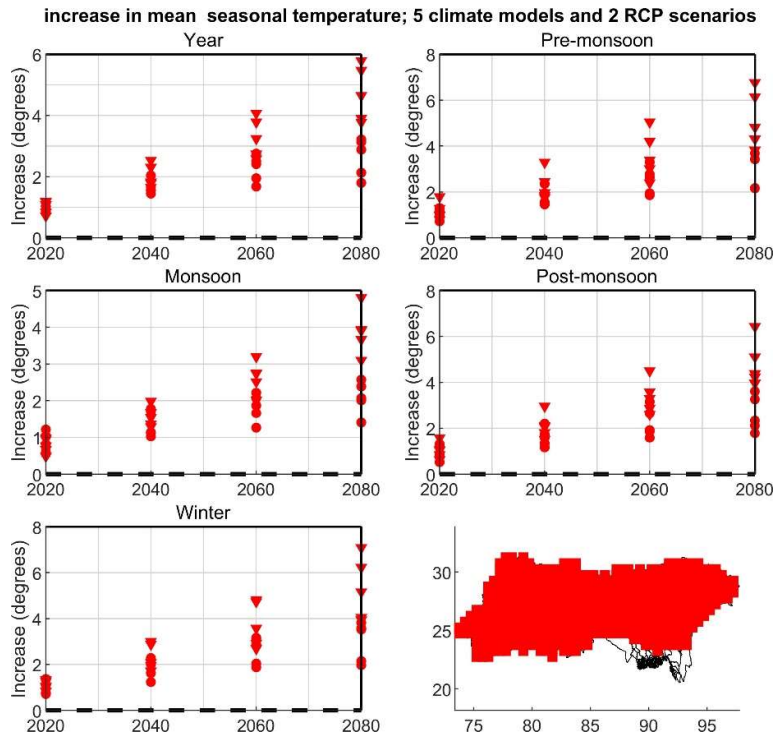
Figure 4.53   Projected change in temperature, relative to climate year 1990, in the GBM basin for 4 different seasons and for the entire year. Each vertical column of dots (RCP4.5) and triangles (RCP8.5) represents the variation in increase for combinations of RCP-scenarios (2) and climate-models (5).

4.4.2.3   Bangladesh

Figure 4.54 shows the projected increase in annual mean temperature according to five different GCMs, over Bangladesh, and according to RCP-scenario 4.5 in the year 2020. Figure 4.55 shows similar plots for the RCP8.5 scenario in the year 2080. It shows there are substantial differences between the projections of the five different GCM models. Figure 4.56 shows the projected increase in mean annual temperature at the 5 selected polders for the four different seasons and for the entire year. From these figures and underlying data, we can conclude:

- All projections indicate an increase in temperature in each season and each time horizon
- Projected temperature increases with time
- The variation between GCM results increase with time
- Projected increases for the monsoon season are generally lower than for the other seasons.
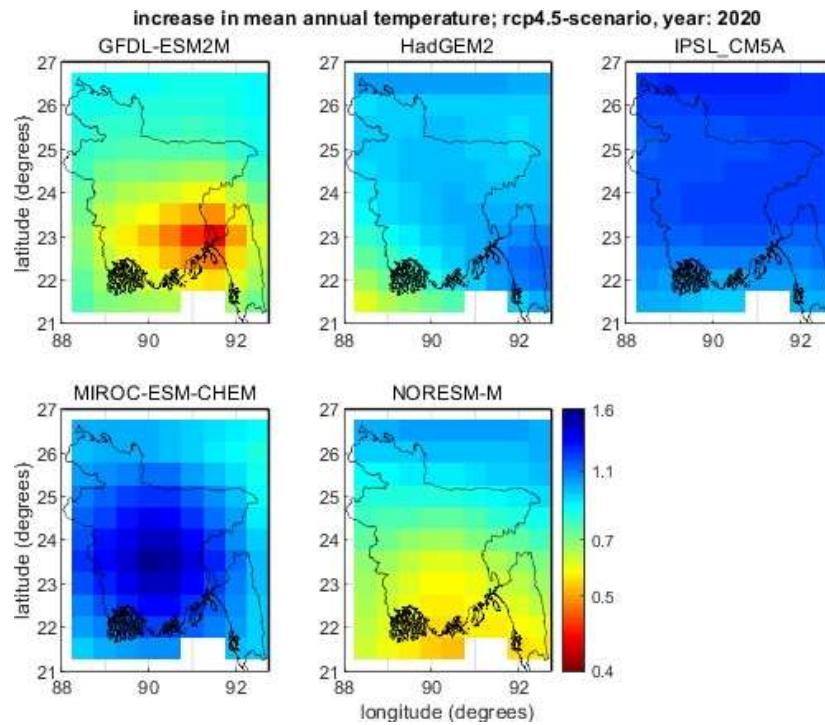
Figure 4.54   Projected change in annual mean temperature, relative to climate year 1990, according to five different GCMs; RCP-scenario 4.5, year 2020.
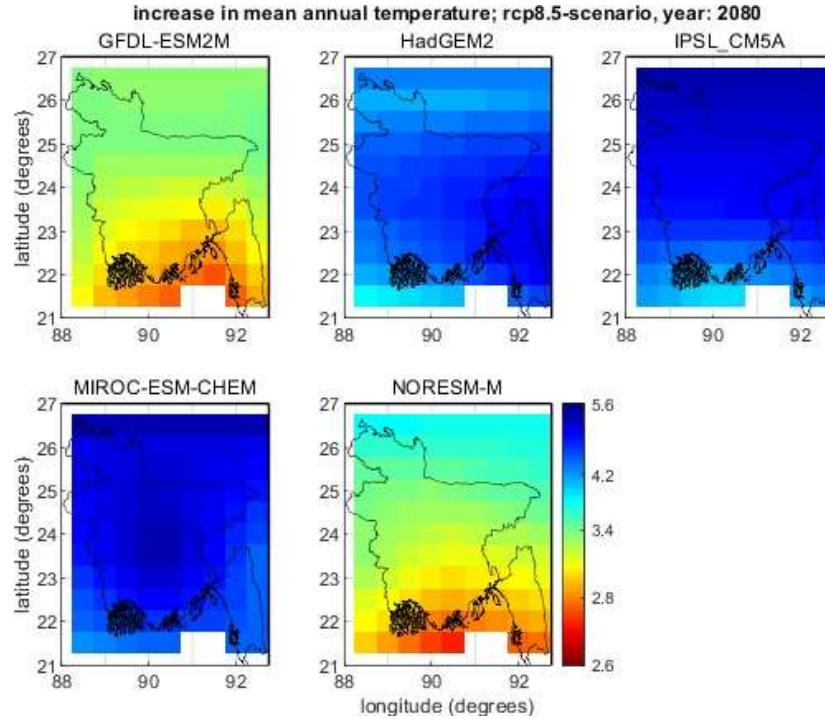
Figure 4.55   Projected change in annual mean temperature, relative to climate year 1990, according to five different GCMs; RCP-scenario 8.5, year 2080.

increase in seasonal temperature; results of 5 GCMs & 2 RCP scenarios
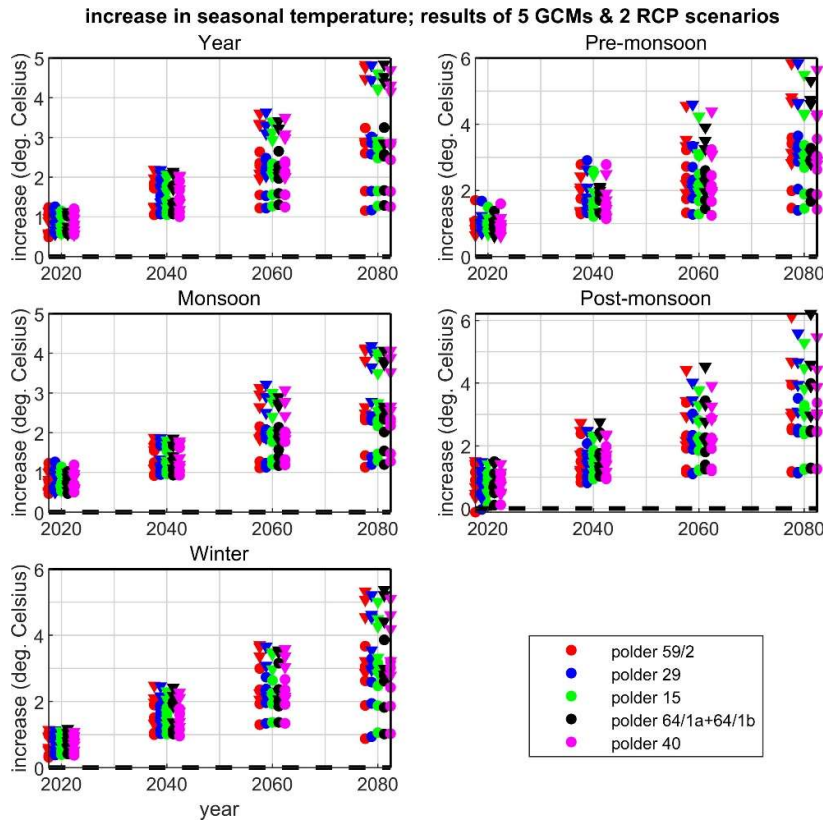
Figure 4.56   Projected change in mean annual temperature, relative to climate year 1990, in the 5 selected polders for 4 different seasons and for the entire year. Each vertical column of dots (RCP4.5) and triangles (RCP8.5) represents the variation in increase for combinations of RCP-scenarios (2) and climate-models (5).

4.4.3   Sea level rise

Regional ASLR projections were extracted at the five closest locations along the Bangladesh coast (Figure 4.57) and based on SROCC (Special Report on the Ocean and Cryosphere in a Changing Climate) regional projections (IPCC, 2019; Oppenheimer et al. 2019). This study represents the most recent published update of the IPCC AR5 report (IPCC, 2013), and before the new IPCC AR6 projections will be published. In the study, the upper bound of the likely range for a high emission scenario has been adjusted upwards with respect to the previous IPCC AR5 projections to account for new insight on climate change and resulting accelerated sea level rise.
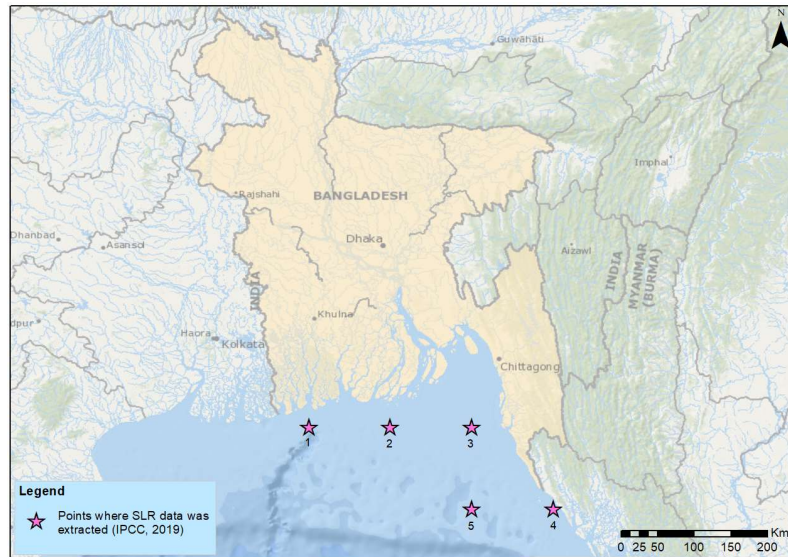
Figure 4.57   Locations at which ASLR value were extracted.

Averaged ASLR values along the Bangladesh coastline are shown in Figure 4.58, both for RCP 4.5 and RCP 8.5 scenarios and including the 5%-95% confidence interval. Predicted values at the different locations (see Figure 4.57) are shown in Table 4.10 and Table 4.11, respectively for RCP 4.5 and RCP 8.5. The values suggest relatively minor difference in ASLR at the different locations, in the order of a few centimetres only, and well within the confidence interval. Therefore, it is suggested that mean values among the different stations will be further used in the project. By 2100, predicted ASLR following an RCP 8.5 scenario, are expected to reach a mean value of 0.76 m, and with a 95% equal to 1.1 m.
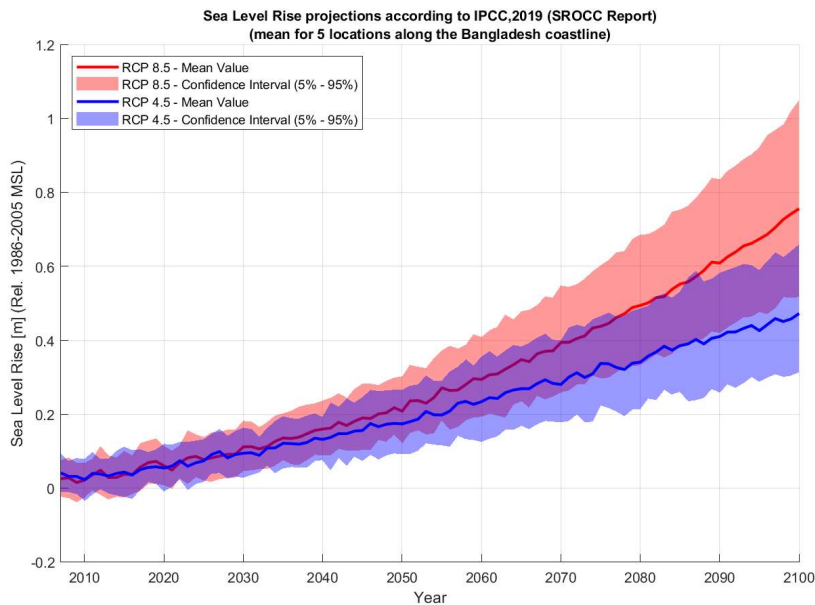
Figure 4.58   Averaged SLR projections for the 21st century and associated uncertainties.

Table 4.10 Regional and global ASLR projections for the 21st century at the five closest locations along the Bangladesh coast (Figure 4.57) and averaged values of the five locations, according to RCP 4.5 scenario. Mean values are provided in bolds while associated uncertainties (5 and 95%) are included in brackets. Long-term estimates for 2200 and 2300 are only available based on global projections (GMSL).

| Time | Total Sea Level Rise – RCP 4.5 [m] (Rel. to 1986 to 2005) | | | | | | |
	1	2	3	4	5	MEAN	GMSL
2020	**0.057** [-0.006 to 0.121]	**0.053** [-0.016 to 0.123]	**0.055** [-0.01 to 0.121]	**0.054** [-0.001 to 0.109]	**0.055** [-0.014 to 0.124]	**0.055** [-0.009 to 0.12]	**0.081** [0.057 to 0.104]
2040	**0.135** [0.067 to 0.208]	**0.137** [0.069 to 0.21]	**0.126** [0.078 to 0.179]	**0.129** [0.082 to 0.183]	**0.133** [0.088 to 0.184]	**0.132** [0.077 to 0.193]	**0.172** [0.124 to 0.221]
2050	**0.181** [0.079 to 0.297]	**0.185** [0.081 to 0.301]	**0.164** [0.09 to 0.247]	**0.164** [0.103 to 0.233]	**0.176** [0.104 to 0.255]	**0.174** [0.091 to 0.266]	**0.228** [0.165 to 0.293]
2060	**0.235** [0.115 to 0.373]	**0.234** [0.111 to 0.366]	**0.230** [0.126 to 0.345]	**0.231** [0.137 to 0.34]	**0.240** [0.137 to 0.354]	**0.234** [0.125 to 0.356]	**0.288** [0.206 to 0.373]
2080	**0.351** [0.207 to 0.515]	**0.350** [0.201 to 0.515]	**0.329** [0.211 to 0.466]	**0.336** [0.221 to 0.468]	**0.341** [0.229 to 0.47]	**0.341** [0.214 to 0.487]	**0.417** [0.296 to 0.545]
2100	**0.487** [0.301 to 0.699]	**0.489** [0.303 to 0.702]	**0.458** [0.324 to 0.627]	**0.457** [0.315 to 0.628]	**0.471** [0.323 to 0.648]	**0.473** [0.313 to 0.661]	**0.549** [0.385 to 0.724]
2200				- -			**1.03** [0.710 to 1.380]
2300				- -			**1.53** [1.020 to 2.090]

Table 4.11 Regional and global ASLR projections for the 21st century at the five closest locations along the Bangladesh coast (Figure 4.57) and averaged values of the five locations, according to RCP 8.5 scenario. Mean values are provided in bolds while associated uncertainties (5 and 95%) are included in brackets. Long-term estimates for 2200 and 2300 are only available based on global projections (GMSL).

| Time | Total Sea Level Rise – RCP 8.5 [m] (Rel. to 1986 to 2005) | | | | | | |
	1	2	3	4	5	MEAN	GMSL
2020	**0.059** [0.008 to 0.114]	**0.058** [0.007 to 0.11]	**0.059** [0.004 to 0.115]	**0.064** [0.011 to 0.118]	**0.062** [0.012 to 0.114]	**0.061** [0.008 to 0.114]	**0.085** [0.061 to 0.109]
2040	**0.165** [0.084 to 0.25]	**0.166** [0.088 to 0.251]	**0.153** [0.084 to 0.227]	**0.154** [0.09 to 0.223]	**0.162** [0.096 to 0.233]	**0.160** [0.088 to 0.237]	**0.195** [0.142 to 0.250]
2050	**0.216** [0.117 to 0.325]	**0.213** [0.112 to 0.325]	**0.197** [0.115 to 0.287]	**0.206** [0.135 to 0.284]	**0.209** [0.133 to 0.295]	**0.208** [0.122 to 0.303]	**0.268** [0.196 to 0.343]
2060	**0.295** [0.187 to 0.416]	**0.296** [0.19 to 0.416]	**0.286** [0.19 to 0.398]	**0.296** [0.197 to 0.407]	**0.299** [0.203 to 0.41]	**0.294** [0.193 to 0.409]	**0.353** [0.259 to 0.454]
2080	**0.505** [0.323 to 0.715]	**0.506** [0.326 to 0.711]	**0.475** [0.332 to 0.652]	**0.486** [0.332 to 0.672]	**0.500** [0.344 to 0.681]	**0.494** [0.331 to 0.686]	**0.568** [0.415 to 0.738]
2100	**0.764** [0.506 to 1.081]	**0.764** [0.509 to 1.078]	**0.741** [0.514 to 1.021]	**0.750** [0.521 to 1.028]	**0.760** [0.532 to 1.037]	**0.756** [0.516 to 1.049]	**0.842** [0.609 to 1.105]
2200				- -			**2.080** [1.340 to 2.920]
2300				- -			**3.700** [2.280 to 5.37]

As a reference, the scenarios reported in the Delta Plan (GED, 2018) and based on the IPCC (2013) report indicate ASLR ranging from 0.2 m up to 1.0 m in 2100. Design conditions of embankment crest levels during CEIP-I were derived assuming a RSLR of 50 cm with reference to the current situation (see e.g. IWM & Royal Haskoning, 2018) accounting for sea level rise, regional subsidence and the effect of sediment deposition from upstream rivers. In addition, embankment design included an additional allowance for initial subsidence at the embankment equal to 30 cm, to account for initial compaction, consolidation and other local effects after construction.

Recent studies have described physically plausible mechanisms leading to high-end SLR scenarios (see e.g. DeConto et al., 2016, Kopp et al., 2017), increasing the concerns about risks to high-end SLR impacts. Important mechanisms which could lead to these high-end SLR scenarios are an accelerated ice mass-loss from Antarctica and Greenland as a result of both surface and basal melt and ice sheet instabilities. A recent expert judgement study by Bamber et al. (2019) argued that a global SLR of 2 m by 2100 lies within the 90% confidence range. Haasnoot el al. (2020) used low likelihood but plausible high-end SLR scenarios to assess the potential consequences for coastal adaptation in The Netherlands, focusing on coastline, flood risk and fresh water resources management. According to these scenarios, under the high-emission scenario RCP 8.5, leading to an increase of global temperature of 3.2°C - 5.4°C, sea level could rise up to 3 m in 2100 (median value 1.95 m). The main conclusion from the study is that high and accelerated SLR scenarios will lead to a very short time to adapt, having large consequence for decision making. Therefore, we suggest also the inclusion of high-end SLR scenario for further use in the project and for long-term planning purposes.

4.4.4 Cyclone frequency and intensity

The effect of changes in cyclone frequency and intensity on water level and wave conditions at the polders will be analysed in detail in the deliverables part of Component-4D ("The effect of climate change on water levels, salinity intrusion and storm surges"). In this section, we will describe plausible scenarios for possible changes in cyclone frequency and intensity supported by recent literature and data analysis (section 3.2.4 and 3.3.3).

Considering that cyclones depend on warm sea temperatures and the difference between temperatures at the ocean and in the upper atmosphere, it is likely that if global warming increases temperatures at the earth's surface but not the upper atmosphere, tropical cyclones will be provided with more power (Emmanuel et al. 2008). This will be then also reflected in the (relative) increase of the number of intense cyclones.

To account for a possible increase in tropical cyclone (TC) intensity as a result of climate change effects, design conditions of crest levels during CEIP-I were derived assuming an increase of 10% in maximum TC wind speed (see e.g. IWM & Royal Haskoning, 2018; Islam et al., 2013).

Knutson et al. (2015) carried out a numerical modelling study to assess projection in TC frequency and intensity for different oceanic basins. CMIP5 multi-model ensembles were used to compare conditions under RCP 4.5 for the late twenty-first century to the period 1982-2005. For the North Indian Ocean, an average increase in the frequency of all TCs (cat. 0-5) equal to 19.5% was found and of 25.6% for TCs (cat. 1-5). This was also accompanied by an increase in TC lifetime maximum intensity for TCs of all categories 1-5 and equal to 1.6%, and a precipitation rate increase of 10.5% (cat. 0-5) and 12.8% (cat. 1-5). Such increases are all well within the range of projected changes in precipitation of section 4.4.1.3 (see, for example, Figure 4.46).

Sugi et al (2017) further investigated the possible change in TC due to climate change. The authors found a decrease in frequency of 10.1% over all TC categories (cat. 0-5) for the northern Indian Ocean. However, for the more intense TC, an increase in yearly cyclone frequency was predicted (i.e. 4.4% increase for cat. 1-5, 21.1% for cat. 3-5 and 21.2% for cat. 4-5). Although not all changes are statistically significant, the trends towards an increase in frequency of the most intense events is consistent to the trends reported by Knutson et al (2015) as well as our data analysis presented under Section 4.2.4.

Knutson et al. (2019, 2020 and 2021) provided the most recent updates of TC climate change assessment after the IPCC AR5. Projections are derived based on changes in TC activity associated with an anthropogenic warming of the order of 2°C. To provide some context, a mean 2°C global mean surface temperature increase, according to CMIP5 climate models, would be reached by around mid-century under the RCP 8.5 scenario. According to the authors, a +2°C warming scenario is projected to yield to a global +5% increase (range: 1% - 10%) in maximum wind speed when considering all TC categories. For very intense TCs (category 4 and 5), there is a medium-to-high confidence that the median projected change could reach about +13%. Regional projections for the North Indian Ocean indicate a median change in frequency for all TC equal to about -5%, with an interquartile range equal to -15% / +6% and with a 5th/95th percentiles equal to about -35% / +30%. When looking at the very intense TC only (cat 4-5), the prediction suggests a mean increase in frequency of about +5% with an interquartile range equal to -15% / +40% and a 10th/90th percentile equal to -70% / +80%.

Changes in TC intensity suggest an overall increase of about +4% with an interquartile range equal to +2% / +6% and a 10th/90th percentile equal to -1% and +8%. Change in TC induced precipitation suggest a median increase equal to about +18% with an interquartile range equal to +14% / +19% and a 10th/90th percentile equal to +12% and +20%.

Leijnse et al. (submitted) modelled the possible effect that changes in TC intensity and frequency could have on predicted water levels and waves around the Bay of Bengal. The assessment was carried out using synthetic tropical cyclone tracks generated with the TCWiSE Tool (Tropical Cyclone Wind Statistical Estimation; Nederhoff et al. 2021). Climate change scenarios based on Knudson et al. (2015) were used as a basis for the assessment (i.e. +25.6% in TC frequency and +1.6% in TC intensity). Based on 4000+ synthetic cyclones simulations carried out on a rather coarse (but computational efficient) hydrodynamic and wave model, the authors concluded that the effect of climate change on TCs could lead to a possible increase in storm surge height ranging between 6% and 11%, depending on the return period analysed, and between 6% and 9% in offshore wave height along the Bangladesh coast.

Regarding the exact values of increase there is still uncertainty in literature since not all changes modelled by climate models have been found to be statistically significant for the north Indian Ocean, though the trends seem consistent, as discussed by Walsh et al. (2015). Future research will continue to improve predictions as discussed by Walsh et al. (2020).

5 Conclusions and proposed climate scenarios

5.1 Conclusions

The main conclusions from the study have been summarized in the following sub-sections for each different variable analysed in this report. Based on these conclusions, a number of suggestions for possible climate scenarios to be further used in the study are identified.

5.1.1 Precipitation

An analysis of historical precipitation and temperature records, available for the period 1948-2007 for ~30 stations in Bangladesh, revealed a number of statistically significant trends. Several tests indicate that the winter season has an overall negative trend in precipitation, whereas the post-monsoon season and the whole year have an increasing trend. Note that this conclusion is based on the combination of all stations, individual stations sometimes have trends that are opposite of the general trend.

- Measured past precipitation data over Bangladesh indicate a slightly increase in monsoon rainfall, annual and maximum daily rainfall. On the other hand, winter rainfall appeared to decrease overall (drier winters).

- Future projections by most models indicate a tendency over Bangladesh towards an increase in monsoon and annual precipitation but accompanied by drier winters.

- The range in projected changes in annual mean precipitation in Bangladesh is about 15% in 2020 (-5% to +10%), 20% in 2040 (-10% to +10%), 30% in 2060 (-10% to +20%) and 30% in 2080 (-5% to +25%)

- The conclusions for Bangladesh are also valid for the five polders analysed in detail under this project (15, 29, 40 (1&2), 59/2, 64/1a and 64/1b). In particular at these polders an increase in precipitation in the monsoon season after 2050 is observed, and a decrease in precipitation in the winter season.

- Differences in future projections based on our study and as reported in the Delta Plan are observed (see Figure 4.47).

- For the GBM basin as a whole, future projections by most models indicate an increase in monsoon precipitation as well, and a decrease in winter precipitation. Projected percentage changes for the Ganges basin are larger than for the Brahmaputra basin.

5.1.2 Temperature

- Measured past temperature data over Bangladesh indicate an overall increase in mean temperature, mostly as a result of an increase in mean and maximum temperature during monsoon and post-monsoon seasons. More variability can be seen during pre-monsoon and winter. Overall, this suggests a trend towards warmer and wetter monsoon and post-monsoon, and towards (slightly) colder and drier winters.

- Future projections for different models are consistent, indicating a temperature increase over the entire GBM basin. Increases are largest in winter and especially in the Himalaya region.

- The RCP 8.5 scenarios is projected to causes bigger temperature increases than the RCP 4.5 scenario.

- Also, for Bangladesh there is consistency among all models towards a clear increase in future temperature in all seasons.

5.1.3 Sea level rise

- Relative sea level rise across the GBM delta can be locally several time larger than global absolute sea level rise as a result of local subsidence (see e.g. Syvitski et al., 2009; Becker et al., 2020, Steckler et al., 2021).

- It is expected that the effect of subsidence will have a similar (or locally even larger) effect than absolute sea level rise in the future, at least in the short- and medium-term (see Table 5.4).

- Differences in absolute sea level rise scenarios across the delta are minimal (Table 4.10 and Table 4.11) and can be well approximated by one averaged value. However, local differences in relative sea level rise are important and are related to local differences in subsidence levels. In addition, changes in high water, tidal range and mean water levels within (some of) the river channels and resulting from long-term morphological processes can be locally much larger than the rise in global absolute sea level rise (see Deliverable D4A-2; "Effect of human interventions on tidal and sediment dynamics in the Pussur-Sibsa basin").

- Regional absolute sea level rise projections following SROCC data (IPCC, 2019; Oppenheimer et al. 2019), indicate mean sea level rise values by 2100 for Bangladesh equal to 0.473 m (95% = 0.661m) according to RCP4.5 and 0.756 m (95% = 1.049m) according to RCP8.5 (see Table 4.10 and Table 4.11).

- Recent studies have described physically plausible mechanisms leading to high-end SLR scenarios as a result of accelerated ice mass-loss from Antarctica and Greenland. These processes could lead to a median value increase in mean sea level up to (or beyond) 2 m by 2100 (Section 4.4.3). It is advisable to take these high-end values into account in the long-term planning of the polders across the GBM delta.

5.1.4 Cyclone frequency and intensity

- Warming of the surface oceans as a result of climate change is likely fuelling more powerful TCs.

- Analysis of historical data from 1972 in the North Indian Ocean and Bay of Bengal indicates that the number of most sever cyclones (cat 4-5) has increased over time. Differently, the total number of cyclones does not show a clear trend over time and may even have decreased in time.

- Future changes in TC frequency and intensity depends on the chosen scenario. The most recent regional projections by Knutson et al. (2019, 2020) are derived assuming a 2°C global mean surface temperature increase. These projections indicate, for the North Indian Ocean, a median change in frequency for all TC equal to about -5%, with an interquartile range equal to -15% / +6%, and with a 5th/95th percentiles equal to about -35% / +30%. When looking at the very intense TC only (cat 4-5), the prediction suggests a mean increase in frequency of about +5% with an interquartile range equal to -15% / +40% and a 10th/90th percentile equal to -70% / +80%.

- Following Knutson et al. (2019, 2020), changes in TC intensity suggest an overall increase of about +4%, with an interquartile range equal to +2% / +6%, and a 10th/90th percentile equal to -1% and +8%.

- Following Knutson et al. (2019, 2020), changes in TC induced precipitation suggest a median increase equal to about +18%, with an interquartile range equal to +14% / +19%, and a 10th/90th percentile equal to +12% and +20%.

- TCs induced precipitations are projected to increase due to enhanced atmospheric moisture associated with anthropogenic global warming.

- According to global CMIP5 climate models, as applied in Knutson et al. (2020) a mean 2°C surface temperature increase will be reached around mid-century, under RCP 8.5 scenario. It is likely that these temperature increase will be largely exceeded by the end of the century. However, the uncertainties are currently too large to provide reliable projections for more extreme scenarios, which could be valid for larger temperature increases.

- The impact of individual TCs will be largely amplified by rising sea levels.

5.2 Proposed scenarios to be applied in upcoming deliverables

As described in this report, uncertainties in climate change projections are large, depending on the climate model used. For this reason, multiple climate change scenarios have been considered in this report. It is noted that these projections are regularly updated over time. For example, new updated projections will be published in 2022, by the IPCC Sixth Assessment Report (AR6).

In addition, different scenarios are used for different purposes, for example depending on whether the scenario is used for the design of a specific structure or for long-term planning purposes, and also according to the life-time of the structure to be designed. Also, how a specific variable is described in the scenario depends on the specific application (e.g. averaged precipitation values may be relevant to assess fresh water availability, while extreme values may be more relevant for a flood assessment study).

Therefore, in this section we will provide a "generic" and "fixed" set of plausible scenarios based on the information analysed as part of this report and most recent literature, and which can be used for different applications as part of this project and in follow-up deliverables. "Fixed" means that they will not be linked to a specific year, but rather provide a range of plausible values, while the year can be computed based on the climate projections used. This will allow testing how the system may respond to different changes, following a "tipping point approach" (Kwadijk et al., 2010).

5.2.1 Precipitation

5.2.1.1 Daily mean precipitation

A 'low', median' and 'high' scenario of the percentage change in daily mean precipitation is proposed for:

- five polders;

- four seasons and the whole year;

- three time horizons.

The numbers represent the percentage change in daily mean precipitation, relative to the year 2020. The low, median and high scenarios correspond to 20-, 50- and 80-percentiles of the changes derived from the various GCM runs.

Table 5.1   Proposed precipitation scenarios for the five selected polders. The numbers represent the percentage change in daily mean precipitation, relative to the year 2020.

	Year:	2040			2070			2100		
	Scenario:	low	median	high	low	median	high	low	median	high
Year	polder 59/2	-6.2	-0.1	5.2	-0.5	5.9	15.9	3.0	11.5	21.2
	polder 29	-4.6	0.8	7.8	-0.1	6.5	16.6	5.0	9.8	22.2
	polder 15	-5.2	-0.8	6.6	-0.5	5.2	13.6	2.8	10.0	17.6
	polder 64/1a+64/1b	-4.5	-1.2	4.4	-1.1	5.7	10.3	1.5	7.8	12.8
	polder 40	-6.2	-1.1	5.9	-1.1	5.3	13.4	3.0	10.4	18.2
Pre-monsoon	polder 59/2	-17.1	-4.4	3.1	-7.6	6.5	17.7	8.2	17.9	23.8
	polder 29	-15.5	-3.5	8.1	-4.8	8.0	26.8	7.5	24.7	31.6
	polder 15	-12.5	-0.6	5.1	-3.7	8.7	27.7	8.0	22.0	33.2
	polder 64/1a+64/1b	-15.4	-5.4	-1.5	-8.1	2.6	17.9	0.7	7.3	28.7
	polder 40	-12.3	-1.1	4.3	-5.5	8.1	23.3	8.8	24.5	30.0
Monsoon	polder 59/2	-3.6	1.7	7.0	1.2	5.1	15.8	8.0	10.4	23.4
	polder 29	-4.0	1.2	8.6	0.5	5.5	16.4	7.1	12.4	25.3
	polder 15	-4.7	0.3	6.9	-0.1	4.0	13.8	6.5	9.2	19.6
	polder 64/1a+64/1b	-2.8	0.0	5.8	-1.8	5.4	11.2	0.4	9.0	13.0
	polder 40	-4.6	0.7	6.6	-0.6	4.0	14.3	5.0	9.0	18.9
Post-monsoon	polder 59/2	-21.2	0.3	17.7	-12.1	4.9	26.6	-13.6	4.6	30.1
	polder 29	-22.9	1.5	19.7	-12.3	5.4	27.7	-17.4	4.7	30.8
	polder 15	-23.0	1.2	18.5	-13.2	5.2	27.3	-16.2	5.2	30.7
	polder 64/1a+64/1b	-16.2	-0.4	10.5	-14.0	6.2	24.2	-10.6	7.1	24.8
	polder 40	-22.5	-1.3	19.6	-11.3	4.8	25.9	-12.5	5.9	30.9
Winter	polder 59/2	-9.6	14.1	39.4	-40.1	8.0	49.6	-67.6	-15.8	15.9
	polder 29	-8.1	8.1	43.1	-37.4	5.2	37.3	-55.8	-7.1	13.1
	polder 15	-8.9	8.8	40.5	-40.5	2.8	34.9	-57.9	-11.2	12.7
	polder 64/1a+64/1b	-11.5	6.3	24.2	-36.3	-10.0	47.2	-56.3	-14.8	15.8
	polder 40	-9.8	13.2	42.6	-43.9	4.0	39.9	-66.1	-13.9	12.6

5.2.1.2 Annual maximum daily precipitation

For rainfall-induced flood studies, the annual maximum daily precipitation is a better indicator. A 'low', median' and 'high' scenario of the percentage change in annual maximum daily precipitation are proposed for:

- five polders;

- the whole year;

- three time horizons.

The difference with section 5.2.1.1 is that no scenarios are derived for the various seasons, only for the whole year. The numbers represent the percentage change in annual maximum daily precipitation, relative to the year 2020. The low, median and high scenarios correspond to 20-, 50- and 80-percentiles of the changes derived from the various GCM runs.

Table 5.2 Proposed precipitation scenarios for the five selected polders. The numbers represent the percentage change in annual maximum daily precipitation, relative to the year 2020.

	Year:	2040			2070			2100		
	Scenario:	low	median	high	low	median	high	low	median	high
Year	polder 59/2	-9.2	-1.1	10.2	-0.3	10.6	28.3	7.8	19.0	37.4
	polder 29	-2.1	1.5	13.8	-1.5	7.5	25.1	2.8	10.7	26.6
	polder 15	-2.8	2.6	14.1	-0.5	8.2	23.0	6.0	18.1	26.8
	polder 64/1a+64/1b	-7.9	0.3	7.3	-0.8	10.4	23.2	5.1	13.6	26.7
	polder 40	-7.1	0.8	12.2	-3.6	7.6	23.0	3.4	14.3	28.2

5.2.2 Temperature

A 'low', median' and 'high' scenario of the change in daily mean temperature are proposed for:

- five polders;

- four seasons and the whole year;

- three time horizons.

The numbers represent the change in daily mean temperature in degrees, relative to the year 2020. The low, median and high scenarios correspond to 20-, 50- and 80-percentiles of changes derived from the various GCM runs.

Table 5.3   Proposed temperature scenarios for the five selected polders. The numbers represent the change in daily mean temperature in degrees, relative to the year 2020.

	Year:	2040			2070			2100		
	Scenario:	low	median	high	low	median	high	low	median	high
Year	polder 59/2	0.6	0.7	1.0	1.1	1.5	2.3	1.3	2.2	3.6
	polder 29	0.6	0.7	1.0	1.0	1.4	2.2	1.3	2.2	3.5
	polder 15	0.6	0.7	0.9	1.0	1.4	2.1	1.2	2.1	3.3
	polder 64/1a+64/1b	0.5	0.7	1.0	1.0	1.5	2.2	1.3	2.2	3.5
	polder 40	0.6	0.7	0.9	1.0	1.4	2.1	1.2	2.1	3.3
Pre-monsoon	polder 59/2	0.5	0.7	1.1	1.0	1.5	2.4	1.5	2.2	3.8
	polder 29	0.5	0.7	1.2	0.9	1.6	2.4	1.4	2.2	3.7
	polder 15	0.5	0.6	1.0	0.9	1.5	2.2	1.3	2.1	3.4
	polder 64/1a+64/1b	0.5	0.7	1.1	1.0	1.4	2.4	1.3	2.1	3.7
	polder 40	0.5	0.6	1.1	0.9	1.5	2.1	1.3	2.1	3.3
Monsoon	polder 59/2	0.4	0.6	0.8	0.7	1.2	1.9	1.0	1.8	3.1
	polder 29	0.4	0.6	0.8	0.7	1.3	1.9	0.9	1.8	3.1
	polder 15	0.4	0.6	0.8	0.7	1.2	1.8	0.9	1.8	2.9
	polder 64/1a+64/1b	0.4	0.6	0.8	0.7	1.2	1.9	0.9	1.8	3.0
	polder 40	0.4	0.6	0.8	0.7	1.2	1.8	1.0	1.7	2.9
Post-monsoon	polder 59/2	0.6	0.9	1.0	1.1	1.7	2.1	1.3	2.5	3.2
	polder 29	0.6	0.9	1.0	1.1	1.7	2.1	1.3	2.5	3.2
	polder 15	0.6	0.8	1.0	1.0	1.7	2.0	1.2	2.4	3.1
	polder 64/1a+64/1b	0.6	0.8	0.9	1.1	1.6	2.0	1.3	2.4	3.2
	polder 40	0.6	0.8	1.0	1.1	1.6	2.0	1.2	2.4	3.1
Winter	polder 59/2	0.7	0.8	1.1	1.3	1.7	2.5	1.6	2.5	3.8
	polder 29	0.7	0.8	1.1	1.3	1.6	2.4	1.5	2.4	3.6
	polder 15	0.7	0.8	1.0	1.3	1.5	2.3	1.4	2.3	3.5
	polder 64/1a+64/1b	0.7	0.8	1.1	1.3	1.6	2.4	1.5	2.3	3.8
	polder 40	0.6	0.7	1.0	1.3	1.5	2.3	1.4	2.3	3.5

5.2.3 Sea level rise

For sea level rise, we suggest using a set of four different ASLR scenarios (0.25m, 0.5m, 1.0m and 2.0 m) as described in Table 5.4, depending on the application. The table indicates when the ASLR scenario may be reached, based on SROCC projections (IPCC, 2019; Oppenheimer et al. 2019), according to RCP 4.5 and RCP 8.5 scenarios, and for three different percentile values (5%, median and 95%). Note that as regional projections are only available up to 2100, values beyond this year are based on global projections (Table 4.10 and Table 4.11). As described in Section 5.1.3, these fixed values could be exceeded even earlier if the most extreme accelerated ASLR scenarios will materialize. The table also indicates the estimated subsidence value for each of the four coastal regions and which, depending on the application, should be added to the ASLR in order to get a total RSLR. For Western Ganges (W), Eastern Ganges (E) and Meghna (M) maximum subsidence values are based on Becker et al. (2020) (see Table 4-4), while for Chittagong values are derived based on Ostanciaux et al. (2012) and equal to 6 mm/year, as these are not available from Becker at al. (2020). Note that new subsidence estimates, based on new data collected as part of this project, are also being derived and they will be described as part of Component-4B. Preliminary estimates suggest that subsidence values may be up to ≈15 mm/year in areas of active sedimentation, while values expected for buildings and embankments are lower, and up to ≈ 8 mm/y (Steckler et al., 2021). The differences in reported values between Becker et al. (2020) and Steckler et al. (2021) are most likely related to the different measurement techniques used to collect these measurements (Section 4.2.3).

While ASLR values of 0.25 m and 0.5 m will be relevant for applications with time-scale of decades, as indicated by the exceedance years in Table 5.4, ASLR values of 1.0 and 2.0 m, will be relevant for long-term planning purposes (i.e. 100 years and beyond) or to assess the long-term morphological responses of the GBM delta system to SLR (e.g. deliverable D4A-1).

Design conditions of embankment crest levels during CEIP-I were derived assuming a RSLR of 50 cm with reference to the current situation and which would account for absolute sea level rise, regional subsidence and effect of sediment deposition from upstream rivers (see e.g. IWM & Royal Haskoning, 2018). This value was used for example in CEIP-I as input in the storm surge and wave modelling, across the Bay of Bengal, which was then used to derive the design conditions. Note that the effect of sediment deposition from upstream rivers has an opposite effect than subsidence and could even offset subsidence in case of sufficient sediment input and homogeneous redistribution across the delta. In addition, embankment design in CEIP-I included an additional allowance for initial subsidence at the embankment equal to 30 cm, to account for initial compaction, consolidation and other local effects after construction.

When comparing a RSLR value of 50 cm with the exceeding years as presented in Table 5.4, one can see that a 50 cm value may be sufficient to derive design conditions for a planning scenario of about 20-30 years, depending on the emission scenario and specific subsidence rate. However, design conditions for a longer timeframe (e.g. 50 years) should take into account higher RSLR and up to ≈ 90-100 cm.

Table 5.4 Proposed regional absolute sea level scenarios (i.e. 0.25m, 0.5m, 1.0m and 2.0m) and approximate year when the sea level rise may be reached according to RCP4.5 and RCP8.5 scenarios, based on SROCC projections (IPCC, 2019; Oppenheimer et al. 2019). Years are estimated respectively for a 5, 50 and 95 percentile. In addition to the year when the absolute sea level rise will be reached, subsidence values are provided for each coastal region (W=Western Ganges; E=Eastern Ganges; M=Meghna; C=Chittagong) and estimated based on Becker et al. (2020) (i.e. for E, W, and M) and Ostanciaux et al. (2012) for C.

	%	MSL	0.25 m				0.50 m				1.00 m				2.00 m			
RCP 4.5	5	Year	2083				2147				2294				2416			
		Zone	W	E	M	C	W	E	M	C	W	E	M	C	W	E	M	C
		VLM	0.19	0.55	0.41	0.47	0.34	0.99	0.74	0.85	0.69	2.02	1.50	1.73	0.99	2.88	2.14	2.47
	50	Year	2063				2105				2195				2394			
		Zone	W	E	M	C	W	E	M	C	W	E	M	C	W	E	M	C
		VLM	0.14	0.41	0.30	0.35	0.24	0.70	0.52	0.60	0.46	1.33	0.99	1.14	0.93	2.72	2.02	2.33
	95	Year	2046				2082				2148				2288			
		Zone	W	E	M	C	W	E	M	C	W	E	M	C	W	E	M	C
		VLM	0.10	0.29	0.21	0.25	0.18	0.54	0.40	0.46	0.34	1.00	0.74	0.86	0.68	1.98	1.47	1.70
RCP 8.5	5	Year	2070				2098				2159				2271			
		Zone	W	E	M	C	W	E	M	C	W	E	M	C	W	E	M	C
		VLM	0.16	0.46	0.34	0.39	0.22	0.65	0.48	0.56	0.37	1.08	0.80	0.92	0.64	1.86	1.38	1.60
	50	Year	2055				2081				2119				2194			
		Zone	W	E	M	C	W	E	M	C	W	E	M	C	W	E	M	C
		VLM	0.12	0.35	0.26	0.30	0.18	0.53	0.40	0.46	0.27	0.80	0.59	0.68	0.45	1.32	0.98	1.13
	95	Year	2042				2068				2099				2151			
		Zone	W	E	M	C	W	E	M	C	W	E	M	C	W	E	M	C
		VLM	0.09	0.26	0.19	0.22	0.15	0.44	0.33	0.38	0.23	0.66	0.49	0.56	0.35	1.02	0.76	0.88

5.2.4 Cyclone frequency and intensity

Based on the analysis as described in Section 4.4.4 and in particular the most recent values presented in Knutson et al. (2020), the following scenarios are suggested as described in Table 5-5:

a) A low scenario (roughly corresponding to the mean regional scenario by Knutson et al. (2020)) in which the frequency of TCs of category 4 and 5 is increased with +4% and the intensity with +5%.

b) A high scenario (roughly corresponding to the 90% regional scenario by Knutson et al. (2020)) in which the frequency of TCs of category 4 and 5 is increased with 80% and the intensity with +8%.

To account for a possible increase in TC intensity as a result of climate change effects, design conditions of crest levels during CEIP-I were derived assuming an increase of 10% in maximum TC wind speed (see e.g. IWM & Royal Haskoning, 2018; Islam et al., 2013). It is expected that this value will provide lower estimates of extreme storm surge and wave conditions than the high scenario as suggested in Table 5-5. However, given the fact that the projections by Knutson et al. (2020), used as a basis for this table, were derived assuming a 2°C temperature increase, and considering that this temperature increase is likely to be exceeded by mid-century, it seems plausible that also a more extreme scenario as in Table 5-5 should be considered.

Table 5-5 Suggested scenarios of TC changes, both for frequency and intensity (maximum sustained wind speed).

	Low	High
Frequency	+4% TC (cat 4-5)	+80% TC (cat 4-5)
Intensity	+ 5%	+8%

6 References

/1/ Ahmed, M., Suphachalasai, S., 2014. Assessing the Costs of Climate Change and Adaptation in South Asia. Mandaluyong City, Philippines: Asian Development Bank, 2014.

/2/ Alam, M.A., Hossain, A., and Shafee, S., 2003. Frequency of Bay of Bengal Cyclonic Storms and Depression Crossing Different Coastal Zones. *International Journal of Climatology*. 23, 1119-1125. DOI: 10.1002/joc.927.

/3/ Alam, E., Dominey-Howes, D., 2014. A new catalogue of tropical cyclones of the northern Bay of Bengal and the distribution and effects of selected landfalling events in Bangladesh. *International Journal of Climatology*. 35, 801-835. DOI: 10.1002/joc.4035.

/4/ Bamber, J.L., Oppenheimer, M., Kopp, R.E., Aspinall, W.P. and Coole, R.M., 2019. Ice sheet contributions to future sea-level rise from structures expert judgement. Proc. Natl. Academ. Sci., 116, 11195-200.

/5/ Bhatla, R., Raj, R., Shivani, 2019. Tropical cyclones over the North Indian Ocean in changing climate. Techniques for Disaster Risk Management and Mitigation, Geophysical Monograph 244. American Geophysical Union. Published by John Wiley & Sons, Inc.

/6/ Becker, M., Papa, F., Karpytchev, M., Delebecque, C., Krien, Y., Uddin Khan, J., Ballu, V., Durand, F., Le Cozannet, G., Saiful Islam, A.K.M., Calmant, S., and Shum, C.K., 2020. Water level changes, subsidence, and sea level rise in the Ganges-Brahmaputra-Meghna delta. Proceedings of the National Academy of Sciences Jan 2020, 117 (4) 1867-1876; DOI: 10.1073/pnas.1912921117.

/7/ Best, D.J. & Roberts, D.E. (1975). Upper Tail Probabilities of Spearman's Rho. *Applied Statistics*, 24 (3).

/8/ CCC, 2016. Assessment of sea level rise on Bangladesh coast through trend analysis. Climate Change Cell, Department of Environment, Ministry of Environment and Forests, Dhaka, Bangladesh.

/9/ Church, J.A., P.U. Clark, A. Cazenave, J.M. Gregory, S. Jevrejeva, A. Levermann, M.A. Merrifield, G.A. Milne, R.S. Nerem, P.D. Nunn, A.J. Payne, W.T. Pfeffer, D. Stammer and A.S. Unnikrishnan, 2013: Sea Level Change. In: Climate Change 2013: The Physical Science Basis. Contribution of Working Group I to the Fifth Assessment Report of the Intergovernmental Panel on Climate Change [Stocker, T.F., D. Qin, G.-K. Plattner, M. Tignor, S.K. Allen, J. Boschung, A. Nauels, Y. Xia, V. Bex and P.M. Midgley (eds.)]. Cambridge University Press, Cambridge, United Kingdom and New York, NY, USA.

/10/ Cleveland, William S.; Devlin, Susan J. (1988). "Locally-Weighted Regression: An Approach to Regression Analysis by Local Fitting". *Journal of the American Statistical Association*. **83** (403): 596–610. doi:10.2307/2289282. JSTOR 2289282.

/11/ Dasgupta, S., Huq, M., Khan, Z.H., Masud, M.S., Ahmed, M.M.Z., Mukherjee, N., Pandey, K., 2010. Climate Proofing Infrastructure in Bangladesh. The World Bank Development Research Group.

/12/ Dasgupta, P., J. F. Morton, D. Dodman, B. Karapinar, F. Meza, M. G. Rivera-Ferre, A. Toure Sarr, and Vincent, K., 2014: Rural areas. *Climate Change 2014: Impacts, Adaptation, and Vulnerability. Part A: Global and Sectoral Aspects. Contribution of Working Group II to the Fifth Assessment Report of the Intergovernmental Panel on Climate Change*. C.B. Field et al., Eds., Cambridge University Press, Cambridge, United Kingdom and New York, NY, USA, 613–657.

/13/ DeConto, R.M. and Pollard, D., 2016. Contribution of Antarctica to past and future sea-level rise. Nature, 531 591

/14/   Kopp R.E., DeConto, R.M., Bader, D.A., Hay, C.C., Horton, R.M., Kulp, S., Oppenheimer, M., Pollard, D., and Strauss, B.H., 2017. Evolving Understanding of Antarctic Ice-Sheet Physics and Ambiguity in Probabilistic Sea-Level Projections. Journal of Earth's Future. 5, 12, 1217-1233.

/15/   Deo, A.A., Ganer, D.W., and Nair, G., 2011. Tropical cyclone activity in global warming scenario. *Journal of Natural Hazards.* 59(2), 771-786. 10.1007/s11069-011-9794-8.

/16/   Emmanuel, K., 2008. The hurricane – Climate Connection. DOI:10.1175/BAMS-89-5-Emanue.

/17/   FFWC, 2012. Annual flood report 2012. Flood Forecasting & warning Centre, Bangladesh Water Development Board, Dhaka, Bangladesh.

/18/   General Economic Division (GED), 2018. Bangladesh Delta Plan 2100.

/19/   Germanwatch, 2019. Global Climate Risk Index 2020. David Eckstein, Vera Künzel, Laura Schäfer, Maik Winges. Germanwatch e.V.

/20/   Haasnoot, M., Kwadijk, J., van Alphen, J., Le Bars, D., van den Hurk, B., Diermanse, F., van der Spek, A., Essink, G. O., Delsman, J. and Mens, M.: Adaptation to uncertain sea-level rise; how uncertainty in Antarctic mass-loss impacts the coastal adaptation strategy of the Netherlands, Environ. Res. Lett., 15(3), 34007, doi:10.1088/1748-9326/ab666c, 2020.

/21/   Hempel, S., Frieler, K., Warszawski, L., Schewe, J., and Piontek, F.: A trend-preserving bias correction – the ISI-MIP approach, Earth Syst. Dynam., 4, 219–236, https://doi.org/10.5194/esd-4-219-2013, 2013.

/22/   Higgins, S.A, Overeem, I., Steckler, M.S., Syvitski, J.P.M., Seeber, L., Akhter, H., 2014. InSAR measurements of compaction and subsidence in the Ganges-Brahmaputra Delta, Bangladesh. Journal of Geophysical Research Earth Surface. 119, 1768-1781.

/23/   Hoarau, K., Bernard, J., Chalonge, L., 2011. Review Intense Tropical Cyclone Activities in the Northern Indian Ocean. International Journal of Climatology. 32, 1935-1945. DOI: 10.1002/joc.2406.

/24/   Huang, et al. 1998 The empirical mode decomposition method and the Hilbert spectrum for non-stationary time series analysis. *Proc. R. Soc. Lond.* A**454**, 903–995.

/25/   IPCC, 2013. Climate Change 2013: The Physical Science Basis. Contribution of Working Group I to the Fifth Assessment Report of the Intergovernmental Panel on Climate Change Stocker, T.F., D. Qin, G.-K. Plattner, M. Tignor, S.K. Allen, J. Boschung, A. Nauels, Y. Xia, V. Bex and P.M. Midgley (eds.). Cambridge University Press, Cambridge, United Kingdom and New York, NY, USA, 1535 pp.

/26/   IPCC, 2019. IPCC Special Report on the Ocean and Cryosphere in a Changing Climate. H.-O. Pörtner, D.C. Roberts, V. Masson-Delmotte, P.Zhai, M. Tignor, E. Poloczanska, K. Mintenbeck, A. Alegria, M. Nicolai, A. Okem, J. Petzold, B. Rama, N.M. Weyer (eds.).

/27/   Oppenheimer, M., B.C. Glavovic, J. Hinkel, R. van de Wal, A.K. Magnan, A. Abd-Elgawad, R. Cai, et al. 2019. "Sea Level Rise and Implications for Low-Lying Islands, Coasts and Communities." In IPCC Special Report on the Ocean and Cryosphere in a Changing Climate, edited by H.-O. Pörtner, D.C. Roberts, V. Masson-Delmotte, P. Zhai, M. Tignor, E. Poloczanska, K. Mintenbeck, et al.

/28/   Islam, T., Peterson, R.E., 2008. Climatology of landfalling tropical cyclones in Bangladesh 1877–2003. *Journal of Natural Hazards*. 48, 115–135 (2009). https://doi.org/10.1007/s11069-008-9252-4.

/29/ Islam, S., Alam, R., Haque Khan, Z., Al Azad Khan, N., Nur-A-Jahan, I., 2013. Methodology of crest level design of coastal polders in Bangladesh. 4th International Conference on Water & Flood Management (ICWFM-2013).

/30/ IWM & Royal Haskoning, 2018. Technical Report on Storm Surge, Wave, Hydrodynamic Modelling and Design Parameters on Drainage System and Embankment Crest Level (Volume 3: Package 3).

/31/ Jackson, L.P. and Jevrejeva, S., 2016. A probabilistic approach to 21st century regional sea-level projection using RCP and High-end scenarios. Global Planetary Change 146, 179-89.

/32/ Karim, M.F., Mimura, N., 2008. Impact of climate change and sea-level rise on cyclonic storm surge floods in Bangladesh. Journal of Global Environmental Change. Vol. 18, Issue 3, 490-500.

/33/ Kendall, M. G. (1975). *Rank Correlation Method*s. Griffin, London, UK.

/34/ Knapp, K.R., Kruk, M.C., Levinson, D.H., Diamond, H.J., and Neuman, C.J., 2010. *The International Best Track Archive for Climate Stewardship (IBTrACS): Unifying Tropical Cyclone Data*. American Meteorological Society. https://doi.org/10.1175/2009BAMS2755.1.

/35/ Knapp, K.R., Diamond, H.J., Kossin, J.P., Kruk, M.C., Schreck, C.J., 2018. International Best Track Archive for Climate Stewardship (IBTrACS) Project, Version 4. NOAA National Centers for Environmental Information. https://doi.org/10.25921/82ty-9e16.

/36/ Knutson, T. R., Sirutis, J. J., Zhao, M., Tuleya, R. E., Bender, M., Vecchi, G. A., Villarini, G., and Chavas, D. (2015). Global projections of intense tropical cyclone activity for the late twenty-first century from dynamical downscaling of CMIP5/RCP4.5 scenarios. Journal of Climate, 28(18), 7203–7224. http://doi.org/10.1175/JCLI-D-15-0129.1.

/37/ Knutson, T., Camargo, S.J., Chan, J.C.L., Emanuel, K., Ho, C.-H., Kossin, J., Mohapatra, M., Satoh, M., Sugi, M., Walsh, K., and Wu, L., 2019. Tropical cyclones and climate change assessment. Part I: Detection and Attribution. Bulletin of the American Meteorological Society, Vol. 100, Issue 1, 1987-2007, https://doi.org/10.1175/BAMS-D-18-0189.1

/38/ Knutson, T., Camargo, S.J., Chan, J.C.L., Emanuel, K., Ho, C.-H., Kossin, J., Mohapatra, M., Satoh, M., Sugi, M., Walsh, K., and Wu, L., 2020. Tropical cyclones and climate change assessment. Part II: Projected Response to Anthropogenic Warming, Vol. 101, Issue 3, https://doi.org/10.1175/BAMS-D-18-0194.1

/39/ Knutson, T.R., Chung, M.V., Vecchi, G., Sun, J., Hsieh, T.-L., Smith, A.J.P., 2021. Climate change is probably increasing the intensity of tropical cyclones. Science Brief Review. In: Critical Issues in Climate Change Science, edited by: Corine Le Quéré, Peter Liss, Piers Forster.

/40/ Kwadijk, J.C.J., Haasnoot, M., Mulder, J.P.M., Hoogvliet, M.M.C., Jeuken, A.B.M., Vander Krogt, R.A.A., Oostrom, N.G.C., Schelfhout, H.A., Van Velzen, E.H., Van Waveren,H., De Wit, M.J.M., 2010. Using adaptation tipping points to prepare for climatechange and sea level rise: a case study in the Netherlands. WIREs Clim. Change 1,729–740.http://dx.doi.org/10.1002/wcc.64.

/41/ Leijnse, T., Giardino, A., Nederhoff, K., and Caires, S., submitted. Generating reliable estimates of tropical cyclone induced coastal hazards along the Bay of Bengal for current and future climate conditions using synthetic tracks. Journal of Natural Hazards and Earth System Sciences.

/42/ Mann, H.B. (1945). Nonparametric tests against trend. *Econometrica* 13, 245–259.

/43/ Mann, H. B. & Whitney, D. R. (1947). On a test of whether one of two random variables is stochastically larger than the other. *Annals of Mathematical Statistics*, 18, 50–60.

/44/ MOEF, 2018: Ministry of Environment and Forest Government of the People's Republic of Bangladesh Climate Change Profile, Report April 2005.

/45/ Monirul Qader Mirza, M., 1997: Hydrological changes in the Ganges system in Bangladesh in the post-Farakka period, *Hydrological Sciences-Journal,* 42(5) October 1997.

/46/ Nederhoff, K., Hoek, J., van Ormondt, M., Caires, S., Leijnse, T., Giardino, A., 2021. Simulating Synthetic Tropical Cyclone Tracks for Statistically Reliable Wind and Pressure Estimations. Journal of Natural Hazards and Earth System Sciences. 21, 861-878.

/47/ Nuzzo, P. (2014). Statistical errors; P values, the 'gold standard' of statistical validity, are not as reliable as many scientists assume, Nature vol 506.

/48/ Ostanciaux, É., Husson, L., Choblet, G., Robin, C., Pedoja, K. Present-day trends of vertical ground motion along the coast lines. Earth Scientific Reviews, Vol. 110, 1-4, 74-92.

/49/ Rahman, M. and Rahaman, M.M., 2018: Impacts of Farakka barrage on hydrological flow of Ganges river and environment in Bangladesh, Sustain. Water Resour. Manag. (2018) 4:767–780 https://doi.org/10.1007/s40899-017-0163-y.

/50/ Sarwar, M.G.M., 2013. "Sea level rise along the coast of Bangladesh" in Disaster Risk Reduction Approaches in Bangladesh, R. Shaw, F. Mallick, A. Islam, Eds pp 217-231.

/51/ SAARC Meteorological Research Centre (SMRC), 2003. The Vulnerability Assessment of the SAARC Coastal Region due to Sea Level Rise: Bangladesh Case, Dhaka, Bangladesh: SMRC-No.3, SMRC Publications.

/52/ Shahid, S., 2009: Rainfall variability and the trends of wet and dry periods in Bangladesh *Int. J. Climatol.* 30: 2299–2313 (2010) DOI: 10.1002/joc.2053.

/53/ Shahid, S., 2011: Trends in extreme rainfall events of Bangladesh, Theoretical and Applied Climatology (2011) 104:489–499 DOI 10.1007/s00704-010-0363-y.

/54/ Schultz, J.M., Russel, J., and Espinel, Z. 2005. Epidemiology of tropical cyclones: the dynamics of disaster, disease, and development. *Epidemiologic Review* 27, 21-35.

/55/ Singh, O. P., Khan, T.M.A., Rahman, S, 2000. Changes in the frequency of tropical cyclones over the North Indian Ocean. *Journal of Meteorology and Atmospheric Physics*. 75, 11-20. https://doi.org/10.1007/s007030070011.

/56/ Singh, O.P., 2002. Spatial variation of sea level trend along the Bangladesh coast. Marine Geodesy, 25, 205-212.

/57/ Singh, O.P., 2010. Recent Trends in Tropical Cyclone Activity in the North Indian Ocean. *Indian Ocean Tropical Cyclones and Climate Change*. 51-54. 10.1007/978-90-481-3109-9_8.

/58/ Steckler, M., Nooner, S.L., Akhter, S.H., Chowdhury, S.K., Bettadpur, S., Seeber, L., Kogan, M.G., 2010. Modeling Earth deformation from monsoonal flooding in Bangladesh using hydrographic, GPS, and Gravity Recovery and Climate Experiment (GRACE) data. Journal of Geophysical Research, 115. https://doi.org/10.1029/2009JB007018.

/59/ Steckler, M.S., Oryan, B., Jaman, M.H., Mondal, D.R., Grall, C., Wilson, C.A., Akhter, S.H., DeWolf, S., and Goodbred, S.L., 2021. Recent measurements of subsidence in the Ganges-Brahmaputra Delta, Bangladesh. Poster, EGU General Assembly. https://doi.org/10.5194/egusphere-egu21-6562.

/60/ Sugi, M., Murakami, H. & Yoshida, K. Projection of future changes in the frequency of intense tropical cyclones. Journal of Climate Dynamics, 49, 619–632 (2017). https://doi.org/10.1007/s00382-016-3361-7.

/61/ Syvitski, J. P. M., Kettner, A. J., Overeem, I., Hutton, E. W. H., Hannon, M. T., Brakenridge, G. R., Day, J., Vörösmarty, C., Saito, Y., Giosan, L., and Nicholls, R. J., 2009, Sinking deltas due to human activities: Nature Geoscience, v. 2, no. 10, p. 681-686.

/62/ Taylor, K. E., R. J. Stouffer, and G. A. Meehl, 2012:Anoverview of CMIP5 and the experiment design. Bull. Amer. Meteor. Soc., 93, 485–498, doi:10.1175/BAMS-D-11-00094.1.

/63/ Warszawski, L., Frieler, K., Huber, V., Piontek, F., Serdeczny, O. and J. Schewe (2013). The Inter-Sectoral Impact Model Intercomparison Project (ISI-MIP): project framework. Proceedings of the National Academy of Sciences of the United States of America. 111. 10.1073/pnas.1312330110.

/64/ Vousdoukas, M., Mentaschi, L., Voukouvalas, E., Verlaan, M., Jevrejeva, S., Jackson, L.P., Feyen, L., 2018. Global probabilistic projections of extreme sea levels show intensification of coastal flood hazards. Nature Communications.

/65/ Walsh, K.J.E., McBride, J.L., Klotzbach, P.J., Balachandran, S., Camargo, S.J., Holland, G., Knutson. T.R., Kossin, J.P., Lee, T., Sobel, A., Sugi, M., 2016. Tropical cyclones and climate change. Wires Climate Change, https://doi.org/10.1002/wcc.371.

/66/ Webster, P.J., Holland, G.J., Curry, J.A., and Chang, H.-R., 2005. Changes in Tropical Cyclone Number, Duration, and Intensity in a Warming Environment. Science, 309, 1844-1846, 1575.

/67/ Whitehead, P. G. Barbour, E., M.N. Futter, S. Sarkar, H. Rodda, J. Caesar, D. Butterfield, L. Jin, R. Sinha, R. Nicholls, M. Salehin,: Impacts of Climate Change and Socio-economic Scenarios on Flow and Water Quality of the Ganges, Brahmaputra and Meghna (GBM) RiverSystems: Low Flow and Flood Statistics, Environmental Science: Processes & Impacts., 2013, 00, 1-3.

/68/ Wilcoxon, F. (1945). Individual comparisons by ranking methods. *Biometrics*, 1, 80-83.

A   Statistical tests and indicators

A.1   Introduction

A climate-induced trend in hydro-meteorological time series is of major concern to decision makers in water management. To detect such changes, time series can be tested for non-stationarity (or non-homogeneity). Non-stationarity refers to a trend or shift in the time series, or a combination of both. The challenge is to distinguish between actual changes in the system and natural variability; in other words, to separate the signal from the noise. The traditional approach is to assess if the following (null) hypothesis can be rejected:

"*the historical time series is a stationary process*"

A process, such as river flow, is stationary if the probability distributions of the metrics that characterize the process, such as annual mean discharge, do not change significantly over time. The objective of statistical tests is to determine whether there is sufficient evidence to reject the null hypothesis that the underlying process is stationary. There are several statistical tests available for this objective. In each test, a test-specific metric, t, is derived from the historical time series. The tests compute a p-value, which is the probability that the deviation of the test statistic from the stationary case is coincidental. Small p-values are an indication that the sequence is non-stationary, and thus that the underlying process is non-stationary. A significance level, α, defines the p-value threshold between acceptance and rejection of the null hypothesis. A time series is considered to be non-stationary (null hypothesis is rejected) if the calculated p value is below α. Commonly used values for the significance level are 0.01 or 0.05 (Nuzzo, 2014).

A.2   Trend tests for single time series

In this report, the following four p-tests are applied to detect trends in time series:

Table A.1   Overview of the statistical tests used in this document and abbreviations

Name	Abbreviation
Pearson t-test	PS
Mann-Kendall test	MK
Spearman's rank correlation test	SM
Wilcoxon-Mann-Whitney test	WMW

Pearson t-test (linear trend test). In this test, the test statistic is the (Pearson) correlation coefficient, ρ, between observed values and the time of observation. The Student's t-test is then applied to quantify the p-value of the test statistic t, where $t = \rho((n\text{-}2)^{0.5}/((1\text{-}\rho^2)^{0.5})$; n is the number of observations.

Spearman's rank correlation test. This test is the non-parametric analogue of the Pearson t-test. The test statistic is Spearman's rank correlation coefficient, which is the correlation between the *ranks* of the annual values and their years of observation. For short series, the p-value can be calculated analytically. For longer series the p-value can be approximated by an Edgeworth series (Best & Roberts, 1975).

Mann-Kendall test. The Mann-Kendall test is another non-parametric significance test for a monotonic trend in a time series based on the Kendall's τ (Mann, 1945; Kendall, 1975). This test compares the ranks for all pairs of annual values. This amounts to $N*(N\text{-}1)/2$ combinations, where N is the number of years of observations. The test statistic, τ, is the difference between the number of pairs that support a positive trend and the number of pairs that support a negative trend, divided by the standard deviation. Large deviations from 0 result in low p-values.

Wilcoxon-Mann-Whitney test. The Wilcoxon-Mann-Whitney (WMW) test (Wilcoxon, 1945), also known as the Wilcoxon ranks sum test or the Mann-Whitney U test, is a non-parametric test for two independent samples. The WMW test can be used for trend analysis by splitting the time series into a first and second half and testing the null hypothesis that the two sub-sets are taken from the same distribution. The test statistic is the sum of the ranks of the elements in each sub-set. Large differences between the sums of ranks of both subsets result in low *p*-values. The two sub-sets need not have identical lengths, as was pointed out by Mann and Whitney (1947).

A.3 Trend tests for multiple time series

If tests on individual time series result in *p*-values that are all above significance level, α, the individual time series do not provide sufficient support for rejection of the null-hypothesis. However, combining information from multiple time series may pool sufficient evidence to reject the null-hypothesis. This requires a (statistical) test method in which the information from the individual stations is efficiently and objectively combined. Another advantage of such test is that it can provide an overall trend indication for an area in which different stations have different trends. For example, some stations may indicate a decreasing trend is happening, while others indicate an increasing trend. A combination test can then quantify if the overall trend for this area is most likely increasing or decreasing.

An example of a combination test is the 'z-test' (Stouffer et al., 1949). In this test, the derived *p*-values of the individual tests are first transformed using the inverse of the standard normal distribution function:

$$z_i = \Phi^{-1}(p_i) \qquad (1)$$

In this equation, p_i is the derived *p*-value of test *i*, Φ is the standard normal distribution function and z_i is a transformed value of p_i. If the null-hypothesis is correct, the *p*-values are uniformly distributed and, hence, the *z*-values are standard normally distributed. Under the assumption of [a] the null hypothesis and [b] independence between the (n) sample sets (or time series), the following test statistic, *Z*, is also standard normally distributed:

$$Z = \frac{\sum_{i=1}^{n} z_i}{\sqrt{n}} \qquad (2)$$

Since *Z* is standard normally distributed under the null-hypothesis, the combined *p*-value of the n tests is equal to $\Phi(Z)$. Large deviations of Z from 0 are indications of non-stationarity. Mosteller & Bush (1954) proposed an adjustment of the z-test by imposing weights on the computed z-values:

$$Z_1 = \frac{\sum_{i=1}^{n} w_i z_i}{\sqrt{\sum_{i=1}^{n} w_i^2}} \qquad (3)$$

These authors proposed to take the weights, w_i, i=1..n, equal to the respective number of samples (observations). This approach gives higher weights to larger sets, i.e. to time series with longer records, as such recognizing that *p*-values from tests on larger sets can be expected to be more reliable as they are less influenced by the factor coincidence. Recently, Zaykin (2011) demonstrated this test can be improved by taking w_i equal to the square root of the number of observations. In this report we adopt this choice of the weights.

A.4 Trend classification

Trend tests are carried out for combinations of different variables (rainfall, temperature and discharge), indicators (minimum, mean and maximum), types of statistical tests (PS, MK, SM and WMW) and different seasons (four plus the whole year). This means a large set of p-values is derived. In order to get a quick overview of results, p-values are classified as follows:

- No trend: $p \geq 0.2$
- Possible trend: $0.05 \leq p < 0.2$
- Likely trend: $0.001 \leq p < 0.05$
- Very likely trend: $p < 0.001$

Note that a p-value < 0.05 is often classified as being "statistically significant", whereas in the above definition this is identified as a likely trend. However, this is rather a discussion of semantics and not relevant for our current objective. The main use of the classification above is to be able to present our results to an audience of non-statistical experts.

The p values and the above classification only indicate the likelihood of the trend, but not whether it is an increasing or decreasing trend. Fortunately, the value of the test statistic will provide the necessary information to make that distinction. A negative value of the test statistic indicates a decreasing trend, a positive value indicates an increasing trend. In total we distinguish seven different trend classes, identified by the combination of the p-value and the test statistic, see Table A.2. Each class has its own unique colour code that helps identify overall trend directions of combinations of stations, seasons etc.

Table A.2. Definition of trend classes.

Color code	Description	Value of test statistic	P-value bounds	
			lower	upper
	Very likely decreasing trend	<0	0	0.001
	Likely decreasing trend	<0	0.001	0.05
	Possible decreasing trend	<0	0.05	0.2
	No trend	≈0	0.2	1
	Possible increasing trend	>0	0.05	0.2
	Likely increasing trend	>0	0.001	0.05
	Very likely increasing trend	>0	0	0.001

It should be emphasized that:

> *The trend class is only a first identification of an ongoing trend. It does not mean the trend will continue in the future. It also does not mean the trend is linear, a sudden "shift" in the data due to for example a human intervention may also result in a low p-value. The trend classes in this report therefore only serve as a first step in the process, further investigation into the underlying time series and physics is always recommended.*

A.5 Indicators

The trend analyses will generally be carried out for three indicators:

- Minimum;
- Maximum;
- Mean.

For example, the first indicator is the minimum daily value of the discharge (or rainfall, temperature) in a year. This value will be derived for each year in the available series. The trend analysis is then subsequently applied to this annual series of minimum values. Minimum values are relevant for water

resources studies, whereas maximum values are relevant for flood risk analyses. The derived trends can be quite different for these indicators. For example, annual minimum low flows might decrease due to an increase in evaporation, but this may not, of hardly, affect the annual maximum discharge.

A.6   Season definition

Trends can also be significantly different for the different seasons in a year. Therefore, the trend analysis is carried out for four different seasons and for the whole year. So, for example, if we consider the pre-monsoon season with the mean value as the indicator, this means for each year the mean discharge in the three months of the pre-monsoon season is computed. This results in an annual series of mean pre-monsoon season flows. The trend analysis is then carried out on this annual series.

Table 6-1   Seasons for which the trend analysis is carried out (including the whole year).

Season	Period	
	from	To
Pre-monsoon	March	May
Monsoon	June	September
Post-monsoon	October	November
Winter	December	February
year	March	February

B   Trends in historical rainfall records

This appendix contains figures of trend classes of historical rainfall records. Results are shown for different seasons (year, winter, pre-monsoon, monsoon and post-monsoon), different indicators (mean rainfall and maximum daily rainfall) and statistical tests (Pearson, Mann-Kendall, Spearman and Wilcoxon-Mann-Whitney). The reader is referred to Section A.4 for the definition of the colour classes.

C   Trends in historical temperature records

This appendix contains figures of trend classes of historical temperature records. Results are shows for different seasons (year, winter, pre-monsoon, monsoon and post-monsoon) and statistical tests (Pearson, Mann-Kendall, Spearman and Wilcoxon-Mann-Whitney). The reader is referred to Section A.4 for the definition of the color classes.

trends in annual (mean) temperature
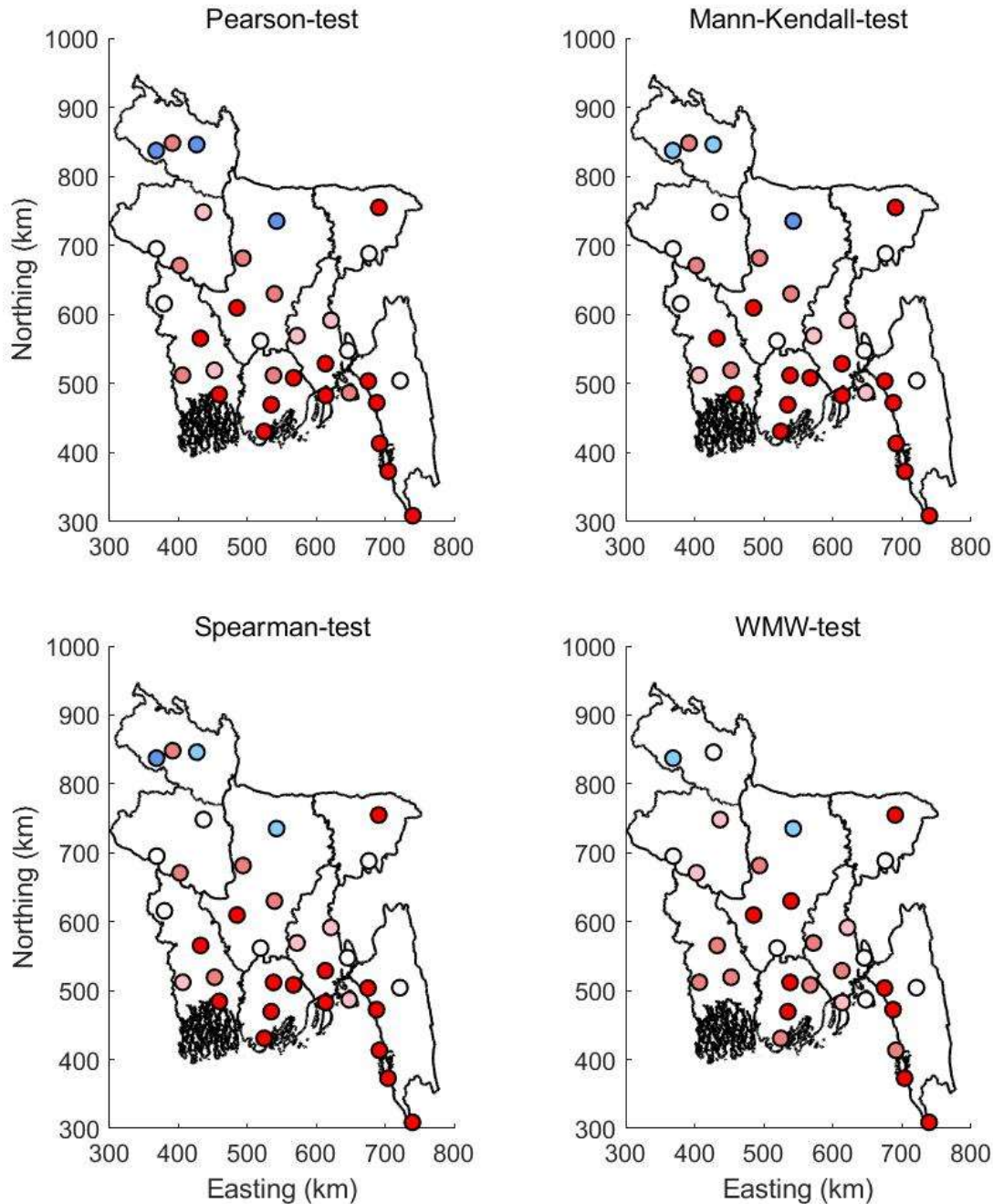
trends in Pre-monsoon (mean) temperature
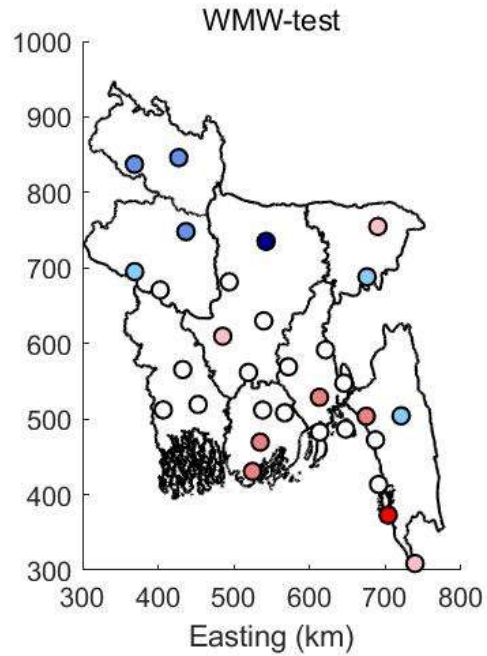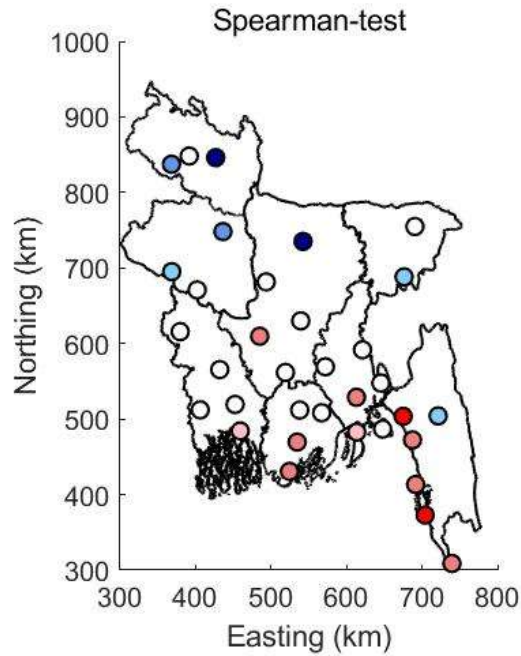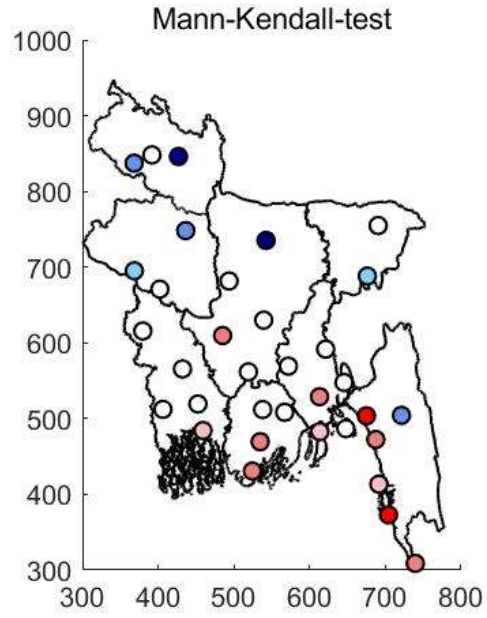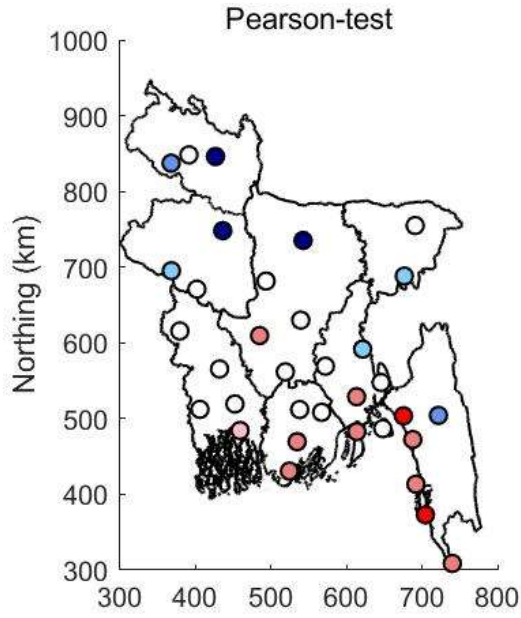
trends in Monsoon (mean) temperature
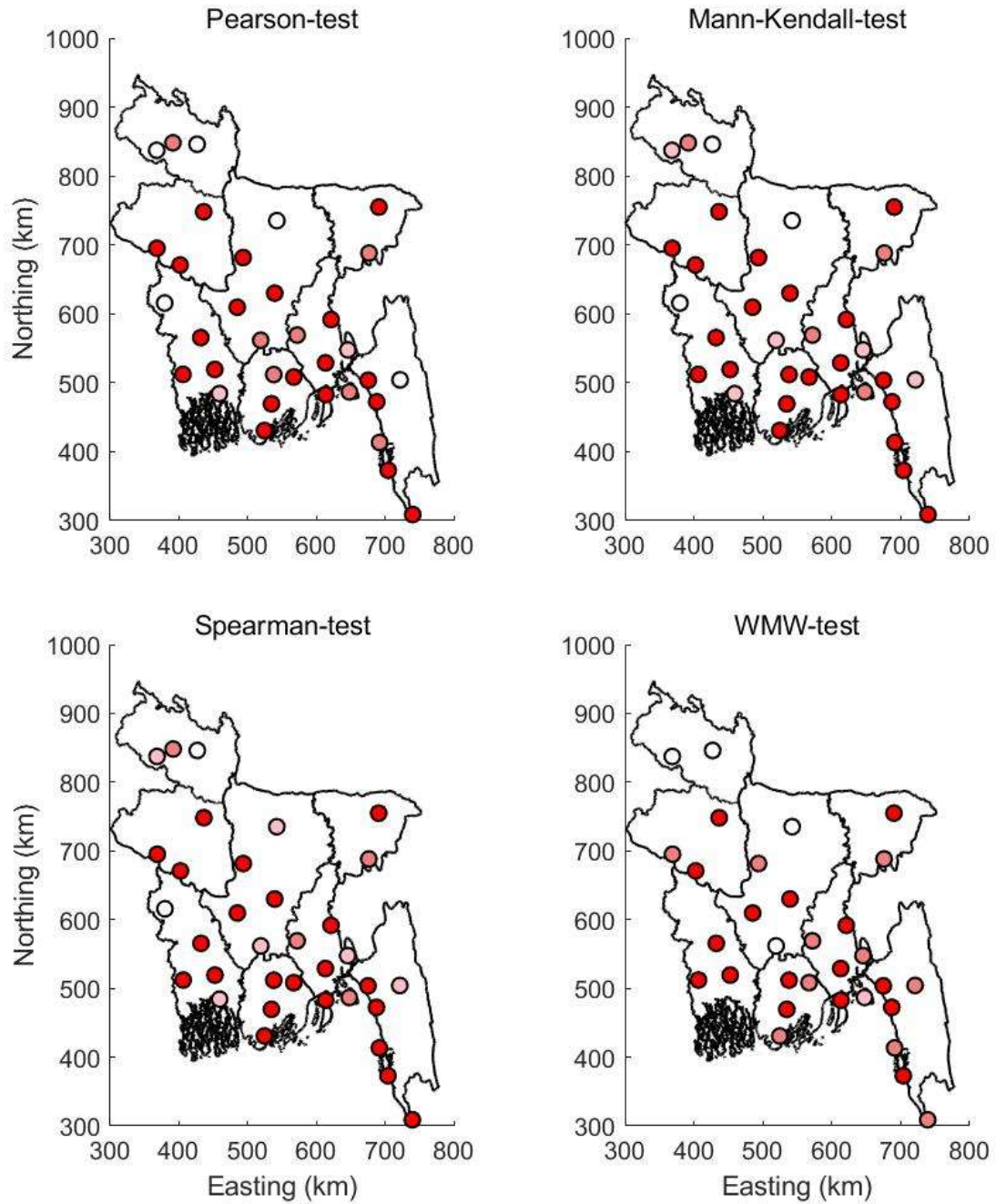
trends in Post-monsoon (mean) temperature
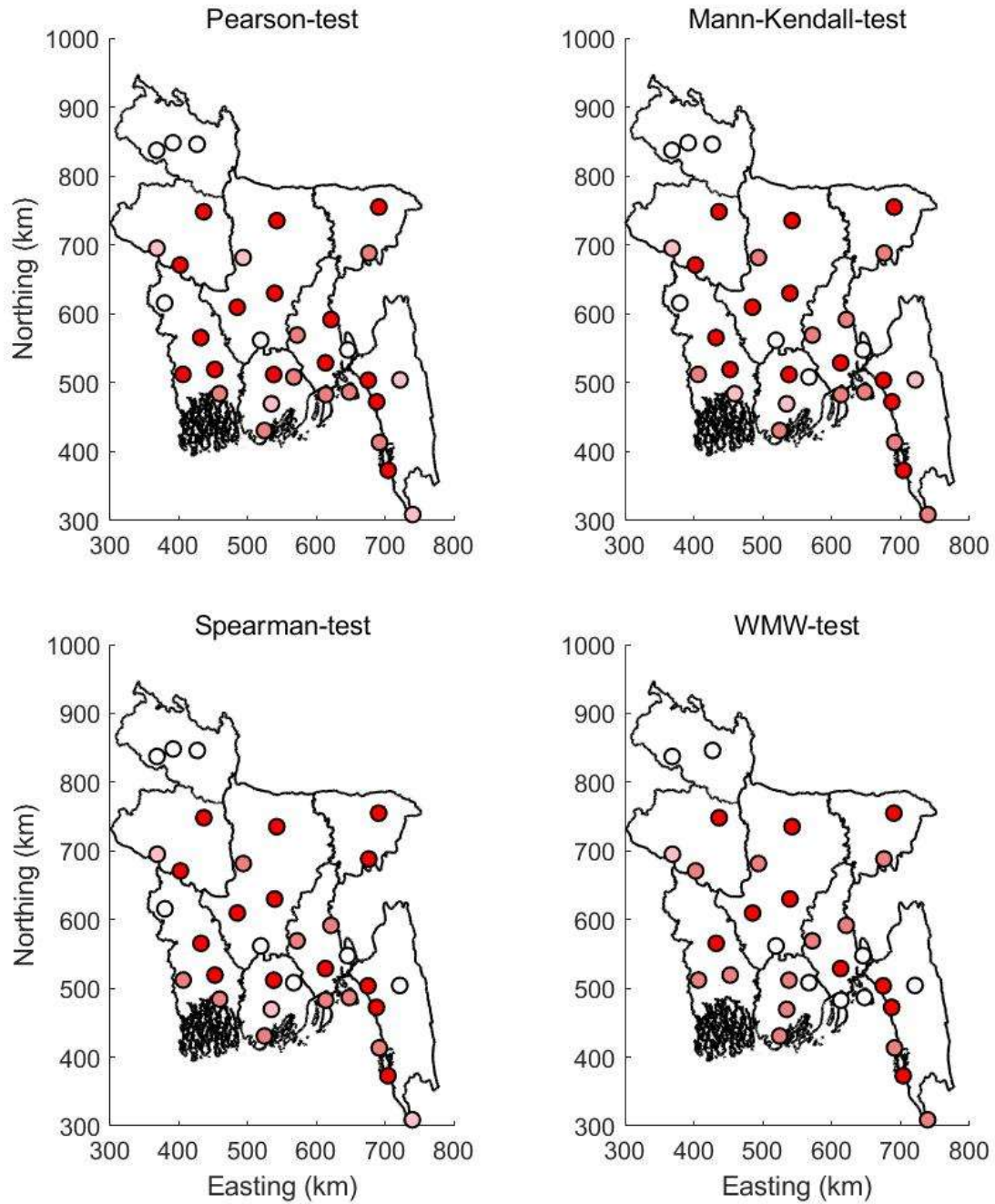
trends in Winter (mean) temperature